DISSERTATION

ORGANOPOLYMERIZATION OF MULTIFUNCTIONAL γ-BUTYROLACTONES

Submitted by

Jing Tang

Department of Chemistry

In partial fulfillment of the requirements

For the Degree of Doctor of Philosophy

Colorado State University

Fort Collins, Colorado

Fall 2018

Doctoral Committee:

Advisor: Eugene Y.-X. Chen

Grzegorz Szamel
Garret M. Miyake
Travis S. Bailey
Laurence A. Belfiore

ABSTRACT

ORGANOPOLYMERIZATION OF MULTIFUNCTIONAL

γ-BUTYROLACTONES

The complexity of polymerizations increases drastically as the functionality of monomers increases, which brings about challenges for elucidation of polymerization mechanisms, establishing control of the polymerization, and characterization of the resulting polymer structures. On the other hand, the increased multifunctionality in monomers and polymers offers new opportunities to create polymers with unique structures and interesting properties. The research described in this dissertation demonstrates both challenges and advantages that multifunctionality brings into the polymerization and polymer structures.

The first successful polymerization of the naturally occurring, OH-containing, tri-functional monomer Tulipalin B (βHMBL) was achieved by utilizing *N*-heterocyclic carbene and phosphazene superbase catalysts. Owing to its presence of both the reactive exocyclic double bond and hydroxyl group, the resulting PβHMBL is a branched vinyl–ether lactone copolymer structure with six different types of substructural units. The results reveal multiple types of reaction pathways and their mechanistic crossovers involved in the polymerization, including conjugate Michael and oxa-Michael additions, proton transfer processes, as well as ene-type dehydration reactions, enabled by proton transfer.

The reactions of other less complicated multifunctional γ-butyrolactone-based monomers under same conditions was also studied to help uncover the polymerization mechanism, including the polymerization of bifunctional (endocyclic double bond, lactone ring) dihydrofuran-2(3H)-one (FO),

3-methylfuran-2(5H)-one (3-MFO), and 5-methylfuran-2(5H)-one (5-MFO), as well as trifunctional (endocyclic or exocyclic double bond, lactone ring, hydroxyl group) 3-(hydroxymethyl) furan-2(5H)-one (3-HMFO). The polymerization of the parent FO leads to a vinyl-addition polymer, while the predominant trimerization and dimerization are observed in the reaction involving the two methyl-substituted derivatives, 3-MFO and 5-MFO. The polymerization of trifunctional 3-HMFO gives a poly(vinyl–ether lactone) copolymer structure, via two different types of base activation mechanisms and a combination of Michael and ox-Michael additions and proton transfer processes.

This thesis work also investigates how different initiation and termination chain ends of poly(γ-butyrolactone) (PγBL) affect the materials properties, including thermal stability, thermal transitions, thermal recyclability, hydrolytic degradation, and dynamic mechanical behavior. Four different chain-end-capped polymers with similar molecular weights have been synthesized. The termination chain end showed a large effect on polymer decomposition temperature and hydrolytic degradation. Overall, by chain-end capping, linear PγBL behaves much like cyclic PγBL in those properties sensitive to the chain ends.

TABLE OF CONTENTS

Chapter 1

Introduction

The dissertation presented hereinafter was conceived in a "journals-format" style, in agreement with the Graduate School guidelines at Colorado State University, and it contains three peer-referred original research manuscripts. Two of the manuscripts have already been published in peer-reviewed chemistry journals, *Eur. Polym. J.* and *Org. Chem. Front.*, while the third manuscript has been accepted by *J. Polym. Sci. Part A: Polym. Chem.* and is currently in press.

Nowadays, fossil fuels are the main sources of energy for the transportation and chemicals, including the coal and petroleum-based polymers. However, fossil resource is finite and the generation of a fossil fuel by natural processes is typically millions of years, and sometimes exceeds 650 million years. Many studies assume that all fossil resources will be depleted within a few centuries. In addition, greenhouse gases emissions caused by consumption of fossil resources kept perturbing the Earth's climate. With all these concerns about using fossil fuels, there is a growing interest in developing polymeric materials derived from renewable sources as the world begins to become much more aware of the need for a sustainable future.

As the only carbon rich material source available on Earth besides fossil resources, biomass is most likely to be the only viable alternative to fossil resources for production of transportation fuels and fine chemicals. The last decade has witnessed the introduction of a wave of new monomers derived from biomass, including simple sugars, starch, lignocelluloses, plant oils, and so on. The unconventional structures of sustainable polymers not only supply a renewable

alternative to the use of petroleum as an industrial feedstock but also broaden the range of accessible polymer properties.

In this context, we focused on the organopolymerization of a bioderived monomer, tulipalin B, or *β*-hydroxy-*α*-methylene-*γ*-butyrolactone ($_{\beta}$HMBL). It is a biologically active (antimicrobial), naturally occurring, trifunctional monomer containing an exocyclic conjugated double bond, a five-membered lactone, and a hydroxyl group. With its multifunctionality, the resulting structure of P$_{\beta}$HMBL is expected to be interesting. However, significant challenges exist in such cases as
the presence of multiple functional groups in the monomer could result in a poor control over the polymer structure and increase the number of pathways to be considered in mechanism study of the reaction.

The results of these fundamental investigations are discussed in detail in the following two chapters:

1) The P$_{\beta}$HMBL polymer produced by AIBN, NHCs I^{t}Bu and TPT as well as superbase ^{t}Bu-P$_4$.
2) Thermal properties of P$_{\beta}$HMBL polymer produced by AIBN, NHCs I^{t}Bu and TPT as well as superbase ^{t}Bu-P$_4$.
3) The homopolymerization of dihydrofuran-2(3H)-one (FO), 3-methylfuran-2(5H)- one (3-MFO), 5-methylfuran-2(5H)-one (5-MFO), and 3-(hydroxymethyl) furan-2(5H)-one (3-HMFO).
4) Mechanistic study of $_{\beta}$HMBL polymerization.

Chapter two reports the first successful polymerization of a βHMBL and investigates its thermal properties. Firstly, we hypothesized several possible pathways based on the previous study of the polymerization of renewable methylene butyrolactones, including Tulipalin A as well as its methyl-substituted derivatives, *γ*-methyl-*α*-methylene-*γ*-butyrolactone (γMMBL) and *β*-methyl-*α*-methylene-*γ*-butyrolactone (βMMBL). Although only homopolymerization was observed in the case of Tulipalin A family, the OH groups in βHMBL is expected to bring more complexity in the polymerization pathways such as proton transfer and oxa-Michael addition. Significant chain transfer occurred in this polymerization limited the molecular weight of the resulting polymer.

The study described in Chapter two realized the polymerization of Tulipalin B, but the resulting polymer structure and the polymerization mechanism remained unclear. To better understand the polymerization mechanism and characterize polymer structures, the research described in Chapter three studied the homopolymerization of the less complex unsaturated five-membered lactones and furanones such as dihydrofuran-2(3H)-one (FO), 3-methylfuran-2(5H)- one (3-MFO), 5-methylfuran-2(5H)-one (5-MFO), and 3-(hydroxymethyl) furan-2(5H)-one (3-HMFO). These results provided critical mechanistic insights into the structurally related, yet more complicated polymerization of βHMBL and revealed the PβHMBL structures.

In Chapter four, we investigated effects of poly(*γ*-butyrolactone) (P*γ*BL) with different initiation and termination chain ends on five types of materials properties, including thermal stability, thermal transitions, thermal recyclability, hydrolytic degradation, and dynamic mechanical behavior.

Chapter five summarizes the research results of the thesis work.

All the experimental details, methods, materials characterizations, supporting figures, and additional tables corresponding to each of the individual chapters are consecutively included in Appendixes at the end of this dissertation. This arrangement keeps the consistency with the already published work and also provides a more readable organization of the research contents within the main chapters.

Chapter 2

Organopolymerization of Naturally Occurring Tulipalin B: A Hydroxyl-functionalized Methylene Butyrolactone

2.1 Summary

The first successful polymerization of the naturally occurring, OH-containing, tri-functional monomer Tulipalin B (βHMBL) is established. N-Heterocyclic carbene and phosphazene superbase catalysts effectively polymerize βHMBL into polymers with M_n up to 13.2 kg mol^{-1}. The possible polymer structure is thought to be a branched copolymer of poly (vinyl-ether lactone)s, derived from proposed crossovers between conjugate Michael and oxa-Michael additions, enabled by proton transfer.

2.2 Introduction

The emergence of organopolymerization[1] has profited from the development of powerful organic catalysts and unique mechanistic pathways in the rapidly growing field of organocatalysis.[2] One such important class of organic catalysts is N-heterocyclic carbenes (NHCs); thanks to their inherently high Brønsted-basicity and nucleophilicity, NHCs have attracted increasing interest for their unique reactivity and selectivity often observed in many different types of organic reactions.[3] The scope of the NHC-mediated polymerization[4] has expanded significantly from the first ring-opening polymerization (ROP) of cyclic esters (lactides)[5] to group transfer polymerization (GTP) of α,β-unsaturated esters (or acrylates);[6] step-growth polyaddition of diols and diisocyanates to polyurethanes;[7] step-growth polycondensation of diols and diesters to polyesters;[8] step-growth polyaddition of dimethacrylates to unsaturated polyesters,[9] which is based on fundamental steps of tail-to-tail dimerization (intermolecular umpolung) of methacrylates;[10] and chain-growth conjugate polyaddition of acrylates.[11] Less utilized is the basicity of the NHC for polymerization via basic

activation of the protic monomer or initiator, but two recent examples invoked such activation mode to achieve oxa-Michael addition polymerization of hydroxyl functionalized acrylates to poly(ester–ether)s with M_n up to 2400 g mol^{-1} (ref. 12) and common (meth)acrylates in the presence of alcohol to α-alkoxy polyacrylates with M_n up to 8000 g mol^{-1}.[13] On the other hand, the phosphazene superbase, 1-tert-butyl-4,4,4-tris(dimethylamino)-2,2-bis[tris (dimethyl amino) phosphoranylid-enamino]-2λ^5 ,4λ^5 -catenadi(phosphazene) (^{t}Bu-P$_4$),[14] is one of the strongest known neutral bases but with low nucleophilicity. Thus, the combination of its strong basicity and low nucleophilicity renders ^{t}Bu-P$_4$ a potent organic initiator or catalyst to promote various types of polymerization reactions, but primarily as a base to deprotonate a protic initiator[15] or monomer[16] directly to generate anionic active species for polymerization reactions. ^{t}Bu-P$_4$ has also been reported as a nucleophilic catalyst for GTP initiated by a silyl ketene acetal.[17]

Renewable or sustainable polymers have recently gained increasing attention, the research of which has been directed at examining the possibility of replacing petroleum-based raw materials by naturally occurring or biomass-derived renewable feedstocks for the production of polymeric materials in large commodity and specialty chemicals markets.[18] In this context, renewable methylene butyrolactones based on the Tulipalin family, Tulipalin A (Figure. 2.1), or α-methylene-γ-butyrolactone (MBL), found in tulips,[19] as well as its methyl-substituted derivatives, *γ*-methyl-*α*-methylene-*γ*-butyrolactone (γMMBL), derived from the biomass sourced levulinic acid,[20] and *β*-methyl-*α*-methylene-*γ*-butyrolactone (βMMBL), derived from the biomass sourced itaconic acid,[21] have been explored for the prospects of substituting the currently petroleum-based acrylic monomers, such as methyl methacrylate (MMA), in the production of acrylic bioplastics and specialty chemicals.[22] Various types of polymerization processes[22a] have been employed to polymerize MBL, γMMBL, and βMMBL,

including radical,[23] anionic,[24] group-transfer,[25] Lewis pair zwitterionic,[26] and metal-mediated coordination[27] polymerization methods. NHC-mediated organopolymerization of such monomers has also been investigated.[11] Regardless of the polymerization mechanism or process, all homo-polymerizations of the above three

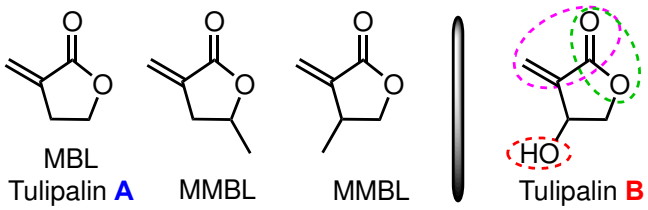

Figure. 2.1 Structures of Tulipalin A, its methyl derivatives, and Tulipalin B.

Tulipalin A-based monomers proceed exclusively through vinyl addition without ring-opening of the five-membered lactone ring. Tulipalin B, or *β*-hydroxy-*α*-methylene-*γ*-butyrolactone (βHMBL) (Figure. 2.1), is a biologically active (antimicrobial), naturally occurring [present as the (S)-enantiomer in tulips],[19] trifunctional monomer containing an exocyclic conjugated double bond, a five-membered lactone, and a hydroxyl group. Recently, its preparation from tulip biomass by a one-step enzyme reaction has been reported.[28] Perhaps owing to its structural complexity and presence of the reactive hydroxyl group, polymerization of βHMBL has not been reported in the open literature. Accordingly, the objective of this study is to investigate organopolymerization of βHMBL (1) by organic NHC and superbase catalysts.

2.3 Results and discussion

Considering the multi-functionality of the βHMBL monomer, we hypothesized that five possible scenarios could be involved in the polymerization of βHMBL by nucleophilic/basic organic NHC catalysts as outlined in Figure 2.1. First, nucleophilic activation leads to a zwitterionic intermediate

that could undergo repeated conjugate Michael addition to form vinyl addition polymer structure type **I**, poly (vinyl lactone) or P$_\beta$HMBL, via pathway **A**. Second, the zwitterionic intermediate could also undergo proton transfer, with another zwitterion or monomer molecule, to generate an alkoxide species that proceeds through oxa-Michael addition[29] followed by proton transfer,[12] thus leading to poly(ether lactone) structure type **II**, via pathway B. Third, basic activation leads an alkoxide ion pair, which initiates the polymerization through oxa-Michael/ proton transfer alternating sequences to form poly(ether lactone) structure type **III** via pathway **C**. Fourth, these different pathways could interchange via pathway **D**, for example, after Michael addition, proton transfer could occur, which crossover to oxa-Michael addition, or vice versa, thereby forming possibly poly(vinyl-ether lactone) copolymers containing both **I** and **II** or **III** structure units, rather than a mixture of homopolymers. Fifth, the above possible pathways focused on the exocyclic conjugated double bond and the hydroxyl functions, but the presence of the third function, the five-membered lactone ring, points to a possible ring-opening polymerization (ROP) pathway (**E**), especially with a system involving alkoxide initiating/propagating species. However, the ROP of five-membered lactones, including the MBL core, is not possible (for repeated ROP enchainment) under normal conditions, due to thermodynamic reasons,[30] but alkoxide species **IV** resulted possibly from a ring-opening event could proceed with oxa-Michael addition for further chain growth, only if this ring-opening pathway is competitive with other pathways described above.

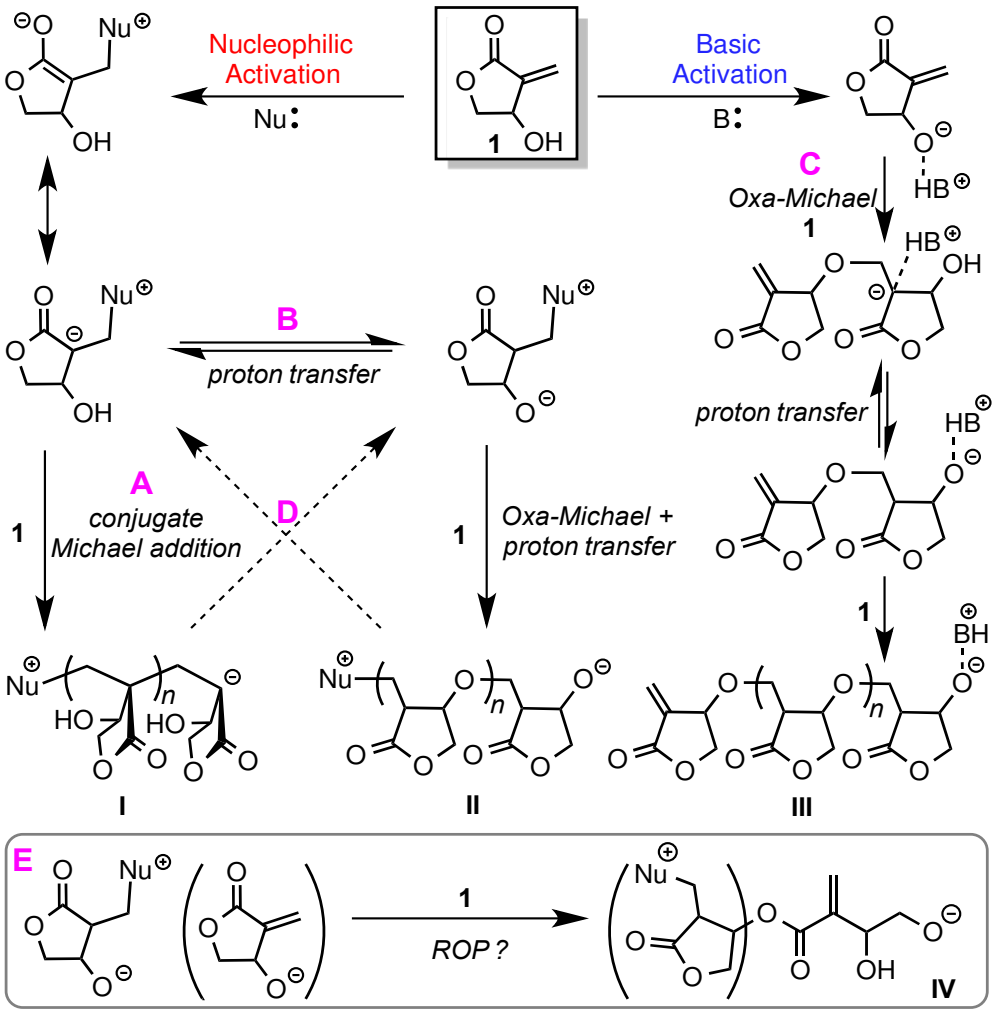

Figure 2.2 Hypothesized possible scenarios involved in the polymerization of βHMBL by nucleophilic/basic organic NHC catalysts.

As outlined above, the polymerization of the tri-functional βHMBL by the nucleophilic/basic organic NHC catalysts can be very complicated. Accordingly, we chose four organic initiators/catalysts including two NHCs, I^{t}Bu (strongest nucleophile) and TPT (weaker nucleophile), one superbase, ^{t}Bu-P$_4$ (strongest base, weak nucleophile), and one radical initiator, AIBN, as a control, for examining their polymerization behavior (Table 2.1). For solubility reasons, DMF was chosen as the solvent. At ambient temperature (~25°C) in a low monomer [M] to initiator [I] ratio of 20, I^{t}Bu promoted βHMBL

polymerization to completion in 24 h, producing a polymer product with M_n = 1.32 × 104 g/mol and $Đ$ = 1.40 (run 1). Increasing the [M]/[I] ratio to 100, the polymerization became sluggish, achieving only 27.9% monomer conversion after 72 h (run 2). The M_n value (9.28 ×103) of the resulting polymer was also lower, due to the low monomer conversion and chain transfer (vide infra). Raising the polymerization temperature to 80 and 100 °C enabled quantitative monomer conversion in 24 h for [M]/[I] = 50, 100, 200 ratio runs or 48 h for the [M]/[I] = 500 run, but the M_n value of the resulting polymers remained in a narrow range from M_n = 7.33 × 103 g/mol to 8.42 × 103 g/mol (runs 3–6), indicating further chain-growth is limited with more monomer presumably due to chain transfer via the OH group. As compared to I^{t}Bu, the polymerization by the less nucleophilic TPT was less effective, achieving lower monomer conversions and producing polymers with lower M_n values for runs with [M]/[I] = 20 (25 °C, run 7) and 50 (80 °C, run 8), but the polymerization with [M]/[I] = 100 (100 °C) was nearly the same (run 9 vs. 4). The results of the polymerization by the superbase ^{t}Bu-P$_4$ (runs 10–14) were rather similar to those by I^{t}Bu, hinting a common polymerization mechanism for both initiators. Control runs by AIBN showed that this free radical polymerization produced P$_\beta$HMBL with lower M_n and $Đ$ values (run 15), especially when carried out in $CHCl_3$ (M_n = 3.0 × 103 g/mol, run 16), due to the poor solubility of the polymer in this solvent and chain transfer by this solvent, and the M_n value was not obviously affected by varying the [M]/[I] ratio from 50 to 1200. Overall, these results showed that $_\beta$HMBL can be effectively polymerized into unimodal polymers with M_n up to 1.32 × 104 g/mol, but the polymerization by the current initiating systems lack control over polymer M_n and $Đ$ values.

Table 2.1 Selected results of βHMBL (M) polymerization by NHC and ^{t}Bu-P$_4$ initiators[a]

Run no.	Initiator (I)	[M]/[I]	temp. (°C)	time (h)	conv. (%)[b]	M_n[c] (kg/mol)	$Đ$[c] (M_w / M_n)
1	I^{t}Bu	20	25	24	100	13.2	1.40
2	I^{t}Bu	100	25	72	27.9	9.28	1.15
3	I^{t}Bu	50	80	24	100	7.43	1.50
4	I^{t}Bu	100	100	24	100	8.27	1.32
5	I^{t}Bu	200	100	24	100	7.33	1.24
6	I^{t}Bu	500	100	48	>99	8.42	1.30
7	TPT	20	25	24	84.3	5.28	1.23
8	TPT	50	80	24	88.8	5.16	1.40
9	TPT	100	100	24	>99	8.77	1.24
10	^{t}Bu-P$_4$	20	25	24	88.4	8.60	1.23
11	^{t}Bu-P$_4$	50	80	24	100	6.37	1.50
12	^{t}Bu-P$_4$	100	100	24	100	10.2	1.35
13	^{t}Bu-P$_4$	200	100	24	86.4	11.0	1.29
14	^{t}Bu-P$_4$	500	100	72	>99	8.26	1.30
15	AIBN	500	80	24	62.8	7.45	1.16
16[d]	AIBN	500	80	24	96.0	3.00	1.10

[a] Monomer concentration [M] = 2.2 mol/L in DMF. [b] Monomer conversion measured by ^{1}H NMR. [c] Number-average molecular weight (M_n) and molecular weight distribution ($Đ = M_w / M_n$) determined by gel-permeation chromatography (GPC) relative to poly (methyl methacrylate) standards. [d] Carried out in $CHCl_3$.

Thermal properties of the resulting polymer materials were analyzed by thermal gravimetric analysis (TGA) and differential scanning calorimetry (DSC). The TGA curves (Figure. 2.3) showed that all the

polymer materials, irrespective of the initiator used, exhibited a similar 3-step decomposition profile as well as similar initial and end onset decomposition temperatures of about 200 °C and 475 °C, respectively. However, the amount of the stable residue left at >600 °C varied significantly, from 15% by AIBN, to 22% by TPT, 29% by I^{t}Bu, and 31% by ^{t}Bu-P$_4$. DSC curves (Figure. 2.4) showed a similar glass-transition temperature (T_g) of –15 °C by I^{t}Bu, –17 °C by TPT, and –18 °C by ^{t}Bu-P$_4$, but no apparent T_g was observed before decomposition for the P$_\beta$HMBL produced by AIBN.

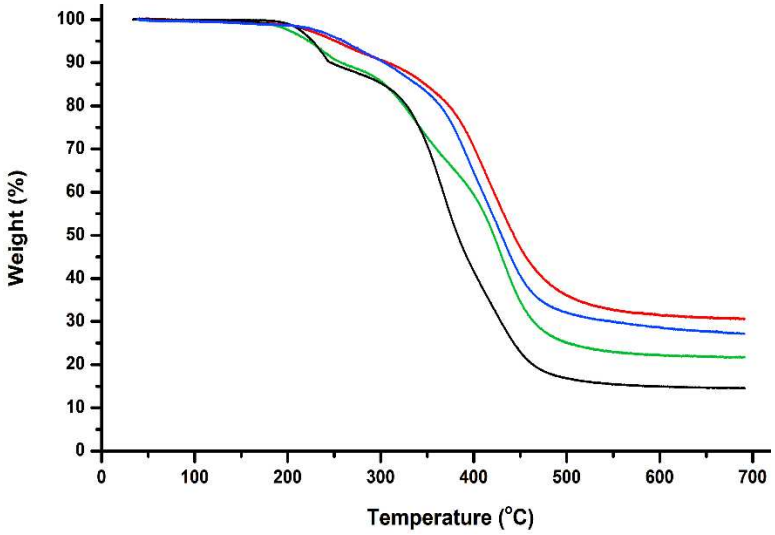

Figure. 2.3 TGA curves of the polymers produced by ^{t}Bu-P$_4$ (red, run 12), I^{t}Bu (blue, run 6), TPT (green, run 9), and AIBN (black, run 15).

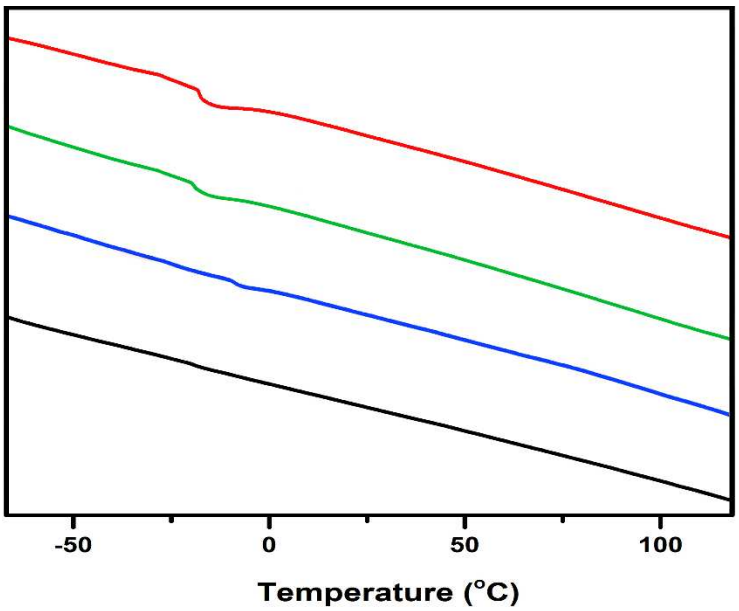

Figure. 2.4 DSC traces of the polymers produced by ^{t}Bu-P$_4$ (red), TPT (green), I^{t}Bu (blue), and AIBN (black).

Intriguingly, ^{1}H NMR spectra (Figure. 2.5) of the polymers produced by I^{t}Bu, ^{t}Bu-P$_4$ and TPT are essentially superimposable, so are their ^{13}C NMR spectra (Figures. S2.5–S2.7), indicating that they all produced the same polymer structure. On the other hand, the P$_\beta$HMBL produced by AIBN is that of a typical vinyl addition (atactic) polymer (Figure. 2.5), and its absence of the apparent T_g before its decomposition is consistent with this structure as the analogous polymer of $_\beta$MMBL exhibited a high T_g of ~290 °C. However, the polymer produced by I^{t}Bu, ^{t}Bu-P$_4$ and TPT is different than that by AIBN. The most visible spectroscopic difference is the appearance of the broad signal centered at δ 7.5 ppm in ^{1}H NMR, which correlates to signals at δ 156–152 ppm in ^{13}C NMR established by ^{1}H-^{13}C gHMQC and TOCSY (Figures. S2.14 and S2.15), assignable to trisubstituted olefinic groups (vide infra). The presence of the OH groups in the polymer was confirmed by the H–D exchange experiment that showed the disappearance of the signal at δ 5.5 ppm upon addition of D$_2$O (Figures.

S2.9 and S2.10) and by FT-IR that revealed a broad absorption band centered at ~ 3400 cm-1 (Figure. S 2.11).

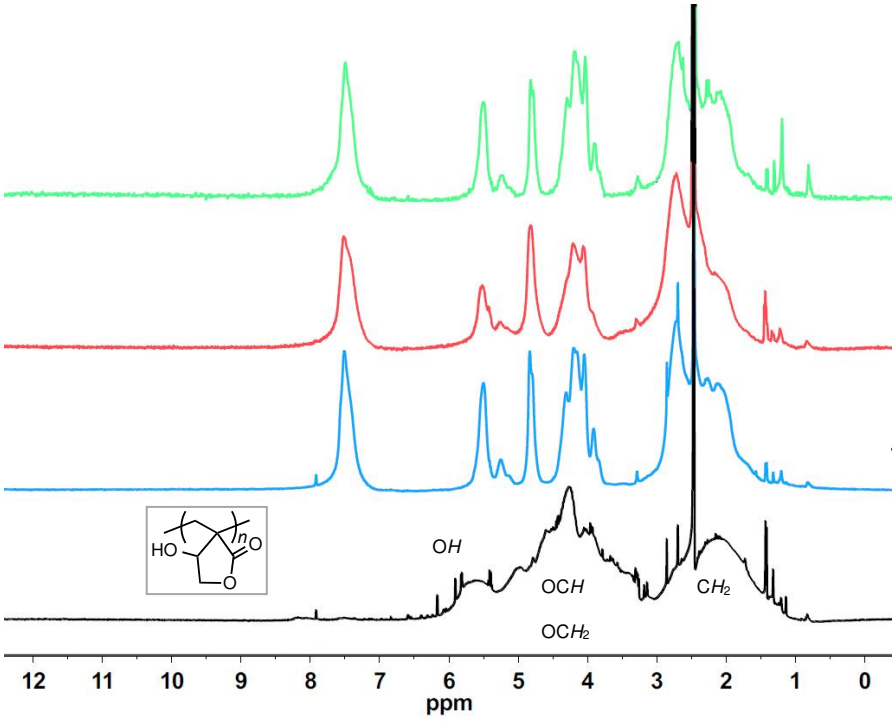

Figure. 2.5 Overlay of ^{1}H NMR (DMSO-d_6, 400 MHz, 25 °C) spectra of the polymers produced by TPT (green, run 9), ^{t}Bu-P_4 (red, run 12), I^{t}Bu (blue, run 6), and AIBN (black, run 15).

Focusing on the polymer produced by I^{t}Bu, we carried out a series of 1D and 2D NMR (500 MHz) studies in DMSO-d_6 at 80 °C. The ^{13}C NMR spectrum (Figure. S2.5) showed a complex pattern of resonances, but the 135-DEPT experiment (Figure. S2.8) enabled initial assignments of carbon resonances as follows: δ 178–172 ppm for *C*=O, 156–152 for >C=*C*H–, 128–126 for >*C*=CH–, 86.8 (m) for atactic main-chain quaternary *C*'s, 79.3 for –O*C*H, 75.0 and 73.3 for –O*C*H$_2$, 72.1 for –O*C*H, 71.0 for –O*C*H2, 68.8 for –O*C*H, 44.4 for *C*H, and 32.1 (m) for CH2. Next, 1H-13C gHMQC and TOCSY spectra (Figures. S2.14 and S2.15) showed correlation between the peak at δ 7.5 ppm in ^{1}H NMR and the peaks at δ 156–152 ppm in ^{13}C NMR, confirming the assignment of the peak at 7.5 ppm

for >C=C*H*–. These correlation spectra also enabled assignments of the resonances from δ 2.7–2.0 ppm in ^{1}H NMR for those of C*H* (lower field) and CH_2 (higher field) protons, as well as the peak at δ 4.8 ppm for –OCH_2 protons and δ 4.4–3.9 ppm for those of –OC*H* and additional –OCH_2 protons. In addition, from the ^{1}H-^{1}H gCOSY spectrum (Figure. S2.12), the proton in >C=C*H*– at δ 7.5 ppm correlates to the protons in –OCH_2 at δ 4.8 ppm, thus revealing a connectivity of >C=CH–CH_2O–. Furthermore, the ^{1}H-^{1}H zTOCSY spectra (Figure. S2.13) revealed that both protons in >C=CH–CH_2O– correlate to CH_2 protons centered at about δ 2.6 ppm, and the OH proton correlates to both types of the methylene protons in –OCH_2 and CH_2, revealing the intact hydroxyl lactone motif in the vinyl addition polymer units. Putting all pieces together, the possible structures present in the resulting polymer contain not only poly- (vinyl lactone) (type **I**) and poly(ether lactone) (type **II** or **III**) but also a structure containing the trisubstituted olefinic moiety >C=CH–CH_2O–, the origin of which is probably due to dehydration (*vide infra*).

The question of whether these structures represent a mixture of different polymers or possibly a copolymer containing all such units was interrogated by solvent fractionation experiments. We reasoned that polyether homopolymers would be soluble in solvents such as chloroform;[31] accordingly, the crude polymer was subjected to Soxhlet extraction in refluxing chloroform for 30 h. There was no soluble fraction extracted, suggesting that the polymer product was not a mixture of different polymers, which is consistent with the unimodal molecular weight distribution on their GPC traces. Another key question concerns the >C=CH–CH_2O– unit derived from the above spectroscopic analysis and how it is generated in the current polymerization system. Figure 2.2 outlines our proposed pathway to such a structure. First, structure **I**, instead of continuing conjugate Michael addition, undergoes proton transfer to form intermediate **II´**, which crossovers to oxa-Michael

addition to yield poly(vinyl-ether lactone) copolymer structure **III´**. Catalyzed dehydration of **III´** leads to structure **V** containing the α,β-unsaturated-γ-butyrolactone unit. The OH group on the vinyl polymer units can participate in proton transfer and subsequently generate a branching structure by following the same pathway as above. The highly branching structure offers a suitable explanation for the high intensity observed for the *α,β*-unsaturated-*γ*-butyrolactone moiety. In addition, the appearance of several types of >C=CH– signals at δ 156–152 ppm in ^{13}C NMR may indicate that dehydration could occur within the vinyl polymer repeat unit to generate more such structure. The observed low T_g of –15 °C for the polymer produced by I^{t}Bu is also consistent with a copolymer containing the soft (branched) polyether units.

MALDI-TOF mass spectrum (Figure. 2.6) of a low molecular weight polymer sample produced by I^{t}Bu showed a series of peaks associated with different sets of isomerides, with the peaks in the same shade-highlighted set representing the same total degrees of copolymerization but with different degrees of dehydration (loss of the mass unit of 18). Therefore, for the polymer produced by I^{t}Bu the masses m/z can be expressed as: $m/z = M_{end} + (114.1 - 18.0) \times m + 114.1 \times n$, where m and n are the degrees of polymerization for βHMBL with dehydration and the degrees of polymerization for βHMBL without dehydration, respectively, while M_{end} is the MW of chain ends. Take the last set as an example, the peaks in this set can be attributed to the 11th-mer poly(vinyl-ether lactone) copolymer, where the peaks at 1417.216, 1399.187, 1381.157, and 1363.135 represent the copolymers containing 11 units of βHMBL with 2 water loss, 11 units of βHMBL with 3 water loss, 11 units of βHMBL with 4 water loss, and 11 units of βHMBL with 5 water loss, respectively. According to this analysis, the MW of the chain end is calculated to be 179.66 g/mol (Figure. 2.7), corresponding to I^{t}Bu$^+$.

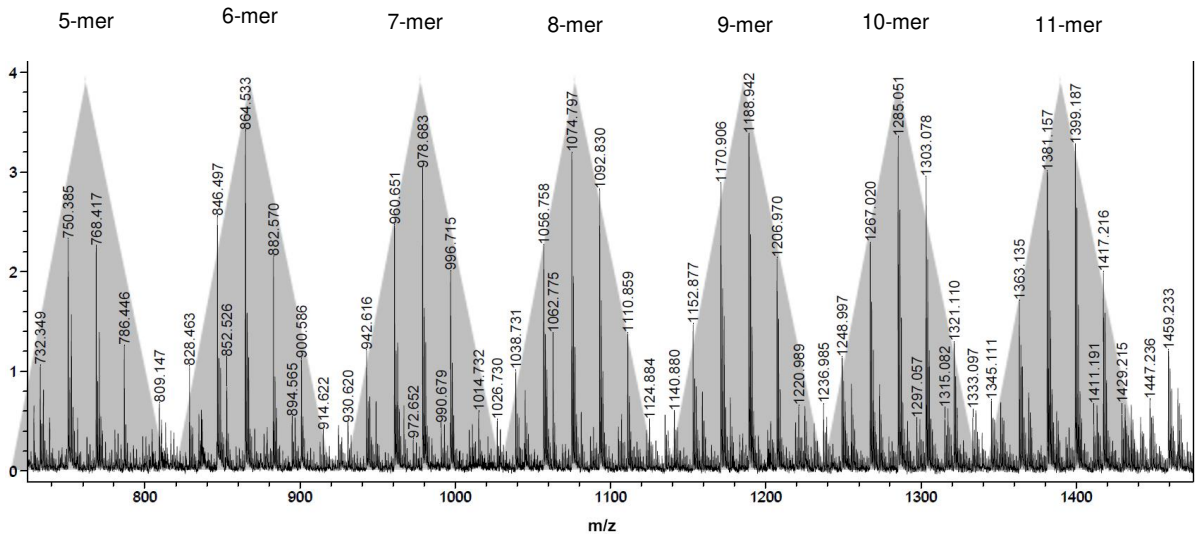

Figure 2.6 MALDI-TOF MS spectrum of the low molecular weight oligomers produced by I^{t}Bu.

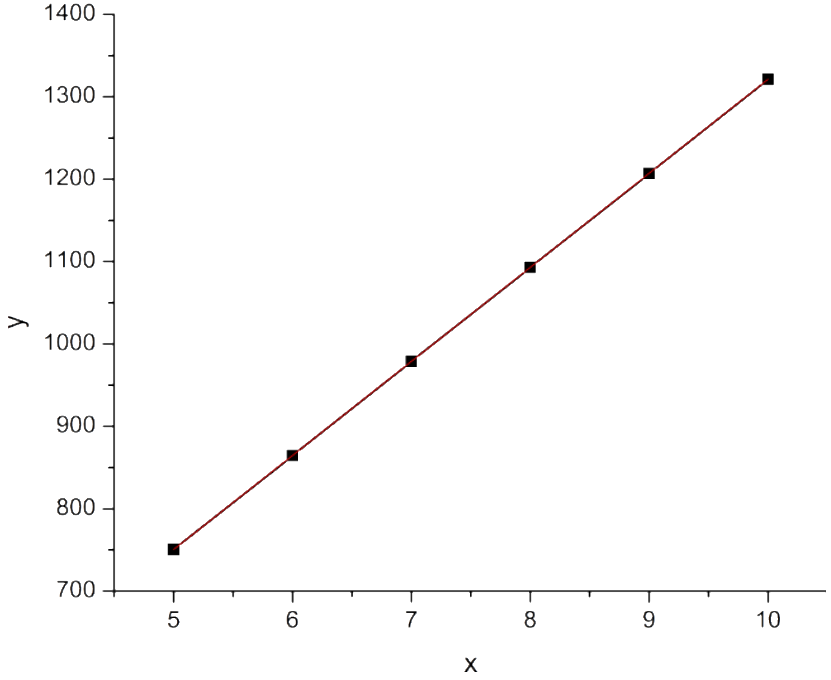

Figure. 2.7 Plot of the m/z value of the molecular ions (y) vs. βHMBL repeat unit (x).

2.4 Conclusions

In summary, we have revealed for the first time the successful polymerization of the naturally occurring, tri-functional monomer Tulipalin B or $_{\beta}$HMBL using nucleophilic/basic organic catalysts and a radical initiator, producing polymer products with molecular weight up to M_n = 1.32 × 104 g/mol. The polymer produced by AIBN is that of a typical vinyl addition (atactic) polymer, but the polymers produced by NHCs I^{t}Bu and TPT as well as superbase ^{t}Bu-P$_4$ have rather complex structures, although the structures by I^{t}Bu, TPT, ^{t}Bu-P$_4$ are essentially the same. Extensive spectroscopic and analytical analyses of the resulting polymer products led to a possible conclusion that the polymer is likely a branched copolymer of poly(vinyl-ether lactone)s, derived from the proposed mechanistic crossovers between conjugate Michael and oxa-Michael additions, enabled by proton transfer due to the presence of OH groups in the monomer and within the polymer chain, followed by dehydration and branching.

References

(1) Selected recent reviews: (a) C. Thomas and B. Bibal, *Green Chem.*, **2014**, *16*, 1687–1699; (b) H. A. Brown and R. M. Waymouth, *Acc. Chem. Res.*, **2013**, *46*, 2585–2596; (c) K. Fuchise, Y. Chen, T. Satoh and T. Kakuchi, *Polym. Chem.*, **2013**, *4*, 4278–4291; (d) H. A. Brown and R. M. Waymouth, *Acc. Chem. Res.*, **2013**, *46*, 2585–2596; (e) M. K. Kiesewetter, E. J. Shin, J. L. Hedrick and R. M. Waymouth, *Macromolecules*, **2010**, *43*, 2093–2107; (f) N. E. Kamber, W. Jeong, R. M. Waymouth, R. C. Pratt, B. G. G. Lohmeijer and J. L. Hedrick, *Chem. Rev.*, **2007**, *107*, 5813–5840.

(2) Selected recent reviews: (a) C. M. R. Volla, I. Atodiresei and M. Rueping, *Chem. Rev.*, **2014**, *114*, 2390–2431; (b) D. Liu and E. Y.-X. Chen, *Green Chem.*, **2014**, *16*, 964–981; (c) R. C. Wende and P. Schreiner, *Green Chem.*, **2012**, *14*, 1821–1849; (d) C. Grondal, M. Jeanty and D. Enders, *Nat. Chem.*, **2010**, *2*, 167–178; (e) T. Marcelli and H. Hiemstra, *Synthesis*, **2010**, 1229–1279; (f) D. W. C. MacMillan, *Nature*, **2008**, *455*, 304–308.

(3) Selected recent reviews: (a) D. M. Flanigan, F. RomanovMichailidis, N. A. White and T. Rovis, *Chem. Rev.*, **2015**, *115*, 9307–9387; (b) M. N. Hopkinson, C. Richter, M. Schedler and F. Glorius, *Nature*, **2014**, *510*, 485–496; (c) D. J. Nelson and S. P. Nolan, *Chem. Soc. Rev.*, **2013**, *42*, 6723–6753; (d) S. J. Ryan, L. Candish and D. W. Lupton, *Chem. Soc. Rev.*, **2013**, *42*, 4906–4917; (e) A. Grossmann and D. Enders, *Angew. Chem., Int. Ed.*, **2012**, *51*, 314–325; (f) X. Bugaut and F. Glorius, *Chem. Soc. Rev.*, **2012**, *41*, 3511–3522; (g) T. Dröge and F. Glorius, *Angew. Chem., Int. Ed.*, **2010**, *50*, 6940–6952; (h) S. Díez-González, N. Marion and S. P. Nolan, *Chem. Rev.*, **2009**, *109*, 3612–3676; (i) F. E. Hahn and M. C. Jahnke, *Angew. Chem., Int. Ed.*, **2008**, *47*, 3122–3172; (j) D. Enders, O. Niemeier and A. Henseler, *Chem. Rev.*, **2007**, *107*, 5606–5655; (k) N. Marion, S.

Díez-González and S. P. Nolan, *Angew. Chem., Int. Ed.*, **2007**, *46*, 2988–3000; (l) D. Bourissou, O. Guerret, F. P. Gabbaï and G. Bertrand, *Chem. Rev.*, **2000**, *100*, 39 –91.

(4) Selected recent reviews: (a) S. Naumann and A. P. Dove, *Polym. Chem.*, **2015**, *6*, 3185–3200; (b) M. Fèvre, J. Pinaud, Y. Gnanou, J. Vignolle and D. Taton, *Chem. Soc. Rev.*, **2013**, *42*, 2142–2172.

(5) E. F. Connor, G. W. Nyce, M. Myers, A. Möck and J. L. Hedrick, *J. Am. Chem. Soc.*, **2002**, *124*, 914–915.

(6) (a) K. Fuchise, Y. Chen, T. Satoh and T. Kakuchi, *Polym. Chem.*, **2013**, *4*, 4278–4291; (b) J. Raynaud, A. Ciolino, A. Baceiredo, M. Destarac, F. Bonnette, T. Kato, Y. Gnanou and D. Taton, *Angew. Chem., Int. Ed.*, **2008**, *47*, 5390–5393; (c) M. D. Scholten, J. L. Hedrick and R. M. Waymouth, *Macromolecules*, **2008**, *41*, 7399–7404.

(7) O. Coutelier, M. El Ezzi, M. Destarac, F. Bonnette, T. Kato, A. Baceiredo, G. Sivasankarapillai, Y. Gnanou and D. Taton, *Polym. Chem.*, **2012**, *3*, 605–608.

(8) G. W. Nyce, J. A. Lamboy, E. F. Connor, R. M. Waymouth and J. L. Hedrick, *Org. Lett.*, **2002**, *4*, 3587–3590.

(9) M. Hong and E. Y.-X. Chen, *Angew. Chem., Int. Ed.*, **2014**, *53*, 11900–11906.

(10) (a) T. Kato, Y. Ota, S.-I. Matsuoka, K. Takagi and M. Suzuki, *J. Org. Chem.*, **2013**, *78*, 8739–8747; (b) S.-I. Matsuoka, Y. Ota, A. Washio, A. Katada, K. Ichioka, K. Takagi and M. Suzuki, *Org. Lett.*, **2011**, *13*, 3722–3725; (c) A. T. Biju, M. Padmanaban, N. E. Wurz and F. Glorius, *Angew. Chem., Int. Ed.*, **2011**, *50*, 8412–8415.

(11) (a) Y. Zhang, M. Schmitt, L. Falivene, L. Caporaso, L. Cavallo and E. Y.-X. Chen, *J. Am. Chem. Soc.*, **2013**, *135*, 17925–17942; (b) Y. Zhang and E. Y.-X. Chen, *Angew. Chem., Int. Ed.*, **2012**, *51*, 2465–2469.

(12) S.-I. Matsuoka, S. Namera and M. Suzuki, *Polym. Chem.*, **2015**, *6*, 294–301.

(13) W. N. Ottou, D. Bourichon, J. Vignolle, A.-L. Wirotius, F. Robert, Y. Landais, J.-M. Sotiropoulos, K. Miqueu and D. Taton, *Chem. Eur. J.*, **2015**, *21*, 9447–9453.

(14) (a) I. Leito, T. Rodima, I. A. Koppel, R. Schwesinger and V. M. Vlasov, *J. Org. Chem.*, **1997**, *62*, 8479–8483; (b) R. Schwesinger, C. Hasenfratz, H. Schlemper, L. Walz,E. M. Peters, K. Peters and H. G. von Schnering, *Angew. Chem., Int. Ed. Engl.*, **1993**, *32*, 1361–1363; (c) R. Schwesinger and H. Schlemper, *Angew. Chem., Int. Ed. Engl.*, **1987**, *26*, 1167–1169; (d) R. Schwesinger, *Chimia*, **1985**, *39*, 269–272.

(15) (a) J. Zhao, N. Hadjichristidis and Y. Gnanou, *Polimery*, **2014**, *59*, 49 –59; (b) B. Esswein and M. Möller, *Angew. Chem., Int. Ed. Engl.*, **1996**, *35*, 623–625; (c) B. Eßwein, N. M. Steidl and M. Möller, *Macromol. Rapid Commun.*, **1996**, *17*, 143–148; (d) A. Molenberg and M. Möller, *Macromol. Rapid Commun.*, **1995**, *16*, 449–453; (e) T. Pietzonka and D. Seebach, *Angew. Chem., Int. Ed. Engl.*, **1993**, *32*, 716– 717.

(16) M. Schmitt, L. Falivene, L. Caporaso, L. Cavallo and E. Y.X. Chen, *Polym. Chem.*, **2014**, *5*, 3261–3270.

(17) (a) Y. Chen, K. Fuchise, A. Narumi, S. Kawaguchi, T. Satoh and T. Kakuchi, *Macromolecules*, **2011**, *44*, 9091–9098; (b) J.-C. Hsu, Y. Chen, T. Kakuchi and W.-C. Chen, *Macromolecules*, **2011**, *44*, 5168–5177; (c) T. Kakuchi, Y. Chen, J. Kitakado, K. Mori, K. Fuchise and T. Satoh, *Macromolecules*, **2011**, *44*, 4641–4647.

(18) Selected recent reviews: (a) M. J.-L. Tschan, E. Brulé, P. Haquette and C. M. Thomas, *Polym. Chem.*, **2012**, *3*, 836– 851; (b) G. W. Coates and M. A. Hillmyer, A virtual issue on "Polymers from Renewable Resources", *Macromolecules*, **2009**, *42*, 7987–7989; (c) A. Gandini, *Macromolecules*, **2008**, *41*, 9491–9504; (d) C. K. Wiliams and M. A. Hillmyer, *Polym. Rev.*, **2008**, *48*,1 –10; (e) M. A. R. Meier, J. O. Metzger and U. S. Schubert, *Chem. Soc. Rev.*, **2007**, *36*, 1788–1802.

(19) (a) R. R. A. Kitson, A. Millemaggi and R. J. K. Taylor, *Angew. Chem., Int. Ed.*, **2009**, *48*, 9426–9451; (b) H. M. R. Ho ffman and J. Rabe, *Angew. Chem., Int. Ed. Engl.*, **1985**, *24*, 94 –110.

(20) (a) L. E. Manzer, *ACS Symp. Ser.*, **2006**, *921*, 40 –51; (b) L. E. Manzer, *Appl. Catal*., A, **2004**, *272*, 249–256.

(21) R. R. Gowda and E. Y.-X. Chen, *Org. Chem. Front.*, **2014**, *1*, 230–234.

(22) Recent reviews: (a) R. R. Gowda and E. Y.-X. Chen, in Encyclopedia of Polymer Science and Technology, ed. H. F. Mark, Wiley, Hoboken, 4th edn, 2013, vol. 8, pp. 235–271, 2014 (print edition) DOI:10.1002/0471440264.pst606 (online edition); (b) S. Agarwal, Q. Jin and S. Maji, *ACS Symp. Ser.*, **2012**, *1105*, 197–212; (c) R. Mullin, Chem. *Eng. News,* **2004**, *82*(45), 29–37.

(23) Selected recent examples: (a) Y. Higaki, R. Okazaki and A. Takahara, *ACS Macro Lett.*, **2012**, *1*, 1124–1127; (b) R. A. Cockburn, R. Siegmann, K. A. Payne, S. Beuermann, T. F. L. McKenna and R. A. Hutchinson, *Biomacromolecules*, **2011**, *12*, 2319–2326; (c) R. A. Cockburn, T. F. L. McKenna and R. A. Hutchinson, *Macromol. Chem. Phys.*, **2010**, *211*, 501–509; (d) J. Mosnáček, J. A. Yoon, A. Juhari, K. Koynov and K. Matyjaszewski, *Polymer*, **2009**, *50*, 2087–2094; (e) J. Mosnáček and K. Matyjaszewski, *Macromolecules*, **2008**, *41*, 5509–5511; (f) G. Qi, M. Nolan, F. J. Schork and C. W. Jones*, J. Polym. Sci., Polym. Chem.*, **2008**, *46*, 5929–5944; (g) C. U. Pittman

Jr. and H. Lee, *J. Polym. Sci., Polym. Chem.*, **2003**, *41*, 1759–1777; (h) J. W. Stansbury and J. M. Antonucci, *Dent. Mater.*, **1992**, *8*, 270–273; (i) M. Ueda, M. Takahashi, Y. Imai and C. U. Pittman Jr., *J. Polym. Sci., Polym. Chem. Ed. Engl.*, **1982**, *20*, 2819–2828; (j) M. K. Akkapeddi, *Polymer*, **1979**, *20*, 1215–1216.

(24) (a) Y. Hu, L. O. Gustafson, H. Zhu and E. Y.-X. Chen, *J. Polym. Sci., Part A: Polym. Chem.*, **2011**, *49*, 2008–2017; (b) J. Suenaga, D. M. Sutherlin and J. K. Stille, *Macromolecules*, **1984**, *17*, 2913–2916; (c) M. K. Akkapeddi, *Macromolecules*, **1979**, *12*, 546–551.

(25) (a) Y. Zhang, L. O. Gustafson and E. Y.-X. Chen, *J. Am. Chem. Soc.*, **2011**, *133*, 13674–13684; (b) G. M. Miyake, Y. Zhang and E. Y.-X. Chen, *Macromolecules*, **2010**, *43*, 4902–4908; (c) D. Y. Sogah, W. R. Hertler, O. W. Webster and G. M. Cohen, *Macromolecules*, **1987**, *20*, 1473–1488.

(26) (a) T. Xu and E. Y.-X. Chen, *J. Am. Chem. Soc.*, **2014**, *136*, 1774–1777; (b) Y. Zhang, G. M. Miyake, M. G. John, L. Falivene, L. Caporaso, L. Cavallo and E. Y.-X. Chen, *Dalton Trans.*, **2012**, *41*, 9119–9134; (c) Y. Zhang, G. M. Miyake and E. Y.-X. Chen, *Angew. Chem., Int. Ed.*, **2010**, *49*, 10158–10162.

(27) (a) R. R. Gowda and E. Y.-X. Chen, *Dalton Trans.*, **2013**, *42*, 9263–9273; (b) Y. Hu, X. Wang, Y. Chen, L. Caporaso,L. Cavallo and E. Y.-X. Chen, *Organometallics*, **2013**, *32*, 1459–1465; (c) X. Chen, L. Caporaso, L. Cavallo and E. Y.-X. Chen, *J. Am. Chem. Soc.*, **2012**, *134*, 7278–7281; (d) Y. Hu, G. M. Miyake, B. Wang, D. Cui and E. Y.-X. Chen, *Chem. Eur. J.*, **2012**, *18*, 3345–3354; (e) Y. Hu, X. Xu, Y. Zhang, Y. Chen and E. Y.-X. Chen, *Macromolecules*, **2010**, *43*, 9328–9336; (f) G. M. Miyake, S. E. Newton, W. R. Mariott and E. Y.-X. Chen, *Dalton Trans.*, **2010**, *39*, 6710–6718.

(28) T. Nomura, E. Hayashi, S. Kawakami, S. Ogita and Y. Kato, Biosci., *Biotechnol., Biochem.*, **2015**, *79*, 25 –35.

(29) E. M. Phillips, M. Riedrich and K. A. Scheidt, *J. Am. Chem. Soc.*, **2010**, *132*, 13179–13181.

(30) (a) M. Hong and E. Y.-X. Chen, *Macromolecules*, **2014**, *47*, 3614–3624; (b) A. Duda and A. Kowalski, Thermodynamics and kinetics of ring-opening polymerization, in Handbook of Ring-Opening Polymerization, ed. P. Dubois, O. Coulembier and J.-M. Raquez, Wiley-VCH, Weinheim, 2009, CH. 3.

(31) (a) T. Wang, M. Yan, X. Sun and D. Quan, *Polymer*, **2015**, *57*, 21 –28; (b) D. Wang, G. Zhang, Y. Zhang, Y. Gao, Y. Zhao, C. Zhou, Q. Zhang and X. Wang, *J. Appl. Polym. Sci.*, **2007**, *103*, 417–424.

Chapter 3

Increasing Complexity in Organopolymerization of Multifunctional γ-Butyrolactones

3.1 Summary

This contribution investigates organopolymerization of five multifunctional γ-butyrolactone-based monomers, including bifunctional (endocyclic double bond, lactone ring) dihydrofuran-2(3H)-one (FO), 3-methylfuran-2(5H)-one (3-MFO), and 5-methylfuran-2(5H)-one (5-MFO), as well as trifunctional (endocyclic or exocyclic double bond, lactone ring, hydroxyl group) 3-(hydroxymethyl) furan-2(5H)-one (3-HMFO) and β-hydroxy-α-methylene-γ-butyrolactone (βHMBL). The complexity of the reaction under nucleophilic and basic conditions using N-heterocyclic carbene (NHC) and superbase organic catalysts increases dramatically on going from the bifunctional monomers to the trifunctional ones. Thus, the polymerization of the parent FO leads to a vinyl-addition polymer, while the reaction of the base catalysts with the two methyl-substituted derivatives, 3-MFO and 5-MFO, affords predominately a trimer and dimer, respectively. The polymerization of trifunctional 3-HMFO gives a poly (vinyl–ether lactone) copolymer structure, via two different types of base activation mechanisms and a combination of Michael and ox-Michael additions and proton transfer processes. The polymerization of βHMBL has the highest degree of the complexity in this monomer series, due to its presence of both the reactive exocyclic double bond and hydroxyl group, producing a branched vinyl–ether lactone copolymer structure having six different types of substructural units. The results reveal multiple types of reaction pathways and their mechanistic crossovers involved in the βHMBL polymerization, including conjugate Michael and oxa-Michael additions and proton transfer processes, as well as ene-type dehydration reactions, enabled by proton transfer.

3.2 Introduction

The growing concern over depleting fossil fuel reserves has stimulated increasing attention to renewable polymers with research directed at examining the possibility of replacing petroleum-based feedstocks by naturally occurring or biomass-derived renewable feedstocks for the production of polymeric materials, as such research could significantly contribute to the sustainable development.[1-3] In this context, the polymerization of naturally occurring, biorenewable Tulipalin B, or *β*-hydroxy-*α*-methylene-*γ*-butyrolactone ($_{\beta}$HMBL, Figure. 3.1), was recently investigated. [4] $_{\beta}$HMBL is a biologically active (antimicrobial), naturally occurring [present as the (S)-enantiomer in tulips],[5,6] trifunctional monomer containing an exocyclic conjugated double bond, a five-membered lactone, and a hydroxyl group. However, owing to its trifunctionality and presence of both the reactive exocyclic double bond and hydroxyl group, this polymerization is expected to proceed via multiple pathways and produce a polymer with complicated structural units; thus, the mechanism of this polymerization and the structure of the resulting P$_{\beta}$HMBL have not been well understood. On the other hand, various types of polymerization processes have been employed to polymerize the less complex derivatives of $_{\beta}$HMBL, such as *α*-methylene-*γ*-butyrolactone (MBL), *γ*-methyl-*α*-methylene-*γ*-butyrolactone ($_{\gamma}$MMBL) and *β*-methyl-*α*-methylene-*γ*-butyrolactone ($_{\beta}$MMBL), including radical,[7-12] anionic,[13-15] group-transfer,[16-18] Lewis pair zwitterionic,[19-2] and metal-mediated coordination [22-26] polymerization methods. N-heterocyclic carbene (NHC)-mediated organo- polymerization of such monomers has also been investigated.[27,28] Very recently, ring-opening polymerization of the typically considered "inert" five-membered lactone ring present in the parent γ-butyrolactone and MBL also has been achieved.[29-31]

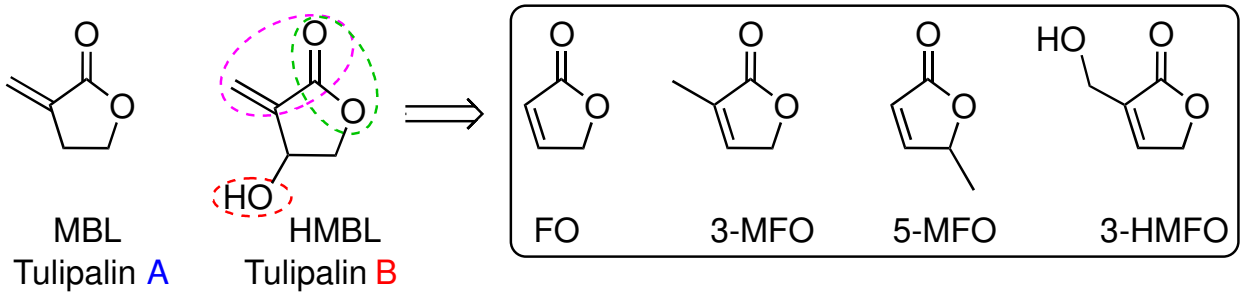

Figure 3.1. Structures of MBL, βHMBL and structurally related furanones employed in this study.

The above described three Tulipalin A-based monomers, MBL, γMMBL and βMMBL, proceed homopolymerizations exclusively through vinyl additions under typical conditions, due to the high reactivity of the exocyclic conjugated double bond, but such typically observed chemoselectivity can be reversed to favor the ring-opening the lactone in MBL under low temperatures using the metalcatalyzed coordination-insertion mechanism.[31] In contrast, the homopolymerization of unsaturated five-membered lactones or furanones with the much less reactive, endocyclic conjugated double bond, such as dihydrofuran-2(3H)-one (FO), 3-methylfuran-2(5H)- one (3-MFO), 5-methylfuran-2(5H)-one (5-MFO), and 3-(hydroxymethyl) furan-2(5H)-one (3-HMFO, Figure. 3.1), is rarely reported. In fact, we were able to find reports only on the copolymerization of 5-MFO with styrene by organoaluminum chlorides,[32] cationic copolymerization of 5-MFO and 1,3-dioxolane,[33-35] and the copolymerization of FO, vinylene carbonate, and methyl bicyclo (2,2,1)-2-heptene-5-carboxylate.[36] Hence, the investigation into the polymerization of these furanone monomers will not only yield fundamental results on the monomer system that has not been previously examined for homopolymerizations, it will also provide important mechanistic insights into the structurally related, yet more complicated polymerization of βHMBL. The utilization of organic catalysts such as NHCs and phosphazene superbases have drawn increasing attention for their unique reactivity in many types

of organopolymerizations.[37–41] With the inherently high Brønsted basicity and nucleophilicity, NHCs have become an important class of organocatalysts in the field of polymerization catalysis.[42,43]

A phosphazene superbase, 1-tertbutyl-4,4,4-tris(dimethylamino)-2,2-bis[tris (dimethyl amino) phosphoranylid-enamino]-2λ^5,4λ^5 -catenadi(phosphazene) (^{t}Bu-P$_4$), exhibiting strong basicity but low nucleophilicity, is also a potent organic initiator or catalyst to promote various types of polymerization reactions.[44–47] Considering the unusual effectiveness of NHCs and superbases for promoting rapid conjugate-addition polymerization of the biorenewable MBL having a reactive exocyclic, conjugated double bond[27,48] and ring-opening polymerization of the biorenewable γ-butyrolactone with the "inert" five-membered lactone ring[30], we hypothesized that such catalysts may possess the potential to effect polymerization of monomers such as bifunctional FO, 3-MFO and 5-MFO, as well as trifunctional 3-HMFO bearing the relatively less reactive endocyclic double bond. In particular, the presence of the reactive hydroxyl group could impart a base-activation initiation mechanism as well proton transfer and oxa-Michael addition propagation pathways, in addition to the typical nucleophilic activation initiation and Michael addition propagation pathways[4,49,50]. Accordingly, the central objective of this study was to examine the polymerization characteristics of such furnanone monomers by organic catalysts or initiators I^{t}Bu and ^{t}Bu-P$_4$; the polymerization of trifunctional βMMBL having the reactive exocyclic double bond was also included in this study to compare the relative complexity of the polymerization behavior.

3.3 Results and discussion

3.3.1. Polymerization of FO

Considering the bifunctionality of FO (and its methyl substituted derivatives), two possible pathways for its potential polymerization can be envisioned and outlined in Figure 3.2. First, nucleophilic attack at the conjugated endocyclic double bond leads to a zwitterionic intermediate that could undergo repeated conjugate Michael additions to form a rigid polymer structure via the vinyladdition polymerization (VAP) pathway. Second, nucleophilic attack at the carbonyl carbon could result in a relative soft polyester main-chain structure via the ring-opening polymerization (ROP) pathway. Guided by these hypotheses, the polymerization of FO was examined with two commonly employed organic catalysts, the strongly nucleophilic (and basic) NHC catalyst I^{t}Bu and superbase ^{t}BuP$_4$, with and without initiator BnOH, the results of which study were summarized in Table 3.1.

Indeed, I^{t}Bu was found to effectively promote the VAP at room temperature or 110 °C, both achieving quantitative monomer conversion in a low [M]/[Cat] ratio of 20/1 in 13 h and affording the corresponding VAP polymer, PFO, with relatively low molecular weights of M_n ~ 2 kg/mol and low Đ values of ~1.05 (runs 1 and 2, Table 4.1). Increasing the [M]/[Cat] ratio to 100/1, the conversion decreased to ~60% at both room temperature and 110 °C (runs 4 and 5), but resulted in a little change in the molecular weight of the resulting polymer. It can be seen that reaction temperature had a negligible effect on polymerization characteristics (run 2 vs. 1, run 3 vs. 4), and increasing the monomer concentration from 1 mol/L to 2.2 mol/L enhanced the conversion from 59.5% to 74.6%,

Table 3.1. Selected results of FO polymerization by I^{t}Bu and ^{t}Bu-P$_4$

Run No.	Cat.	I	Solv.	Conc. (mol/L)	Temp (^{o}C)	[M]/[Cat]/[I][a]	Time (h)	Conv. (%) [b]	M_n [c] (kg/mol)	$Đ$ [c] (M_w/ M_n)
1	I^{t}Bu	-	DMF	1	25	20/1	13	100	1.92	1.06
2	I^{t}Bu	-	DMF	1	110	20/1	13	100	2.03	1.05
3	I^{t}Bu	-	DMF	1	25	100/1	13	59.8	1.57	1.03
4	I^{t}Bu	-	DMF	1	110	100/1	13	59.5	2.05	1.03
5	I^{t}Bu	-	DMF	2.2	110	100/1	13	74.6	2.06	1.03
6	I^{t}Bu	BnOH	DMF	1	25	100/1/1	13	58.6	1.58	1.04
7	^{t}BuP$_4$	-	THF	4	-40	20/1	24	100	1.88	1.06
8	^{t}BuP$_4$	BnOH	THF	4	-40	20/1/1	24	100	1.89	1.06

[a] [M]/[Cat]/[I] = [monomer]/[catalyst]/[initiator]. [b] Monomer conversion measured by ^{1}H NMR. [c] M_n and Đ values determined by GPC relative to PMMA standards.

but the molecular weight of the polymer remained the same (run 4 vs. 5). Addition of BnOH as the initiator did not noticeably change the polymerization characteristics (run 6 vs. 3). Switching to ^{t}BuP$_4$, the polymerization at −40 °C produced also a VAP product with M_n ~ 1.9 kg/mol, with or without BnOH (runs 7 and 8). As expected, when compared to MBL, an analogous fivemembered lactone but with a highly reactive exocyclic double bond, the reactivity of FO, a five-membered lactone bearing an endocyclic double bond, was dramatically reduced under similar reaction conditions, due to the increased steric hindrance at the internal double bond. As a result, chain transfer to monomer and/or polymer chains significantly competes with chain propagation (Figure 3.3), causing formation of

relatively low molecular weight polymer products and the observed insensitivity of the polymer molecular weight to the [M]/[Cat] ratio.

^{1}H NMR spectrum (Figure. 3.4) of the PFO via the VAP pathway features two broad resonances centered at 7.6 and 6.5 ppm, consistent with the VAP polymer chain end group shown in Figure 3.5. The end group, basically the 5-substituted FO monomer structure, was further confirmed by MALDI-TOF mass spectrum (Figure. 3.5). Specifically, the MALDI-TOF mass spectrum showed only one set of major

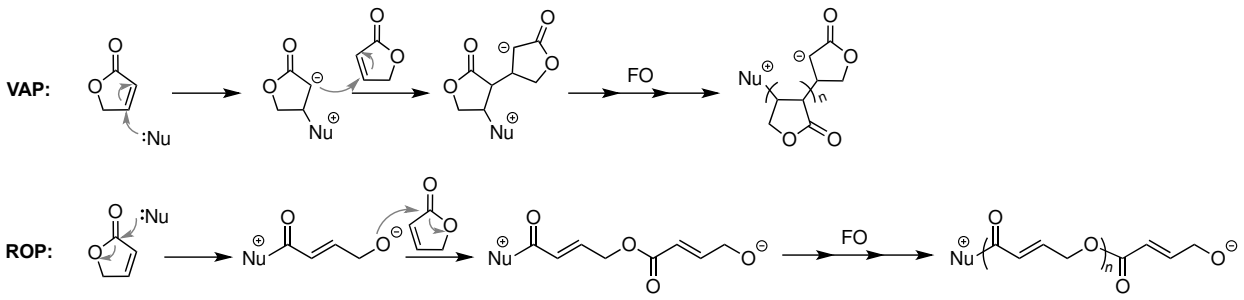

Figure 3.2. Hypothesized two possible scenarios involved in the potential polymerization of FO.

molecular ion peaks, and the plot of m/z values of the peaks vs the number of FO repeat units yielded a perfectly straight line, giving a slope of 84 and an intercept of 23 (Figure. 3.6). Thus, the slope corresponds to the molar mass of the FO monomer, whereas the intercept is the sum of the mass (23) of Na^+ (from the added NaI) and that of end groups, which is 0 in this case (i.e., no end groups, or an equivalent of an additional FO unit). Overall, the above results clearly indicated that the polymerization undergoes the VAP pathway, not the ROP pathway (Figure 3.2) and that I^{t}Bu serves as a base, not a nucleophile, in the activation and initiation steps of polymerization (Figure 3.3).

Thermal properties of the resulting polymer materials were analyzed by thermal gravimetric analysis (TGA) and differential scanning calorimetry (DSC). The TGA curve (Figure. 3.7) showed that the resulting PFO exhibits a one-step decomposition profile and an initial onset decomposition temperatures of about 289 °C. The amount of the stable carbonaceous material residue was 16.6% at > 600 °C. Also consistent with the rigid vinyl polymer structure, the DSC curve (Figure. 3.8) showed a relatively high glass-transition temperature (T_g) of 146 °C.

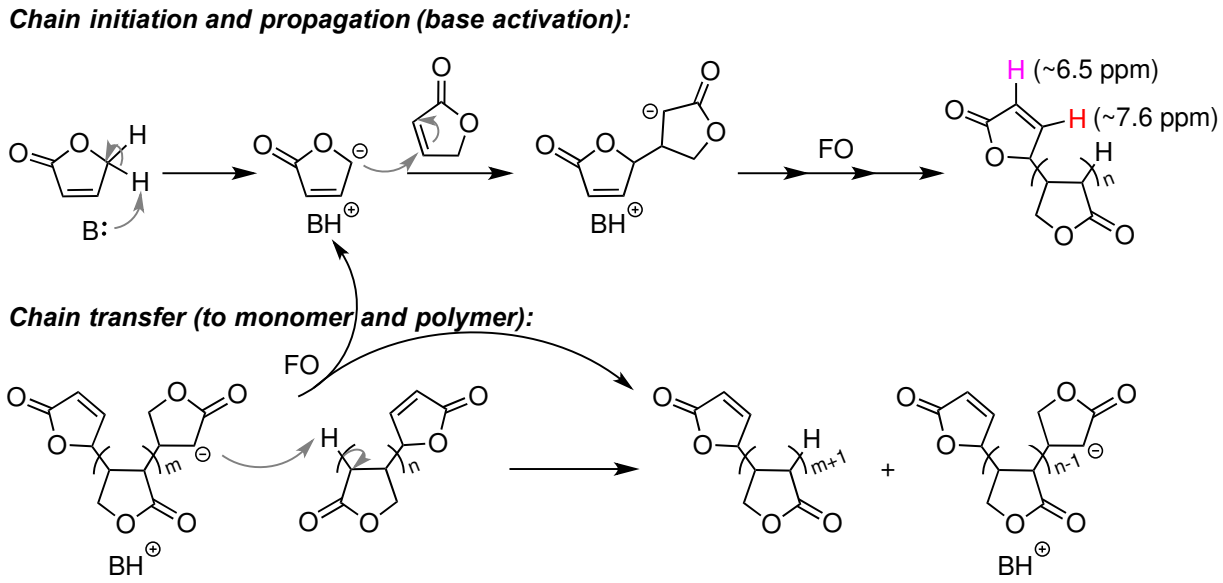

Figure 3.3. Proposed chain initiation and propagation vs. chain transfer involved in the polymerization of FO

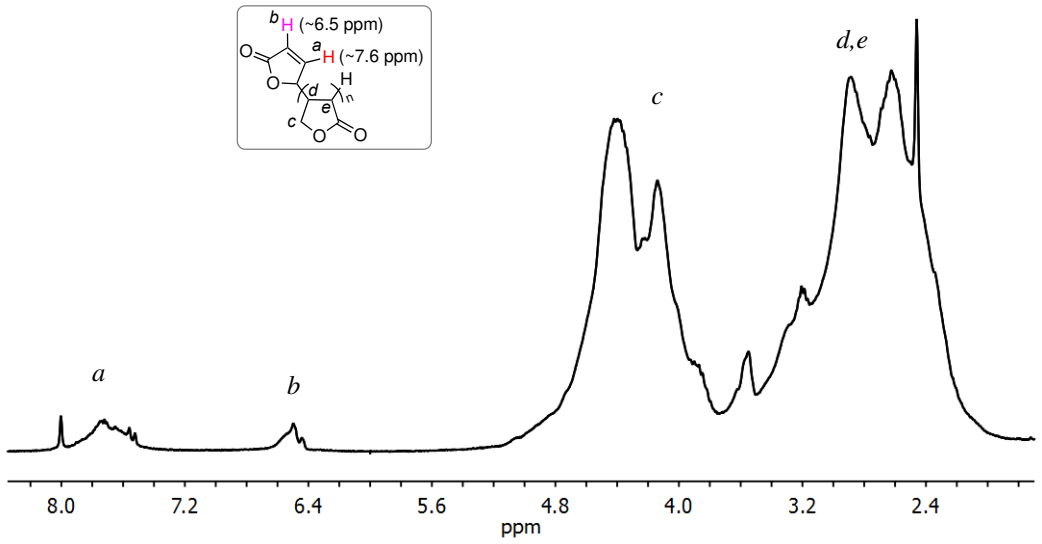

Figure 3.4. ^{1}H NMR (DMSO-d_6, 400 MHz, 25 ºC) spectrum of PFO produced by I^{t}Bu via the VAP pathway.

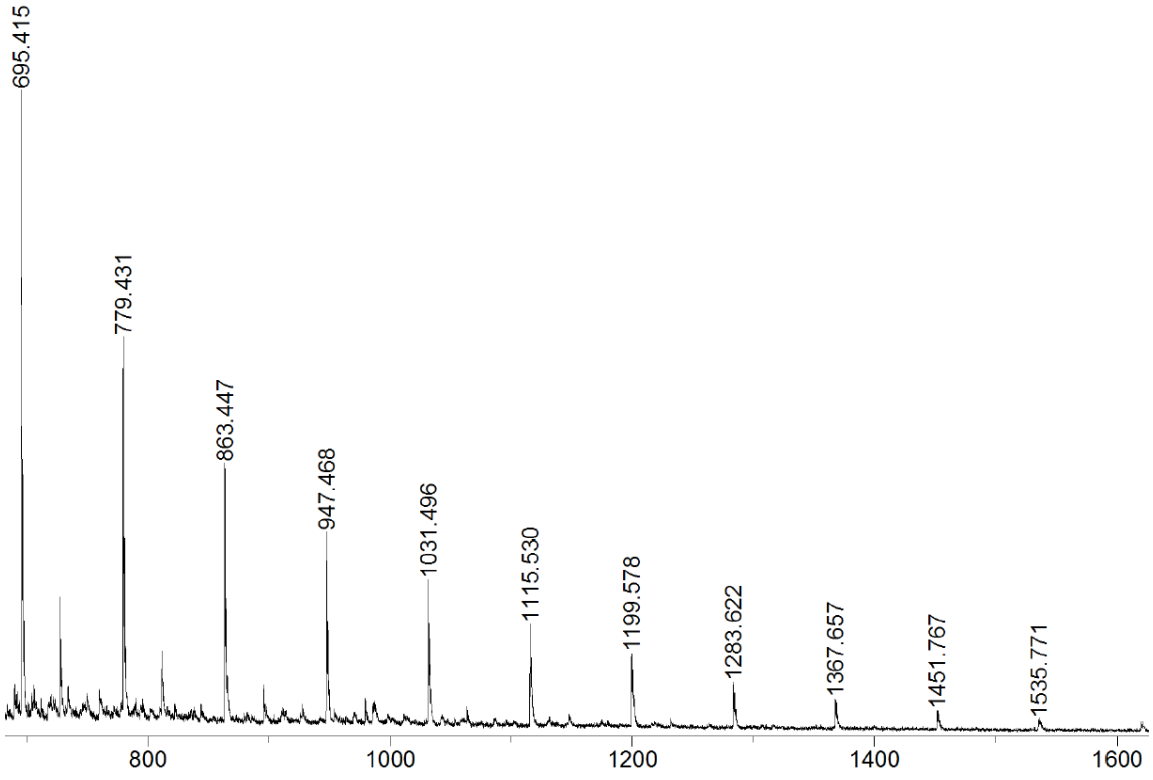

Figure 3.5. A section of the MALDI-TOF MS spectrum of the low molecular weight PFO

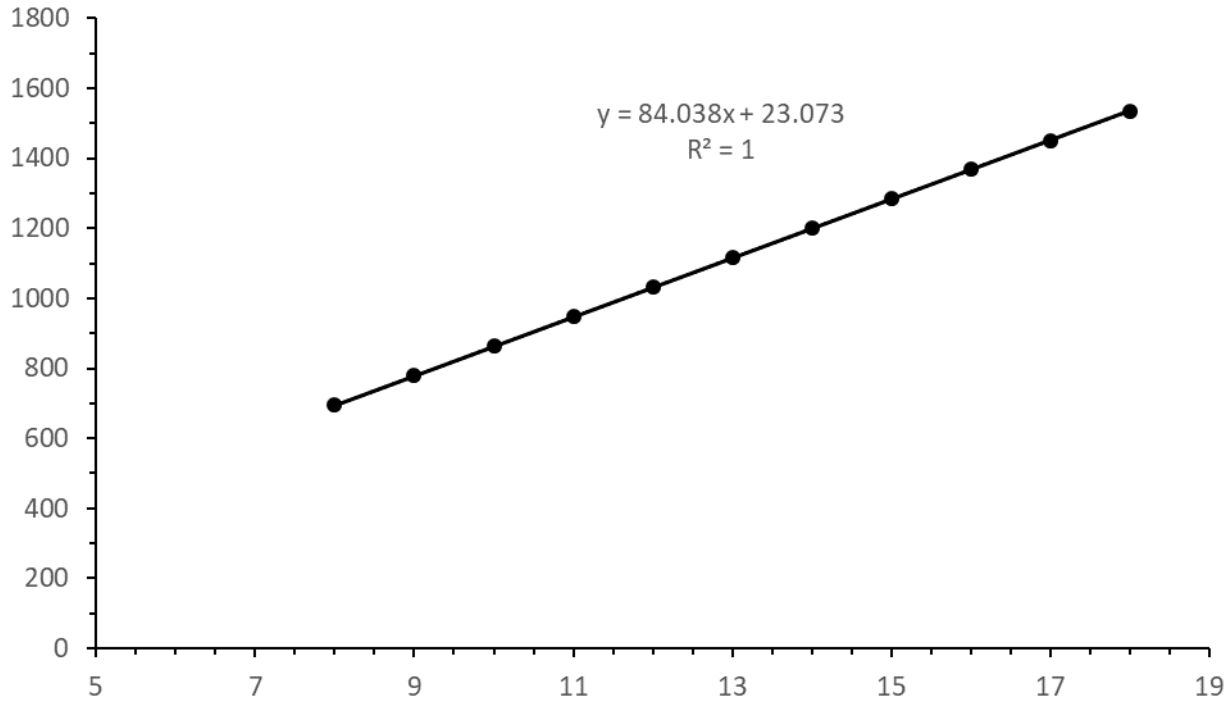

Figure 3.6. Plot of the m/z value of the molecular ions (y) vs. FO repeat unit (x).

Thermal properties of the resulting polymer materials were analyzed by thermal gravimetric analysis (TGA) and differential scanning calorimetry (DSC). The TGA curve (Figure. 3.7) showed that the resulting PFO exhibits a one-step decomposition profile and an initial onset decomposition temperatures of about 289 °C. The amount of the stable carbonaceous material residue was 16.6% at >600 °C. Also consistent with the rigid vinyl polymer structure, the DSC curve (Figure. 3.8) showed a relatively high glass-transition temperature (T_g) of 146 °C.

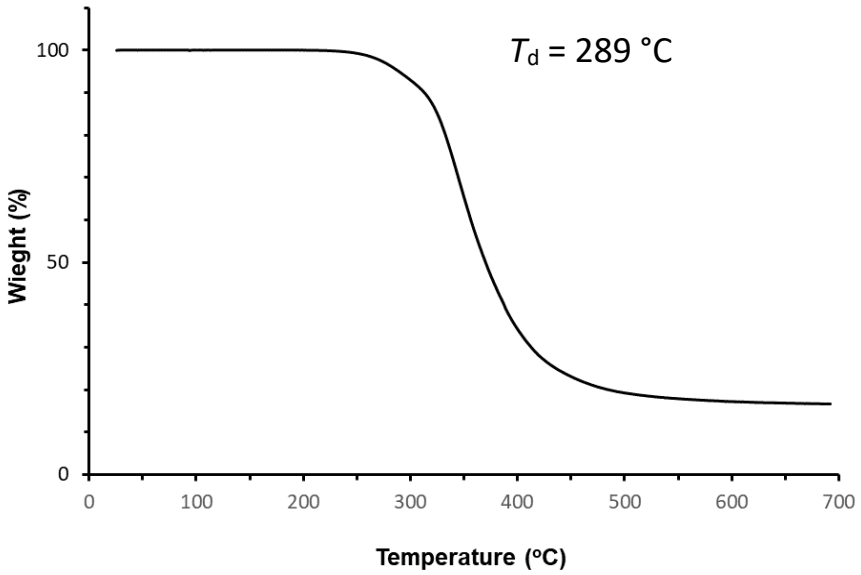

Figure 3.7. TGA curve of the PFO produced by I^{t}Bu (run 6)

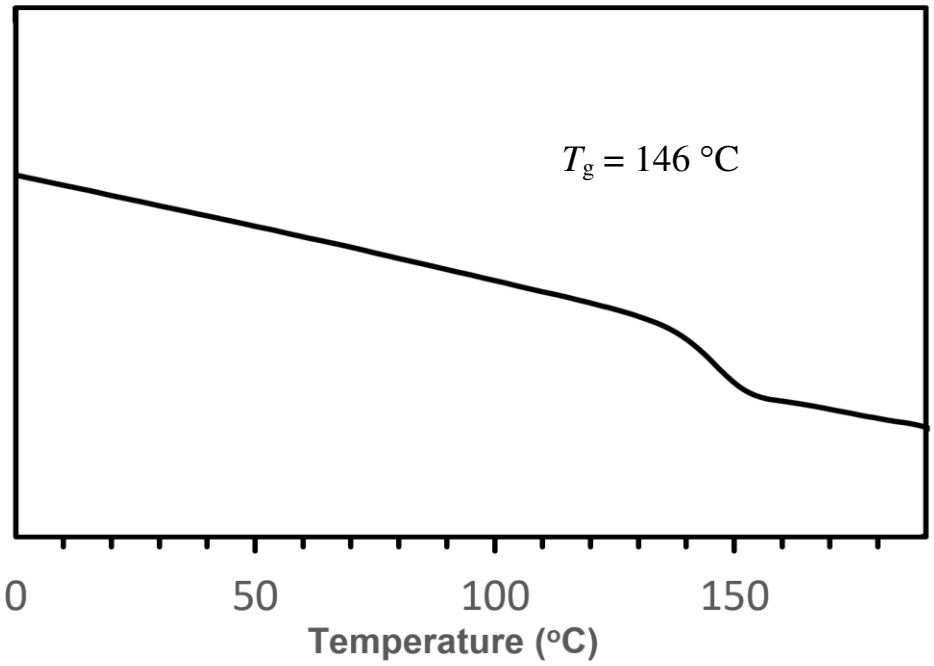

Figure 3.8. DSC trace of the PFO produced by I^{t}Bu (run 6)

3.3.2. Trimerization of 3-MFO and dimerization of 5-MFO

Moving onto 3-MFO, a sterically more hindered monomer relative to FO, its attempted polymerization reactions with NHC and superbase catalysts, such as I^{t}Bu, ^{t}Bu-P$_4$, and other common metal bases such as La[N(SiMe$_3$)$_2$]$_3$, KOH, and K$_2$CO$_3$, in the absence or the presence of the BnOH initiator, all led to a unique trimerization product (with yield up to 78%), plus minor vinyl-addition oligomerization products (Table 3.2). When the reactions were quenched with MeOH (5% HCl), white precipitates formed were found not to be the anticipated VAP product, but a new small molecule compound, 4,4′-(4-methyl-5-oxo-2,5-dihydrofuran-2,2-diyl)bis(3- methyl-dihydrofuran-2(3H)-one) or T(3-MFO), according to its ^{1}H and ^{13}C NMR spectra (Figs.3.7 and 3.8) as well as 2D NMR spectra (Figs. S3.1 and S3.2). Focusing on the isolated small molecule product produced by I^{t}Bu, the ^{13}C NMR spectrum (Fig.3.8) showed a total of 15 carbon resonances, indicative of a trimer structure, which is consistent with its ^{1}H NMR assignments (Fig.3.7). The ^{1}H-^{13}C HSQCAD (Fig.S3.1) and 90-DEPT (Fig.S3.2) experiments enabled the complete assignments of the carbon resonances as follows: δ 172–179 ppm for the three C=O groups, 149 ppm and 132 ppm for the endocyclic double bond C's, 87.5 ppm for the quaternary C connecting the two non-double bond lactones, 66.2 ppm and 66.9 ppm for the C-O on the two non-double bond lactones, 46.3 ppm and 46.6 ppm for the CHs on the two non-double bond lactones, 35.5 ppm and 34.2 ppm for the CHs connecting the endocyclic double bond lactone, 15.7 ppm and 16.0 ppm for the CH$_3$ groups on the lactones with no double bond and 10.7 ppm for the CH$_3$ on the lactone with double bond (c.f., Figure. 3.8 for all the C assignments). The HSQCAD spectrum also enabled the complete assignments of proton resonances as follows: δ 7.54 ppm for the endocyclic double bond proton, 4.08–4.53 ppm for CH$_2$ groups, 2.76 ppm and 2.88 ppm for the CH$_2$ connecting methyl groups on the two non-double bond lactones, 2.29 ppm and 2.13 ppm for the CHs connecting to the quaternary C of the endocyclic double bond lactone, 1.98 ppm for

the methyl group of the endocyclic double bond lactone, and 1.05 ppm and 1.07 ppm for the other two methyl groups on the lactones with no double bonds (c.f., Fig.3.7 for all the H assignments). The structure of the new compound was further confirmed by HRMS data: HRMS (APCI, + mode) m/z calculated for $C_{15}H_{22}NO_6$ ($[M + NH_4]^+$): 312.1442, found: 312.1447.

The formation of the unique trimeric structure from the reaction of 2-MFO under basic conditions can be explained with a mechanism proposed in Figure 3.9. In this base-promoted trimerization mechanism, abstraction of a proton at the 5-poistion of 3-MFO by the base generates a carbanion nucleophile (**A**), which undergoes nucleophilic attack at another 3-MFO molecule via conjugate Michael addition to form carbanion intermediate **B**. Owing to its higher basicity but lower nucleophilicity (the negative charge is located at the 3-carbon of the furanone ring with the substituent), intermediate **B**, instead of continuing on nucleophilic attack at another 3-MFO molecule, undergoes proton transfer to form new nucleophile **C**. Subsequently, **C** proceeds with Michael addition to another 3-MFO molecule to afford a trimeric anion (**D**). For the same reason stated above, this bulky carbanion, instead of attacking another 3-MFO molecule via Michael addition, it abstracts a proton at the 5-position of 3-MFO to regenerate nucleophile **A** and the final product T(3-MFO), Scheme 4. The conjugate acid and charge-compensating cation, [BH]+, could also participate in the proton transfer steps.

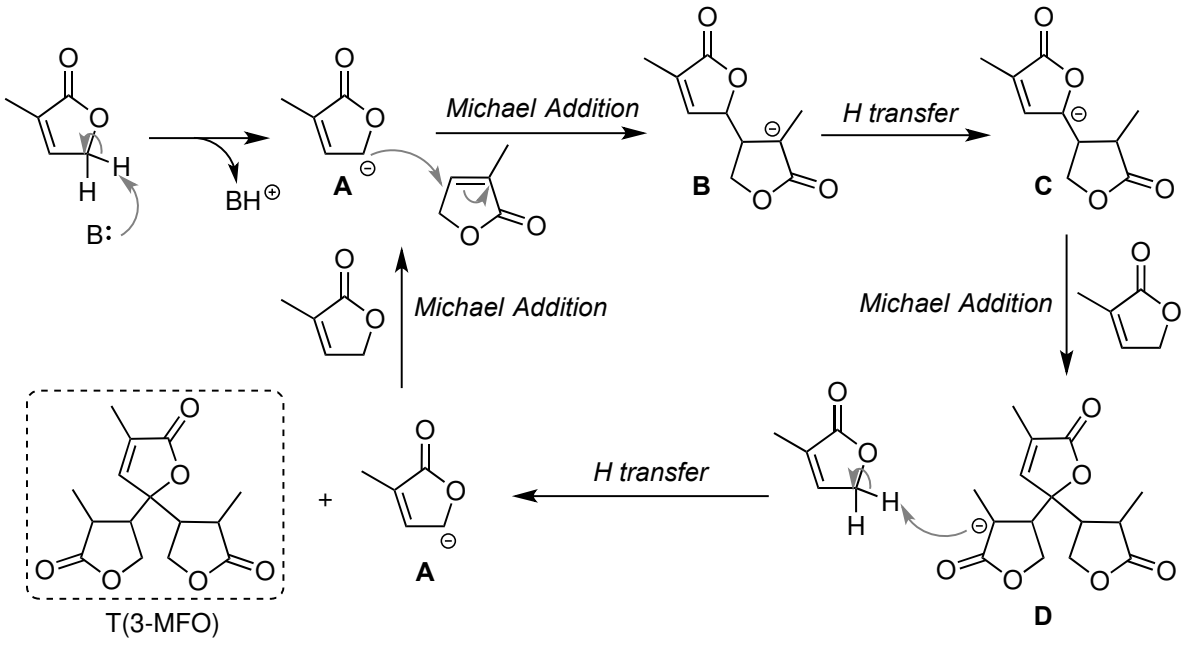

Figure 3.9. Proposed mechanism for the base-promoted trimerization of 3-MFO to form T(3-MFO).

Results from the investigations in the scope of the bases (Table 2) showed the basicity of the catalysts was important for the activity and the relative product ratios of trimerization and vinyl-addition oligomerization. Bases such as DABCO and K_2CO_3 (runs 25, 26, and 28) effected no substrate conversion at −40 °C, while stronger bases such as NHCs, ^{t}Bu-P_4 and KOH readily yielded the trimer product up to 78% yield (runs 17–20 and 27). Further decreasing the temperature to −60 °C led to an apparent drop in substrate conversion (runs 22–24). It appears that lower reaction temperatures favor trimerization over the vinyl-addition oligomerization, and the yield of the trimer was significantly increased with the addition of BnOH (run 11 vs. 10; run 18 vs. 17). The presence of BnOH is proposed to facilitate the proton transfer process involved in the trimerization, via the postulated intermolecular, lower-energy 6-membered ring transition state **E**, relative to the intramolecular, higher-energy 4-membered ring transition state in the absence of BnOH (**B** to **C**, Figure 3.9). Thus,

the highest yield of the trimer was 77.8% (run 20) and achieved by using It Bu/BnOH (1/1) at –40 °C in toluene (run 20). The use of more acidic initiator 4-methoxyphenol (ArOH) in the reaction lowered the trimer yield (run 12 vs. 11).

The observed preference for 3-MFO to form the trimer via the trimerization pathway over the polymer formation via the VAP pathway suggested that the methyl group at the 3-position of the furanone ring suppresses the VAP by further increasing the steric hindrance of the endocyclic double bond. In this context, we also examined the polymerization behavior of 5-MFO under similar conditions. Interestingly, the VAP process was even less preferred, due to facile proton transfer. Since there is only one proton at the 5-position, instead of trimerization, 5-MFO underwent dimerization to form the known dimer product F (Figs. S3.3 and S3.4) [54]. Quantitative conversions to the dimer product were achieved by adding alcohol initiators such as BnOH (runs 29 and 32) and ArOH (run 33).

3.3.3. Polymerizations of 3-HMFO and βHMBL

Another FO derivative, 3-HMFO, was conveniently prepared via isomerization by simply heating βHMBL in water or treating βHMBL with KOH. (Figure 3.1). However, the outcome of this treatment is sensitive to the substrate concentration. Thus, a low concentration condition led to isomerization to 3-HMFO (runs 6 and 7, Table 3.3), while polymerization took place at a higher concentration (runs 8 and 9), affording a polymer product that was shown to be similar to P(3-HMFO) (Fig. S3.5, Table 3.3), which indicated that under such conditions βHMBL was first isomerized to 3-HMFO that was subsequently polymerized to P(3-HMFO). 3-HMFO underwent polymerization at 110 °C without any catalyst, presumably via thermally induced radical processes. In the presence of a base catalyst, the polymerization of 3-HMFO at 110 °C went smoothly, achieving quantitative monomer conversion in

7 h with ^{t}Bu-P$_4$ (run 1, Table 3.3) or with I^{t}Bu (run 2, Table 3.3), but the polymerization was shut down at or below room temperature (runs 3–5, Table 3.3). Since P(3-HMFO) and P(βHMBL) produced in water have the same structure, according to NMR spectra, we will first focus on the discussion on the polymerization mechanism of 3-HMFO.

Figure 3.12 outlines possible mechanistic scenarios for the polymerization of 3-HMFO by basic catalysts. Based on the above study on the polymerizations of FO and MFOs, two basic activation pathways, abstraction of the 5-position proton (pathway 1) and deprotonation of the alcohol (pathway 2), can be envisioned. The resulting respective carbanion and oxyanion can either initiate the polymerization via Michael (oxa-Michael) addition/proton transfer alternating sequences to form a poly(ether lactone) structure, or via repeated Michael additions to form a vinyl polymer, which is less likely, considering the steric hindrance of the propagating carbanion. Thus, in pathway 1, one proton at the 5-postion is abstracted by the base to form the carbanion nucleophile, which undergoes Michael addition to another 3-HMFO molecule. The resulting dimeric carbanion **G** can undergo two different proton transfer processes to generate new carbanion **G-1** (proton transfer type I) or oxyanion **G-2** (proton transfer type II). In pathway 2, protons at the 5-position of the furanone ring are kept intact, while nucleophilic attacks involve oxyanions via oxa-Micheal additions to form poly (ether lactone) linkages. Overall, five different units (u-1–u-5), including main chains, chain ends, and branches, could be present in the polymer structure, with three of them bearing the endocyclic double bonds (u-1 – u-3, Figure 3.12). 1D and 2D NMR spectra, including ^{1}H, ^{1}H-^{1}H g COSY, and ^{1}H-^{13}C HSQCAD spectra (Figs. S3.6-3.8), enabled assignments of ^{1}H NMR resonances. Specifically, resonances centered at δ 7.5 ppm were readily assigned to > C=C*H*- contained in units u-1–u-3, generated from proton transfer processes that keep the double bond intact; resonances at δ 5.3 ppm were assigned to

the 5-position proton of u-2, δ 4.8 ppm to the two 5-position protons of u-1, and δ 2.5–3.0 ppm to the ether linkage > C=CH-C*H*$_2$-O- found in all units. ^{13}C NMR resonances were also assigned: δ 71 ppm to the primary carbon at the 5-position on the furanone ring of u-1, δ 79 ppm for the tertiary carbon at the 5-position on the furanone ring of u-2, δ 167–175 ppm for C=O present in all units, as well as δ 148–154 ppm for H*C*=C-C=O and δ 124–131 ppm for HC=*C*-C=O found in units u-1–u-3.

Table 3.2. Selected results of reactions of 3-MFO or 5-MFO with NHCs, ^{t}Bu-P$_4$, La complex and other common bases[a]

Run No.	M	Cat.	I	Solv.	Conc. (mol/L)	Temp (°C)	[M]/[Cat]/[I]	Time (h)	Conv. (%) & Structure
1	3-MFO	-	-	DMF	3	110	-	21	0
2	3-MFO	I^{t}Bu	-	DMF	3	110	100/1	17	100% (45.5 %T)
3	3-MFO	I^{t}Bu	BnOH	DMF	3	110	100/1/1	17	100% (52.1%T)
4	3-MFO	KOH	BnOH	DMF	3	110	100/1	17	100% (42.7%T)
5	3-MFO	K_2CO_3	BnOH	DMF	3	110	100/1/1	17	100% (13.3%T)
6	3-MFO	I^{t}Bu	-	THF	3	25	20/1	11	100% (0% T)
7	3-MFO	I^{t}Bu	BnOH	THF	3	25	20/1/1	11	100% (0% T)
8	3-MFO	I^{t}Bu	-	DMF	3	25	20/1	13	100% (14.0%T)
9	3-MFO	I^{t}Bu	BnOH	DMF	3	25	20/1	13	100% (16.8%T)
10	3-MFO	KOH		DMF	3	25	3/1	24	100% (12.5%T)
11	3-MFO	KOH	BnOH	DMF	3	25	3/1/1	24	100% (49.7%T)
12	3-MFO	KOH	ArOH	DMF	3	25	3/1/1	24	100% (23.4%T)
13	3-MFO	I^{t}Bu	-	Tol	3	25	20/1	13	96.2% (41.6%T)

14	3-MFO	I^{t}Bu	BnOH	Tol	3	25	20/1/1	13	100% (41.8%T)
15	3-MFO	I^{t}Bu	BnOH	Tol	3	25	20/1/1	20	100% (54.9%T)
16	3-MFO	La	BnOH	THF	3	-40	20/1/3	24	82.2% (38.5%T)
17	3-MFO	^{t}Bu-P$_4$	-	THF	3	-40	20/1	24	100% (37.0%T)
18	3-MFO	^{t}Bu-P$_4$	BnOH	THF	3	-40	20/1/1	24	100% (>52.0%T)
19	3-MFO	IMes	BnOH	THF	3	-40	20/1/1	24	100% (>65.6%T)
20	3-MFO	I^{t}Bu	BnOH	TOL	3	-40	20/1/1	24	100% (>77.7%T)
21	3-MFO	I^{t}Bu	BnOH	THF	3	-40	20/1/1	24	100% (>43.6%T)
22	3-MFO	I^{t}Bu	BnOH	THF	2	-60	20/1/1	24	59.5% (34.4%T)
23	3-MFO	I^{t}Bu	BnOH	THF	3	-60	20/1/1	24	69.3% (33.7%T)
24	3-MFO	I^{t}Bu	BnOH	THF	3	-60	20/1/2	24	86.6% (39.1%T)
25	3-MFO	DABCO	-	TOL	3	-40	20/1	24	0
26	3-MFO	DABCO	BnOH	TOL	3	-40	20/1/1	24	0
27	3-MFO	KOH	BnOH	THF	3	-40	20/1/1	24	100% (>66.8% T)
28	3-MFO	K_2CO_3	BnOH	THF	3	-40	20/1/1	24	0
29	5-MFO	I^{t}Bu	-	THF	3	-40	20/1	24	100% (27.5% D)
30	5-MFO	I^{t}Bu	BnOH	THF	3	-40	20/1/1	24	100% D
31	5-MFO	I^{t}Bu	-	Tol	3	25	20/1	20	100% (57.5 %D)
32	5-MFO	I^{t}Bu	BnOH	Tol	3	25	20/1/1	20	100% D
33	5-MFO	I^{t}Bu	ArOH	Tol	3	25	20/1/1	20	100% D
34	5-MFO	La	BnOH	THF	3	-40	20/1/3	24	100% D

[a] See footnotes in Table 3.1 for further abbreviations and explanations. ArOH = 4-methoxyphenol; La = La[N(SiMe3)2]3; T = trimer; D = dimer.

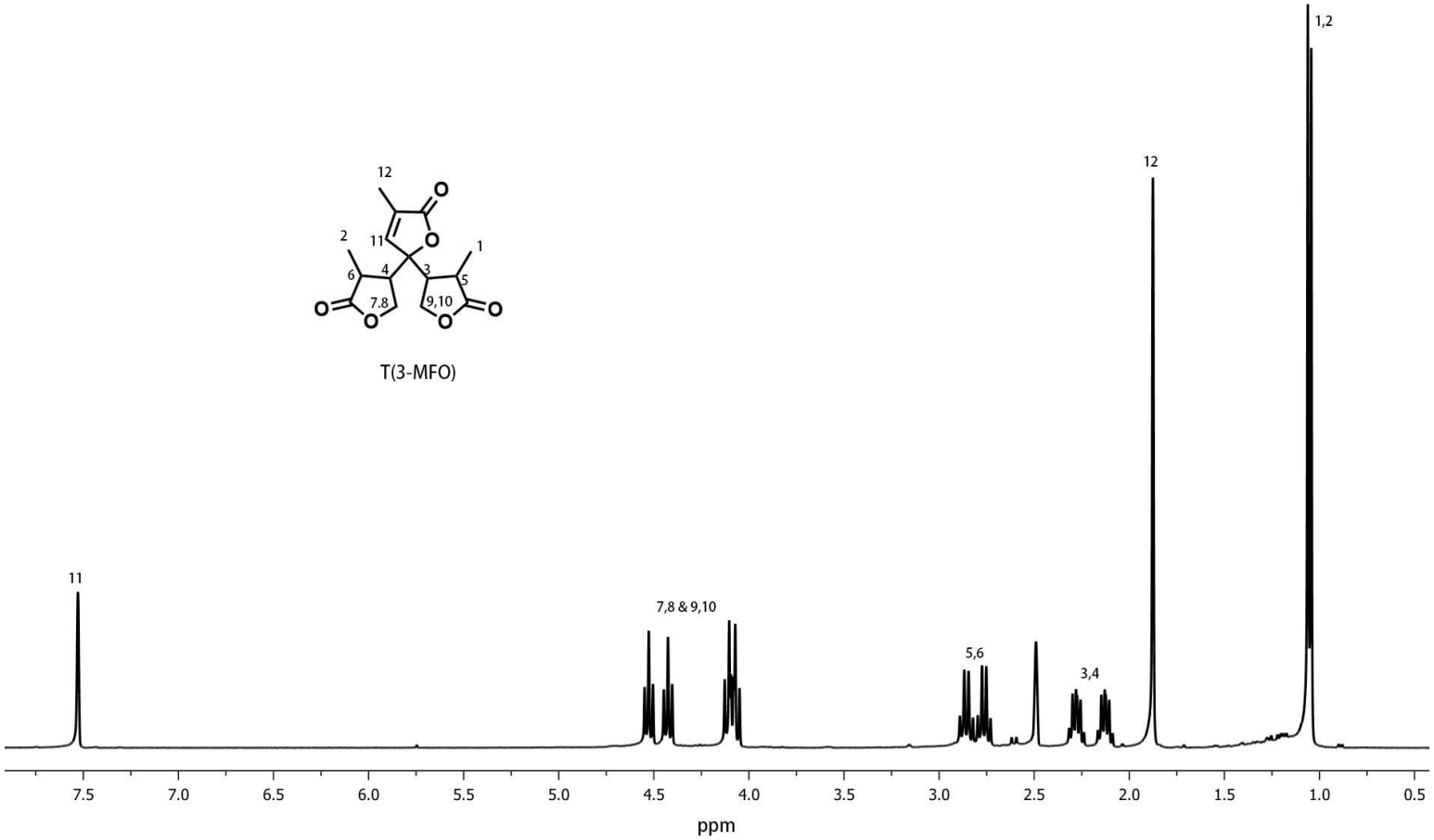

Figure 3.10. ^{1}H NMR (DMSO-d_6, 400 MHz, 25 °C) spectrum of T(3-MFO) produced by I^{t}Bu.

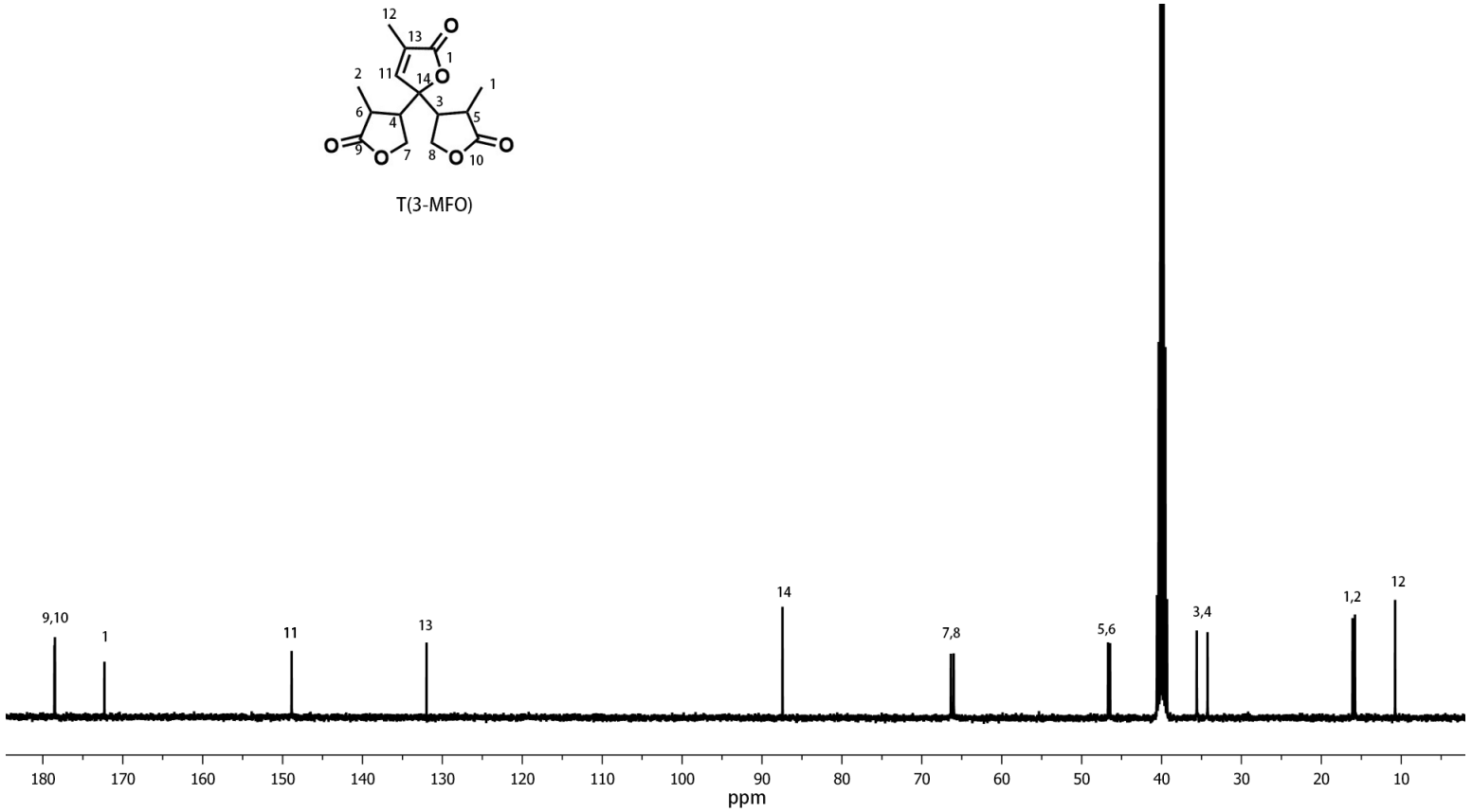

Figure 3.11. ^{13}C NMR (DMSO-d_6, 100 MHz, 25 °C) spectrum of T3-MFO produced by I^{t}Bu.

Although 3-HMFO is not polymerized by base catalysts such as I^{t}Bu at or below room temperature in organic solvents such as DMF and THF (runs 3–5, Table 3.3), βHMBL can be readily polymerized by I^{t}Bu in DMF at room temperature (run 10, Table 3.3). However, the resulting polymer product presented a complex polymer structure consisting of multiple different structural units (Figs. 3.9 and 3.10). The above study on the 3-HMFO polymerization provided some key insights into the understanding of this rather complicated mechanism of the βHMBL polymerization by basic/nucleophilic catalysts in DMF, due to the trifunctionality present in this monomer and multiple possible/competing reaction pathways. The key difference between these two trifunctional monomers is the relatively inert endocyclic double bond in 3-HMFO vs. the highly reactive exocyclic double bond in βHMBL. This difference renders the nucleophilic activation and vinyl addition pathways much more favorable for βHMBL, relative to 3-HMFO, thus further increasing the complexity of the resulting polymer structure in the case of the βHMBL polymerization. In addition, an ene-type mechanism[55] needs to be considered for chain initiation and branching as well (Figure 3.13). Hence, other than the Michael addition, oxa-Michael addition, and proton transfer processes already considered[4], dimerization by the ene-type reaction should generate ether structure **L**, which undergoes either nucleophilic activation or base activation, leading to nucleophiles **M** and **N**, respectively. Subsequent Michael additions afford structures **O** and **P**, consisting of three types of structural units, lactone-type U-I, FO-type U-II, and 3-HMFOtype U-III (Figure 3.13). Worth noting here is that the ene-type reaction loses one H_2O molecule in the resulting structures, which is consistent with the MALDI-TOF spectral analysis[4]. Furthermore, as proposed in the mechanisms for the reactions of FO and its derivatives, the proton transfer process can also take place in the βHMBL polymerization system, thus effectively converting **M** type nucleophile to **N** type nucleophile, both of which can undergo Michael additions to give structures **O** and **P** (vide supra).

Continuing onto chain propagation steps, nucleophile **O** can proceed with Michael additions to form vinyl-addition propagating carbanion **Q**, which can subsequently undergo either proton transfer to give structure **R** having vinyl polymer unit U-IV, or the enetype reaction with another monomer molecule to form structure S with U-II motif, where the branching is introduced via an ether linkage (Figure 3.14) and further branching can be generated via basic activation of unit U-II. Alternatively, nucleophile **O** can also undergo proton transfer first to generate oxyanion **T**, followed by oxa-Michael addition to the monomer to give structure **U** having a lactone-ether U-V motif. Hence, in principle, each vinyl-addition unit could undergo the ene-type reaction to generate unit U-II which could further polymerize via basic activation to form a branched polymer (via Michael addition) or form U-III and U-VI structures (via proton transfer).

Likewise, nucleophile **P** could undergo further propagation steps with multiple pathways, including continued Michael addition to give vinyl polymer structure **V**, type I proton transfer to afford oxyanion **W**, and type II proton transfer to generate carbanion nucleophile **X** (Figure 3.15). Adding to additional complexity, propagating carbanion **V** can undergo type I proton transfer to switch to an oxyanion nucleophile that further propagates into a polyether structure via oxa-Michael additions, while oxyanion **W** can proceed with oxa-Michael addition to produce a polyether structure, which can crossover back to a carbanion nucleophile via type II proton transfer, resulting also in the polymer structure having both vinyl and ether units. Lastly, carbanaion nucleophile **X** can undergo continued Michael additions to produce vinyl polymer Y with unit U-VI that has a quaternary carbon center at the 5-position of the furanone ring. Overall, several pathways described above can be involved in the polymerization of βHMBL by the base catalyst in DMF, and they could also interchange with one

another, thereby resulting in a copolymer structure consisting of possibly six different substructural units, U-I – U-VI.

The above mechanistic analysis, coupled with previously detailed 1D and 2D NMR studies of the resulting P(βHMBL) [4], enabled complete assignments of the resonances of the ^{1}H NMR spectrum shown in Figure. 3.9: δ 7.5 ppm for C*H*=C-C=O in U-II, U-III and U-VI, δ 5.5 ppm for -OH in U-IV, 5.3 ppm for > C=CH-C*H*- in U-III and 4.7 ppm for > C=CH-CH_2 in U-VI. Likewise, the ^{13}C NMR (Figure. 3.10) resonances can be assigned as follows: δ 170–180 ppm for C=O, δ 150–160 ppm for -H*C*=C-C=O-, δ 125–130 ppm for -HC=*C*-C=O-, δ 87 ppm for the quaternary carbon of U-VI, δ 80 ppm for the tertiary carbon of U-III, and δ 71 ppm for the primary carbon of U-II.

The effect of the added initiator BnOH on the polymerization of βHMBL was also examined (run 11, Table 3.3). Consistent with the above analysis for the trimerization of 3-MFO in the presence of BnOH, which significantly enhances proton transfer processes via more favored transition state E, the ^{1}H NMR signals of the resulting P(βHMBL) at 4.7 ppm (for > C=CH-CH_2 in U-VI) nearly disappeared with the addition of BnOH (Figure. 3.11), clearly indicating that the two protons at the 5-position of the furanone ring were largely both substituted, as a result of the accelerated proton transfer processes with the added BnOH.

Table 3.3. Selected results of 3-HMFO and βHMBL polymerization by NHC, ^{t}Bu-P$_4$ and KOH

Run	M	Cat.	I	Solv.	Conc. (mol/L)	Temp (°C)	[M]/[Cat]/[I]	Time (h)	Conv. (%)	Structure	M_n [a] (kg/mol)	$Đ$ [a] (M_w/M_n)
1	3-HMFO	^{t}Bu-P$_4$		DMF	2.2	110	20/1	7	100	Copolymer	1.69	1.10
2	3-HMFO	I^{t}Bu	-	DMF	2.2	110	20/1	7	100	Copolymer	1.54	1.01
3	3-HMFO	I^{t}Bu	-	THF	3	-60	20/1	24	0	-	-	-
4	3-HMFO	I^{t}Bu	BnOH	THF	3	-60	20/1/1	24	0	-	-	-
5	3-HMFO	I^{t}Bu	-	DMF	2.2	25	20/1	23	0	-	-	-
6	βHMBL	-	-	H_2O	0.44	150	-	24	85	3-HMFO	-	-
7	βHMBL	KOH	-	H_2O	0.22	120	100/1	24	85.3	3-HMFO	-	-
8	βHMBL	KOH	-	H_2O	2.2	120	100/1	24	88.7	Copolymer	13.8	2.50
9	βHMBL	KOH	-	H_2O	2.2	150	100/1	24	98	Copolymer	11.4	1.92
10	βHMBL	I^{t}Bu		DMF	2.2	25	20/1/1	24	100	Branched Copolymer	13.2	1.40
11	βHMBL	I^{t}Bu	BnOH	DMF	2.2	25	20/1/1	24	100	Branched Copolymer	6.5	1.21

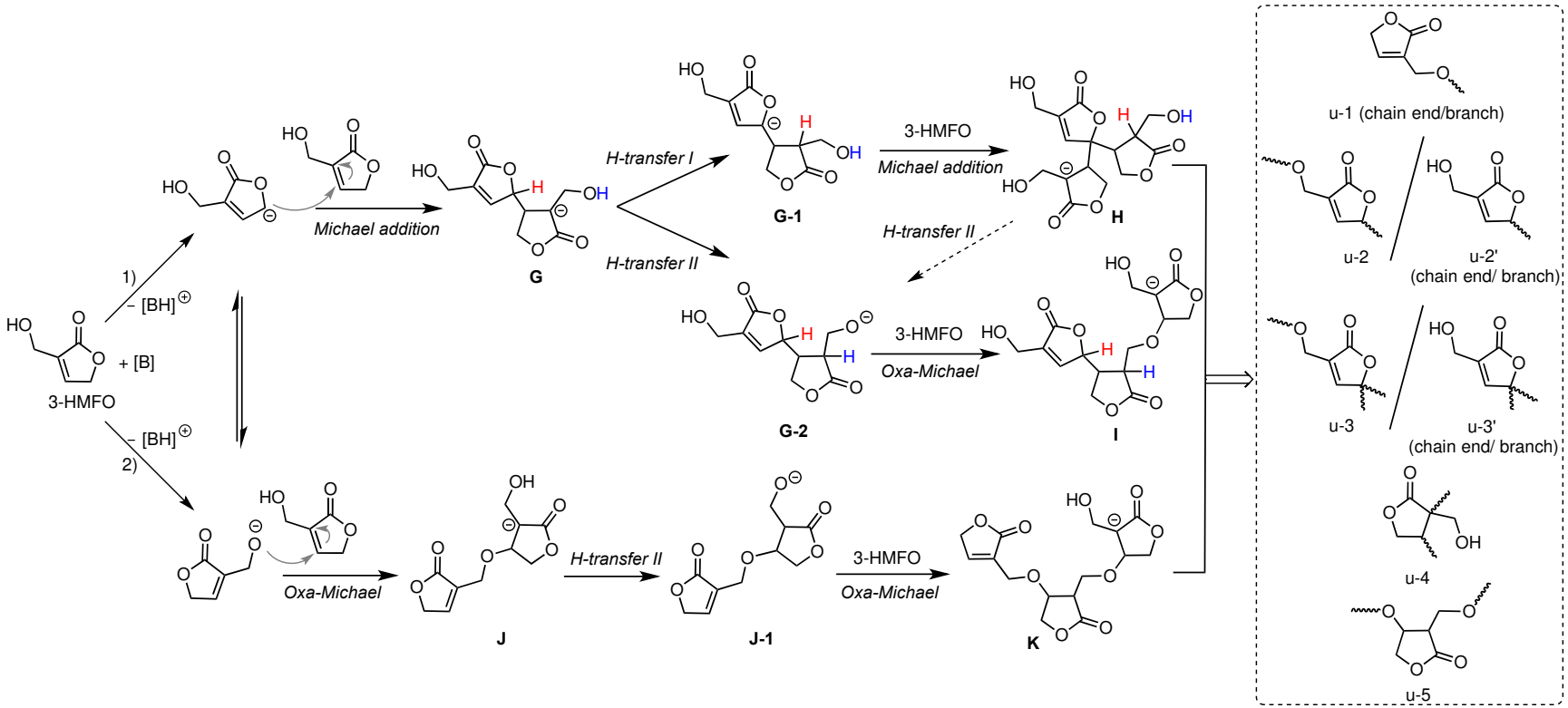

Figure 3.12. Possible mechanistic scenarios proposed for the polymerization of 3-HMFO.

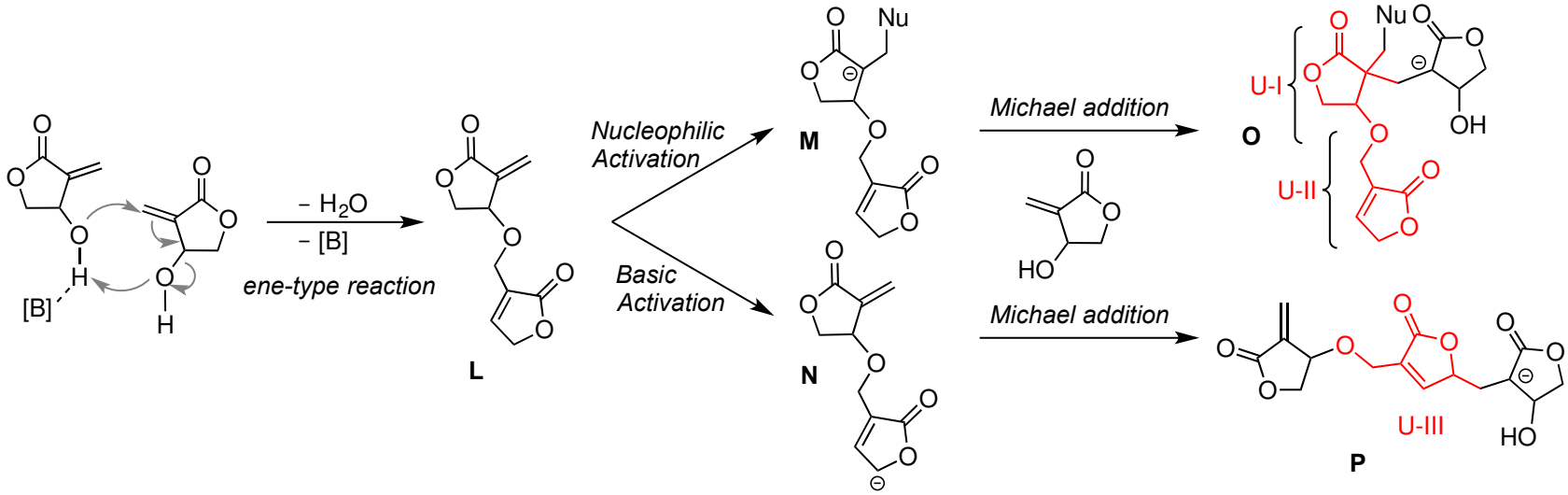

Figure 3.13. Proposed ene-type reaction as well as nucleophilic and basic activation mechanisms for the chain initiation steps of the polymerization of βHMBL

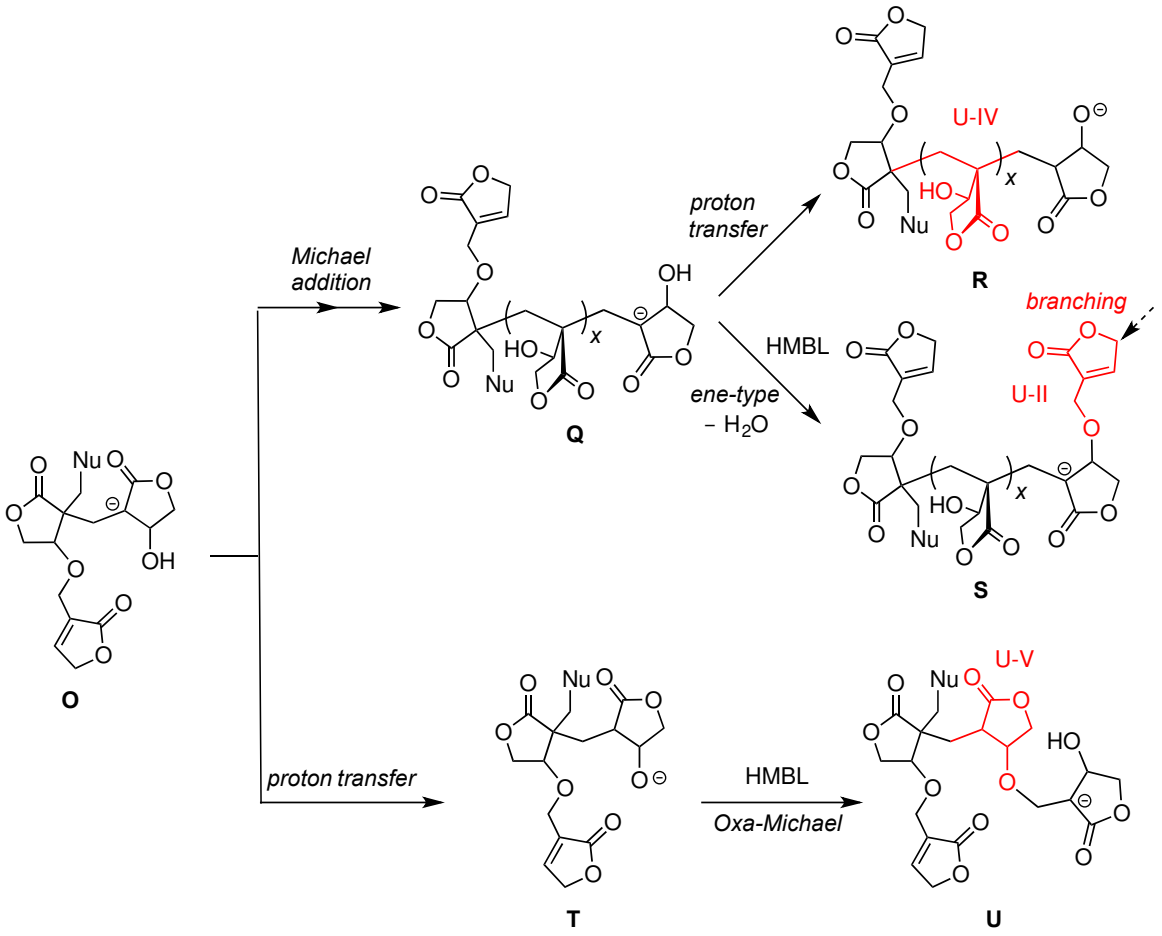

Figure 3.14. Proposed mechanistic scenarios during the chain propagation starting from nucleophile O affording chain branching and structural units U-IV and V.

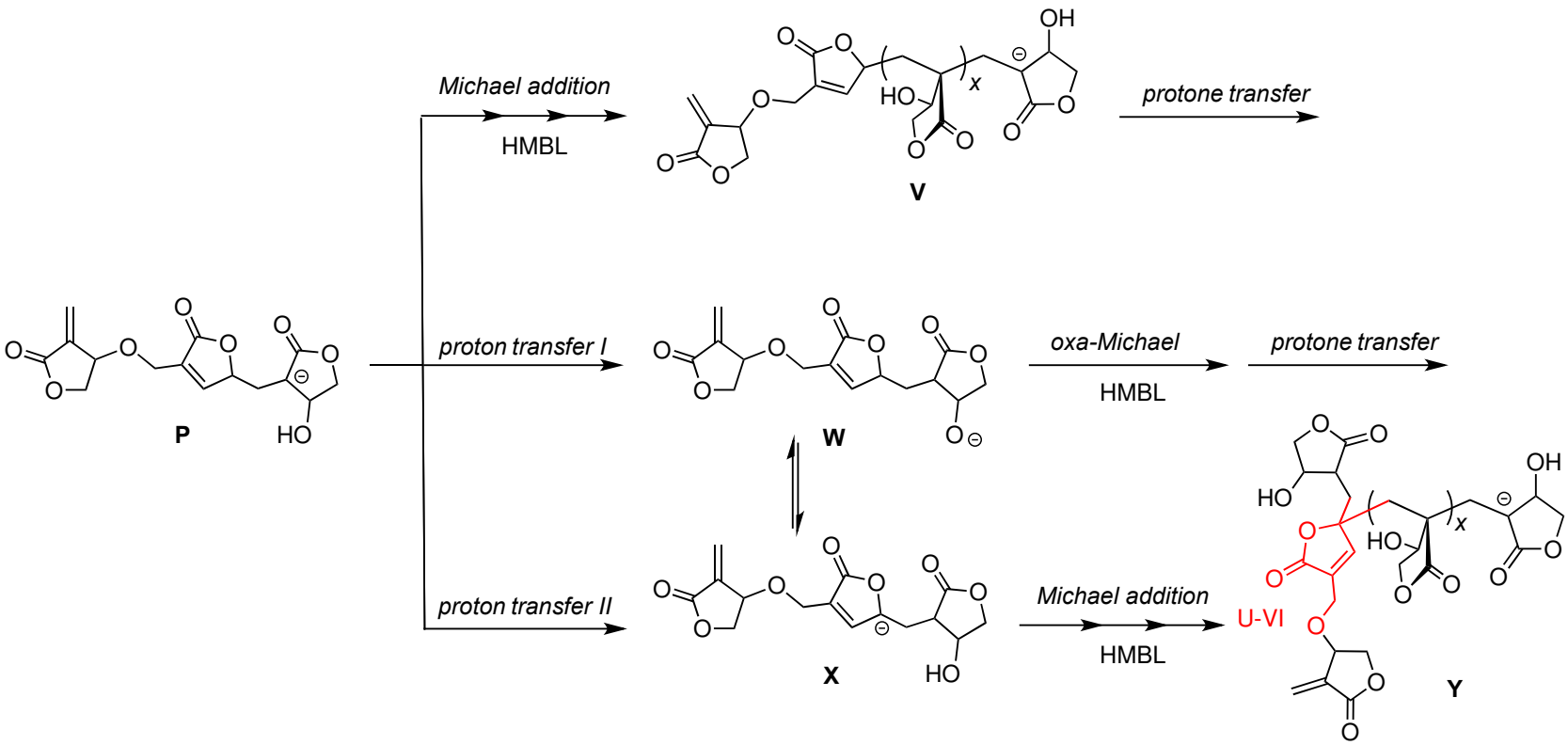

Figure 3.15. Proposed mechanistic scenarios during the chain propagation starting from nucleophile **P**

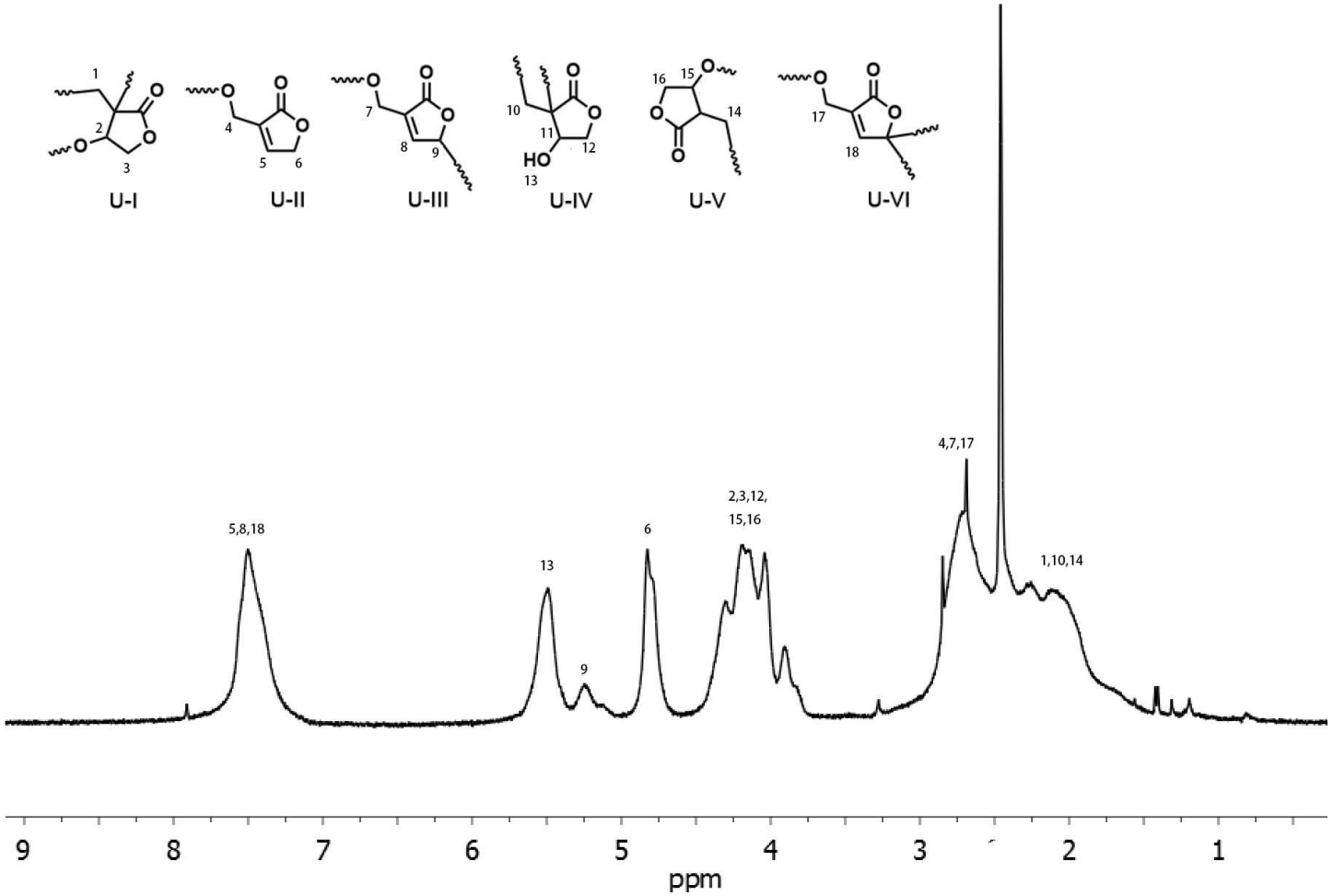

Figure 3.16. ^{1}H NMR (DMSO-d6, 400 MHz, 25 ^{o}C) spectrum of P(βHMBL) produced by I^{t}Bu in DMF.

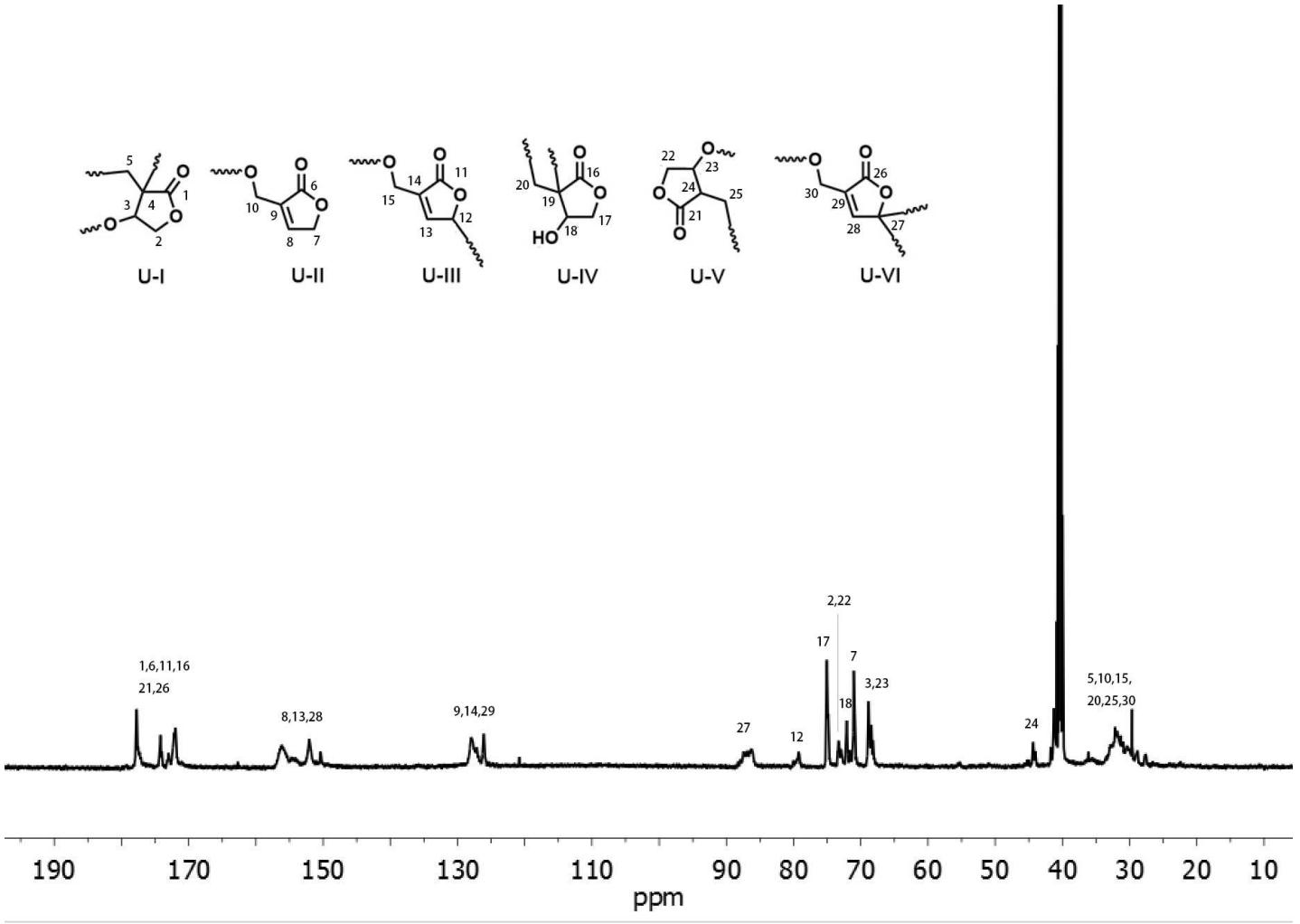

Figure 3.17. ^{13}C NMR (DMSO-d6, 125 MHz, 80 ^{o}C) spectrum of P(βHMBL) produced by I^{t}Bu in DMF.

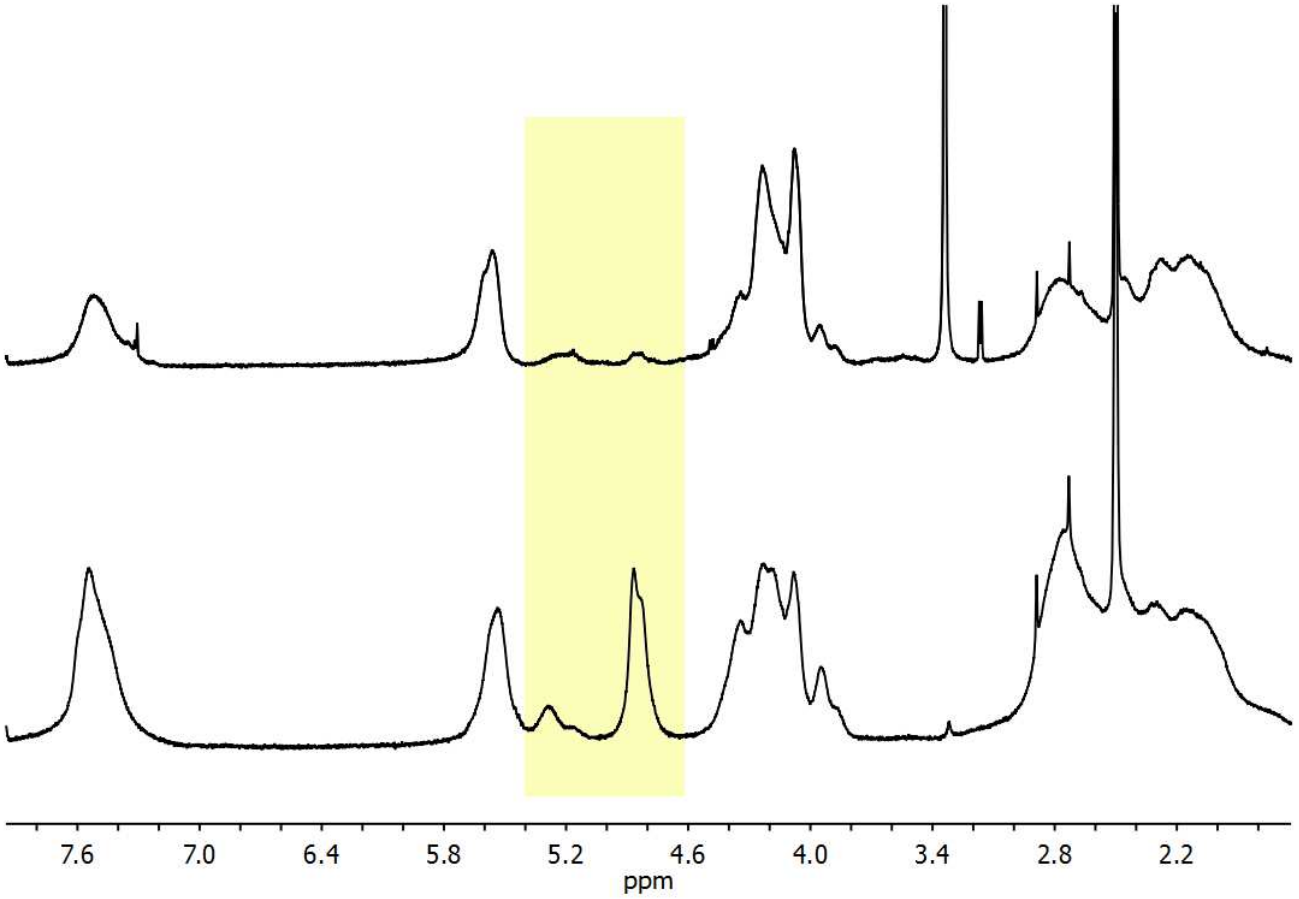

Figure 3.18. Overlay of ^{1}H NMR (DMSO-d6, 400 MHz, 80 °C) spectra of P(βHMBL)s produced by I^{t}Bu with BnOH (top) and without BnOH (bottom).

3.4. Conclusions

In summary, we have investigated the organopolymerization of five multifunctional γ-butyrolactone-based monomers, including bifunctional FO, 3-MFO, and 5-MFO with an endocyclic double bond and a 5-membered lactone ring, as well as trifunctional 3-HMFO and βHMBL with an endocyclic (3-HMFO) or exocyclic (βHMBL) double bond, a 5-membered lactone ring, and a hydroxyl group. The complexity of the reaction under nucleophilic and basic conditions, mediated by organocatalysts such as NHCs and superbases, increases drastically on going from the bifunctional monomers to the trifunctional ones, with the highest degree of the complexity being the polymerization of βHMBL, due to its presence of both the reactive exocyclic double bond and hydroxyl group. The polymerization of the parent bifunctional monomer FO by NHC catalyst I^{t}Bu and superbase ^{t}Bu-P$_4$ produced a vinyl-addition polymer via base-activation chain initiation (through abstraction of the 5-position proton) and Michael-addition propagation pathways, but facile chain transfer to monomer and/or polymer chains via proton transfer limited the molecular weight of the PFO produced. On the other hand, the reaction of base catalysts with FO's two methyl-substituted derivatives proceeds much less frequently towards repeated Michael additions; instead, proton transfer occurs between two consecutive nucleophilic attacks to produce a unique trimer structure in the case of 3-MFO, or proton transfer immediately occurs following a Michael addition to give a dimer structure in the case of 5-MFO. The polymerization of trifunctional 3-HMFO, with a third OH functional group, leads to a copolymer structure, poly(vinyl–ether lactone), via two different types of base activation mechanisms to generate carbanion and oxyanion nucleophiles that undergo respective Michael and ox-Michael additions, followed by repeated proton transfer and vinyl addition events. In the most complicated case of this monomer series, the polymerization of βHMBL by I^{t}Bu and ^{t}Bu-P$_4$ in organic solvents such as DMF afforded a branched copolymer structure having six different types of substructural units, originated

from multiple types of reactions, including conjugate Michael and oxa-Michael additions and proton transfer processes as well as ene-type dehydration reactions, enabled also by proton transfer; mechanistic crossovers between different pathways rendered the formation of the branched copolymer of poly(vinyl–ether lactone). These results highlight the complexity and sensitivity of the polymerization mechanism and its resulting polymer structure to the functional lactone monomer structure, including the type, position, and number of functional groups as well as substitution patterns of functional and non-functional groups on the lactone ring.

References

(1) Y. Zhu, C. Romain, C. K. Williams, *Nature* **2016**, *540*, 354–362.

(2) M. a R. Meier, J.O. Metzger, U.S. Schubert, *Chem. Soc. Rev.* **2007**, *36*, 1788–1802.

(3) M.J.-L. Tschan, E. Brulé, P. Haquette, C.M. Thomas, *Polym. Chem.* **2012**, *3*, 836-851.

(4) J. Tang, E.Y.-X. Chen, *Org. Chem. Front.* **2015**, *2*, 1625–1631.

(5) R.R.A. Kitson, A. Millemaggi, R.J.K. Taylor, *Angew. Chem. Int. Ed.* **2009**, *48*9, 426–9451.

(6) H.M.R. Hoffmann, J. Rabe, *Angew. Chem. Int. Ed. Engl.* **1985**, 24, 94–110.

(7) M.K. Akkapeddi, *Polymer* **1979**, *20*, 1215-1216.

(8) R.A. Cockburn, T.F.L. McKenna, R.A. Hutchinson, *Macromol. Chem. Phys.* **2010**, *211*, 501–509.

(9) R. a Cockburn, R. Siegmann, K. a Payne, S. Beuermann, T.F.L. McKenna, R. a Hutchinson, *Biomacromolecules* **2011**, *12*, 2319-2326.

(10) Y. Higaki, R. Okazaki, A. Takahara, *ACS Macro Lett.* **2012**, *1*, 1124−1127.

(11) J. Mosna, K. Matyjaszewski, *Macromolecules* **2008**, *41*, 5509–5511.

(12) C.U. Pittman, H. Lee, *Polymer Chem.* **2003**,1759–1777.

(13) J. Suenaga, D.M. Sutherlin, J.K. Stille, *Macromolecules* **1984**, *17*, 2913–2916.

(14) M.K. Akkapeddi, *Macromolecules* **1979**, *12*, 546–551.

(15) Y. Hu, L.O. Gustafson, H. Zhu, E.Y.X. Chen, *J. Polym. Sci. Part A Polym. Chem.* **2011**, *49*, 2008–2017.

(16) Y. Zhang, L.O. Gustafson, E.Y.X. Chen, *J. Am. Chem. Soc.* **2011**, *133*, 13674–13684.

(17) D.Y. Sogah, W.R. Hertler, O.W. Webster, G.M. Cohen, *Macromolecules* **1987**, *20*, 1473–1488.

(18) G.M. Miyake, Y. Zhang, E.Y.X. Chen, *Macromolecules* **2010**, *43*, 4902–4908.

(19) Y. Zhang, G.M. Miyake, E.Y.X. Chen, *Angew. Chem. Int. Ed.* **2010**, *49*, 10158–10162.

(20) T. Xu, E.Y.X. Chen, *J. Am. Chem. Soc.* **2014**, *136*, 1774–1777.

(21) Y. Zhang, G.M. Miyake, M.G. John, L. Falivene, L. Caporaso, L. Cavallo, E.Y.-X. Chen, *Dalton Trans.* **2012**, *41*, 9119–9134.

(22) Y. Hu, G.M. Miyake, B. Wang, D. Cui, E.Y.X. Chen, *Chem. Eur. J.* **2012**, *18*, 3345–3354.

(23) Y. Hu, X. Wang, Y. Chen, L. Caporaso, L. Cavallo, E.Y.X. Chen, *Organometallics* **2013**, *32*, 1459–1465.

(24) R.R. Gowda, E.Y.-X. Chen, *Dalton Trans.* **2013**, *42*, 9263-9273.

(25) C.J. Weiss, T.J. Marks, *Dalton Trans.* **2010**, *39*, 6576–6588.

(26) X. Chen, L. Caporaso, L. Cavallo, E.Y.X. Chen, *J. Am. Chem. Soc.* **2012**, *134*, 7278–7281.

(27) Y. Zhang, M. Schmitt, L. Falivene, L. Caporaso, L. Cavallo, E.Y.X. Chen, *J. Am. Chem. Soc.* **2013**, *135*, 17925–17942.

(28) S. Naumann, A.W. Thomas, A.P. Dove, *Angew. Chem. Int. Ed.* **2015**, *54*, 9550–9554.

(29) M. Hong, E.Y.-X. Chen, *Nat. Chem.* **2016**, *8*, 42–49.

(30) M. Hong, E.Y.X. Chen, *Angew. Chem. Int. Ed.* **2016**, *55*, 4188–4193.

(31) X. Tang, M. Hong, L. Falivene, L. Caporaso, L. Cavallo, E.Y.X. Chen, *J. Am. Chem. Soc.* **2016**, *138*, 14326–14337.

(32) T. Hirabayashi, K. Yokota, *Polym. J.* **1982,** *14*, 789–796.

(33) Y. Yokoyama, M. Okada, H. Sumitomo, *Die Makromolekulare Chemie* **1975**, *176*, 3537–3550.

(34) Y. Yokoyama, M. Okada, H. Sumitomo, *Die Makromol. Chem.* **1975**, *176*, 2815–2832.

(35) Y. Yokoyama, M. Okada, H. Sumitomo, *Die Makromol. Chem.* **1974**, *175*, 2525–2538.

(36) J.M. Judge, C.C. Price, *J. Polym. Sci.* **1959**, *41*, 435–443.

(37) C. Thomas, B. Bibal, *Green Chem.* **2014**, *16*, 1687–1699.

(38) Sardon, H.; Pascual, A.; Mecerreyes, D.; Taton, D.; Cramail, H.; Hedrick, J. L. *Macromolecules*, **2015**, *48*, 3153−3165.

[39) M.K. Kiesewetter, E.J. Shin, J.L. Hedrick, R.M. Waymouth, *Macromolecules* **2010**, *43*, 2093–2107.

(40) N.E. Kamber, W. Jeong, R.M. Waymouth, R.C. Pratt, B.G.G. Lohmeijer, J.L. Hedrick, *Chem. Rev.* **2007**, *107*, 5813–5840.

(41) K. Fuchise, Y. Chen, T. Satoh, T. Kakuchi, *Polym. Chem.* **2013**, *4*, 4278-4291.

(42) M. Fèvre, J. Pinaud, Y. Gnanou, J. Vignolle, D. Taton, *Chem. Soc. Rev.* **2013**, *42*, 2142–2172.

(43) S. Naumann, A.P. Dove, *Polym. Chem.* **2015**, *6*, 3185–3200.

(44) R. Schwesinger, C. Hasenfratz, H. Schlemper, L. Walz, E.-M. Peters, K. Peters, H. G. Schering, *Angew. Chem. Int. Ed. English.* **1993**, *32*, 1361–1363.

(45) I. Leito, T. Rodima, I. a. Koppel, R. Schwesinger, V.M. Vlasov, *J. Org. Chem.* **1997**, *62*, 8479–8483.

(46) U. Kohn, M. Schulz, A. Schramm, W. Gunther, H. Gorls, S. Schenk, E. Anders, *Eur. J. Org. Chem.* **2006**, 4128–4134.

(47) R. Schwesinger, H. Schlemper, *Angew. Chem. Int. Ed. English.* **1987**, *26*, 1167–1169.

(48) M. Schmitt, L. Falivene, L. Caporaso, L. Cavallo, E.Y.-X. Chen, *Polym. Chem.* **2014**, *5*, 3261–3270.

(49) S.-I. Matsuoka, S. Namera, M. Suzuki, *Polym. Chem.* 2015, *6*, 294–301.

(50) W. N. Ottou, D. Bourichon, J. Vignolle, A.-L. Wirotius, F. Robert, Y. Landais, J.-M. Sotiropoulos, K. Miqueu, D. Taton, *Chem. Eur. J.* **2015**, *21*, 9447–9453.

(51) C.Yuan, Y.Qi, *Synthesis* **1986**, *10*, 821-825.

(52) Y. Wu, R.P. Singh, L. Deng, *J. Am. Chem. Soc.* **2011**, *133*, 12458–12461.

(53) T. Mendgen, T. Scholz, C.D. Klein, *Bioorganic Med. Chem. Lett.* **2010**, *20*, 5757–5762.

(54) J. Xin, S. Zhang, D. Yan, O. Ayodele, X. Lu, J. Wang, *Green Chem.* **2014**, *16*, 3589-3595.

(55) R.F. Colletti, R.J. Halley, L.J. Mathias, *Macromolecules* **1991**, *24*, 2043–2047.

Chapter 4

Effects of Chain Ends on Thermal and Mechanical Properties and Recyclability of Poly(*γ*-butyrolactone)

4.1 Summary

This work investigates effects of poly(*γ*-butyrolactone) (P*γ*BL) with different initiation and termination chain ends on five types of materials properties, including thermal stability, thermal transitions, thermal recyclability, hydrolytic degradation, and dynamic mechanical behavior. Four different chain-end-capped polymers with similar molecular weights, BnO-$[C(=O)(CH_2)_3O]_n$-R, R = C(=O)Me, $C(=O)CH=CH_2$, C(=O)Ph, and $SiMe_2CMe_3$, along with a series of uncapped polymers R'O-$[C(=O)(CH_2)_3O]_n$-H (R' = Bn, Ph_2CHCH_2) with M_n ranging from low (4.95 kg/mol) to high (83.2 kg/mol), have been synthesized. The termination chain end R showed a large effect on polymer decomposition temperature and hydrolytic degradation, relative to H. Overall, for those properties sensitive to the chain ends, chain-end capping renders R-protected linear P*γ*BL behaving much like cyclic P*γ*BL.

4.2 Introduction

Ring-opening polymerization (ROP) of cyclic esters (lactones and lactides) with relatively high strain energy through the rapid chain-growth mechanism provides a highly effective, commonly adopted method to prepare aliphatic polyesters, a class of technologically important biodegradable and/or biocompatible polymers.[1-13] Highly stable five-membered *γ*-butyrolactone (*γ*-BL) is as a key downstream chemical of bio-derived succinic acid that was ranked first[14] in the DOE's top 12 biomass-derived compounds[15-16] and commonly used as industrial solvent and cleaning agent. As a cyclic ester monomer for the corresponding poly(*γ*-butyrolactone) (P*γ*BL),

however, it was not accomplished until 2015 when the first successful chemical ROP of γ-BL was realized by our group,[17] as γ-BL was commonly considered as "non-polymerizable" in textbooks[18-20] and literature[21] due to its unfavorable thermodynamics of the polymerization. Utilizing metal (La, Y)-catalyzed coordination ROP, relatively high molecular weight PγBL with number-average molecular weight (M_n) up to 30 kg/mol and high monomer conversion up to 90% was achieved. Significantly, the resulting PγBL can exhibit either a linear or cyclic topology, controlled by the catalyst/initiator nature and ratio, and it can be depolymerized back to its monomer completely by heating the bulk material at 220 °C (for linear PγBL) or 300 °C (for cyclic PγBL) for 1 h. Subsequently, effective organopolymerization of γ-BL was also achieved later with tetrameric phosphazene superbase ^{t}Bu-P$_4$ as the initiator or catalyst (in combination with benzyl alcohol, BnOH, as the initiator), producing linear PγBL with M_n up to 26.7 kg/mol.[22] Most recently, Liu, Li and co-workers also produced linear PγBL with M_n up to 22.9 kg/mol using a new cyclic trimeric phosphazene base and BnOH as the initiator.[23]

To broaden practical applications of the PγBL material, it is important to demonstrate the tunability of the overall materials properties of PγBL, including thermal and mechanical properties, hydrolytic degradation behavior, and chemical recyclability. Recently, we introduced a polymer system based on γ-BL with a *trans*-ring fusion at the α and β positions; this *trans*-fusion renders its room-temperature polymerizability under solvent-free conditions to yield a high-molecular weight polymer with mechanical properties comparable to those of common plastics, but with intrinsically infinite recyclability.[24-25] Copolymerizing γ-BL with ε-caprolactone and δ-valerolactone was utilized to effectively change and regulate many composition-dependent properties such as thermal, cocrystallization, and degradation

properties.[26] Metal-free copolymerization of γ-BL and L-lactide was also realized by sequential ROP.[27] Other than changing the composition of the main chain through copolymerization, other approaches could be utilized to modify homopolymer P*γ*BL. For example, it is known that the overall properties of the polymers can be significantly affected by the polymer topology.[17,28-37] In this context, the decomposition temperature [T_d, defined by the temperature of 5% weight loss in the thermal gravimetric analysis (TGA) curve] of the linear P*γ*BL was around 220 °C, while the cyclic P*γ*BL with similar M_n exhibited a significantly higher T_d of around 300 °C.[17] Besides the decomposition temperature, the hydrolytic degradation rates and mechanical properties of P*γ*BL were also found to be affected by the polymer topology.

The critical difference between the linear and cyclic topologies is the presence and absence of chain ends for the respective topology. An interesting question then arises: can linear P*γ*BL be modified to behave just like its cyclic analog in properties most sensitive to the OH group in the chain end (e.g., thermal and hydrolytic stability) by protecting the OH group with the more robust OR group? According to a proposed decomposition mechanism shown in Figure 4.1, a bulkier end group (R) should increase the steric hindrance of the nucleophilic attack at the carbonyl carbon by OR (vs. OH), and at the same time it should hinder the transfer of the chain end group to the penultimate in-chain O atom, thus imposing a higher activation barrier for the polymer degradation. Based on this hypothesis, we carried out a study to examine the P*γ*BL properties with different chain ends via either *in-situ* end-capping or post-functionalization, both of which are common methods employed to modify functional polymers.[38-42] For example, thermal stability of polyoxymethylene glycols was effectively modified by esterification.[43-45] Self-immolative polymers degrade by an end-to-end deploymerization mechanism in response to

the cleavage of the end cap.[46-49] Through the use of stimuli-responsive end-caps, poly(glyoxylate)s can serve as a new class of self-immolative linear polymer backbones. It was shown that degradation occurred at higher temperatures for end-capped poly(ethyl glyoxylate) than for non-terminated ones.[50] The presence of an appropriate end-capping group at the ω-chain-end protects the polyphthalaldehyde (PPA) from spontaneous depolymerization by increasing the PPA thermal stability up to 150–200 °C.[51,52]

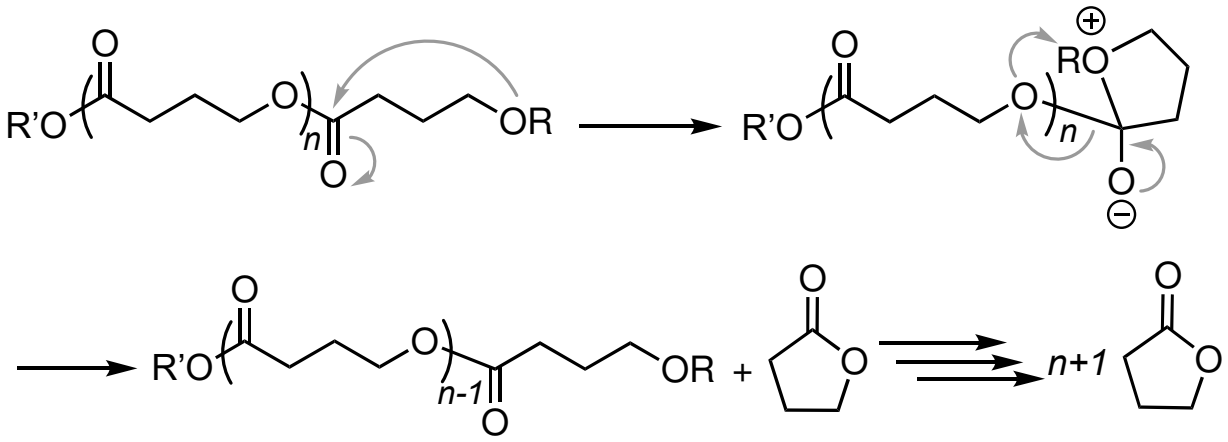

Figure 4.1 Proposed backbiting decomposition mechanism for thermal degradation of P*γ*BL.

Hydroxyl groups are very reactive towards many reagents and can be readily protected by formation of an ether, [53-62] a silyl ether,[63-66] or an ester.[67-68] In this work, by taking advantage of the reactive OH group located at each P*γ*BL chain end, we first utilized the above reactions to convert P*γ*BL-OH chains into P*γ*BL-OR by end-capping with reactive acyl chloride, silyl chloride, or anhydride reagents. Subsequently, we investigated the effects of such chain-end capping on the thermal and mechanical properties, hydrolytic degradation behavior, and chemical recyclability of P*γ*BL materials.

4.3 Exprimental

4.3.1 Materials, Reagents, and Methods

All syntheses and manipulations of air- and moisture-sensitive materials were carried out in flamed Schlenk-type glassware on a dual-manifold Schlenk line, on a high-vacuum line, or in an inert gas (Ar or N_2)-filled glovebox. *γ*-Butyrolactone (*γ*-BL) was purchased from Acros Organics Co, dried over CaH_2 overnight, vacuum–distillated, and stored in a brown bottle with activated molecular sieve in the glovebox for further use. Lanthanum(III) amide complex $La[N(SiMe_3)_2]_3$, *tert*-butylchlorodimethylsilane, acetyl chloride, acryloyl chloride, and benzoyl chloride were purchased from Aldrich Chemical Co. and used as received. Literature procedures were employed or modified for the preparation of P*γ*BL with M_n under 10 kg/mol.[17] Yttrium catalyst **Y-1**[69] was utilized for the synthesis of P*γ*BL with M_n over 40 kg/mol.

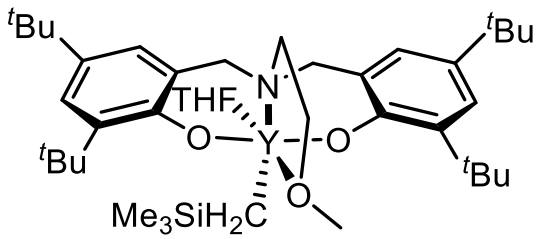

Y-1

4.3.2 Polymerization Procedures for Preparation of PγBL with M_n > 40 kg/mol

Polymerizations were performed in 25 mL flame-dried Schlenk flasks interfaced to a dual-manifold Schlenk line. After a catalyst solution in THF containing a predetermined amount of **Y-1** was cooled using an external temperature bath at –40 °C for 20 min, *γ*-BL (17.2 g, [*γ*-BL] = 10

mol/L) was added to the flask. The ratio of [γ-BL]/[**Y-1**] = 500 was used to prepare PγBL with M_n = 42.2 kg/mol, and the ratio of [γ-BL]/[**Y-1**] = 700 was used to prepare PγBL with M_n = 83.2 kg/mol. After 12 h, the reaction was quenched with benzoic acid in chloroform and precipitated into cold methanol, filtered, washed with methanol to remove any unreacted monomer, and dried in a vacuum oven at room temperature for 24 h to a constant weight.

4.3.3 General Post-Polymerization Chain-end Capping Procedures

PγBL was added to a dry CH_2Cl_2 solution ([PγBL] = 0.1 mol/L) containing imidazole (10 equiv. relative to PγBL-OH) in a 25 mL flame-dried Schlenk flask interfaced to a dual-manifold Schlenk line. After equilibration at 0 ^oC in an ice-water bath for 20 min, acyl chloride (2.5 equiv. relative to PγBL-OH) was added to the flask via a gastight syringe, and the reaction was allowed to warm up to 25 ^oC. After a desired period of time specified in Table 4.1, the product mixture was poured into brine and extracted with chloroform for three times. The combined organic layer was dried over anhydrous Na_2SO_4. The resulting polymer was precipitated into 100 mL of cold methanol, filtered, washed with methanol to remove any unreacted reagents, and dried in a vacuum oven at room temperature after 24 h to a constant weight.

4.3.4 Hydrolytic Degradation Tests of Polymers

Square-shaped polymer specimens for degradation tests were cut from polymer films prepared by compression molding at 80–85 ^oC for 5 min. For the samples with a melting-transition temperature below room temperature, the polymer films were remolded after solidifying at –40 ^oC for 10 min in the freezer and cut as quickly as possible. The weighted three polymer films were separately immersed in 4 mL of deionized water, acidic aqueous ([H^+] = 1.0 M), and basic

aqueous ([OH^-] = 1.0 M) solutions. After a predetermined degradation time, the supernatant liquid was decanted off and the remaining specimen was washed thoroughly with distilled water and methanol, and then dried under vacuum at room temperature for 2 days to a constant weight. After the thoroughly dried specimen was weighed, it was reimmersed in the above aqueous solutions again, and such a process was repeated at each time point.

4.3.5 Polymer Characterizations

Polymer weight-average molecular weight (M_w), number-average molecular weight (M_n), and dispersity index ($Đ = M_w/M_n$) were measured by gel permeation chromatography (GPC) analysis carried out at 40 °C and a flow rate of 1.0 mL/min, with DMF as the eluent on a Waters University 1500 GPC instrument equipped with one PLgel 5 µm guard and two PLgel 5 µm mixed-C columns (Polymer Laboratories; linear range of molecular weight = 200–2,000,000). The instrument was calibrated with 10 PMMA standards, and chromatograms were processed with Waters Empower software (version 2002).

Melting transition (T_m) and glass transition (T_g) temperatures were measured in ambient condition by differential scanning calorimetry (DSC) on an Auto Q20, TA Instrument. All T_m and T_g values were obtained from a second scan after the thermal history was removed from the first scan. The second heating rate was 10 °C/min and cooling rate was 5 °C/min. Decomposition temperatures (T_d), defined by the temperature of 5% weight loss, and maximum rate decomposition temperatures (T_{max}), obtained from derivative (wt %/°C) vs. temperature (°C) plots, of the polymers were measured by thermal gravimetric analysis (TGA) on a Q50 TGA Analyzer, TA Instrument. Polymer samples were heated under N_2 atmosphere from 25 °C to 600 °C at a heating rate of 20 °C/min.

The isolated low molecular weight samples were analyzed by matrix-assisted laser desorption/ ionization time-of-flight mass spectroscopy (MALDI−TOF MS); the experiment was performed on an Ultraflex MALDI-TOF mass spectrometer (Bruker Daltonics) operated in positive ion, reflector mode using a Nd:YAG laser at 355 nm and 25 kV accelerating voltage. A thin layer of a 1% NaI solution was first deposited on the target plate, followed by 0.6 µl of both sample and matrix (dithranol, 10mg/mL in 50% ACN, 0.1% TFA). External calibration was done using a peptide calibration mixture (4 to 6 peptides) on a spot adjacent to the sample. The raw data was processed in the FlexAnalysis software (version 2.4, Bruker Daltonics).

Dynamic mechanical analysis (DMA) was performed on PγBL thin films (ca. 16 × 10 × 1.4 mm) with an RSAG2 analyzer (TA Instruments) in tension film mode at a maximum strain of 0.3% and a frequency of 1 Hz. The PγBL thin films for DMA tests were prepared by compression molding at 80–85 ºC for 5 min. The sample was heated from –125 ºC to 25 ºC or 30 ºC at a heating rate of 3 ºC /min. The DMA T_g was selected as the temperature at the maximum (peak) value of the loss modulus.

4.4 Results And Discussion

4.4.1 Post-functionalization of PγBL-OH to PγBL-OR

To prepare P*γ*BL-OR with molecular weights similar to P*γ*BL-OH, we initially attempted *in situ* chain-end capping of the *γ*-BL polymerization by addition of an acyl chloride at the end of the polymerization. However, this approach worked only partially because the *γ*-BL polymerization was carried out at –40 ºC for thermodynamic reasons, and the resulting polymer precipitated out of the solution at the end of the reaction, which makes the *in-situ* end capping infeasible. Hence, post-functionalization of the preformed P*γ*BL-OH was adopted in this study. As some of the most frequently used OH-protecting agents, the following six (Figure 4.2) were selected for post-

functionalization of PγBL-OH: acetyl chloride **(1),** acetic anhydride (**2**), acryloyl chloride (**3**), benzoyl chloride (**4**), *tert*-butyldimethylsilyl chloride (**5**), and 2,2,2-triphenyl-acetyl chloride (**6**).

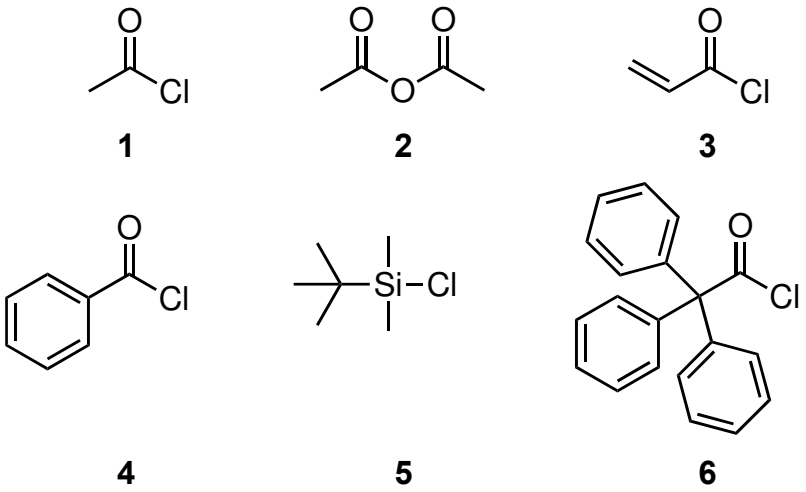

Figure 4.2 Structures of the protecting agents.

Table 4.1 Selected Results of the Post-functionalized PγBL-OR

Run	Initiator	End Group	Time (h)	R %[a]	T_d (°C)	T_g (°C)	T_m (°C)	T_{max} (°C)	M_n (kg/mol)	M_w
1	BnOH	H	-	0	222	-45.1	45.1, 57.4	260	7.56	1.59
2[b]	BnOH	C(=O)Me	43	100	300	-44.0	44.7, 62.2	373	7.63	1.31
3	BnOH	C(=O)CH=CH$_2$	4	84.9	287	-47.3	41.2, 59.6	367	7.19	1.29
4	BnOH	C(=O)Ph	30	95.8	277	-44.9	43.7, 58.1	358	7.28	1.30
5	BnOH	SiMe$_2$CMe$_3$	47	100	334	-47.1	55.8, 60.2	402	7.42	1.53
6	Ph$_2$CHCH$_2$OH	H	-	0	227	-48.3	48.6, 50.1	260	7.35	1.94

[a]Calculated percentage of OH groups protected (in the form of PγBL-OR) in the polymer chain based on ^{1}H NMR spectra (Figure 4.3). [b] Postfunctionalized by acetyl chloride.

Table 4.1 summarized the results selected from those highly effective conversion runs. Overall, the acyl chlorides were found to be very effective in converting the OH end group to the

OR end group, achieving high to quantitative (100%) conversions. Even with the bulky 2,2,2-triphenyl-acetyl group in **6**, the reaction went rather smoothly (83.6% conversion, Figure S4.1). Compared to acetyl chloride, the performance of acetic anhydride was relatively poor, achieving only 70.8% of the OH to OR conversion based on the analysis by ^{1}H NMR spectra (Figure S4.2). To also examine the effect of the initiating chain end, PγBL samples of BnO-PγBL-OH and Ph_2CHCH_2O- PγBL-OH were also synthesized by using BnOH and Ph_2CHCH_2OH as the corresponding initiator (runs 1 and 6, Table 4.1)

Figure 4.3 depicts an overlay of ^{1}H NMR spectra of the resulting end-capped polymers, represented as BnO-$[C(=O)(CH_2)_3O]]_n$-R, clearly showing the newly formed R groups as -C(=O)Me, -C(=O)CH=CH_2, -C(=O)Ph, and –$SiMe_2CMe_3$. These end groups were further confirmed by analysis with matrix-assisted laser desorption/ionization time-of-flight mass spectroscopy (MALDI-TOF MS). Take BnO-$[C(=O)(CH_2)_3O]_n$-C(=O)CH=CH_2 for example (Figure 4.4), there was only a trace fraction of cyclic PγBL without end groups (at m/z < 1500), and the predominate structure is that of the linear PγBL. The spacing between the two neighboring molecular ion peaks in the major series corresponds to the molar mass of the repeating unit γ-BL (m/z = 86.02), which was shown as the slope (86.22) from the plot of m/z values (y axis) versus the number of repeat units (x axis). The intercept of the plot, 164.13, represents the total mass of chain ends + H^+, thus corresponding to linear structure BnO-$[C(=O)(CH_2)_3O]_n$-C(=O)CH=CH_2. MALDI-TOF MS analysis of two other end-capped polymers, BnO-$[C(=O)(CH_2)_3O]_n$-C(=O)OMe and BnO-$[C(=O)(CH_2)_3O]_n$-$SiMe_2CMe_3$ (Figure S4.3-S4.4),

also confirmed their chain-end structures of the major linear polymers, with some amounts of cyclic structures as well.

4.4.2 Thermal Properties of Chain-End Capped PγBL-OR

Thermal properties of P*γ*BL with similar molecular weights (7.2–7.6 kg/mol) but different chain ends were investigated by thermal gravimetric analysis (TGA) and differential scanning calorimetry (DSC). The TGA curves of the BnO-$[C(=O)(CH_2)_3O]_n$-R (Figure. 4) exhibited essentially a one-step degradation profile with much higher decomposition temperature T_d (277 – 334 °C) and maximum rate decomposition temperature T_{max} (358 – 402 °C) than the T_d and T_{max} values of the unprotected polymer BnO-$[C(=O)(CH_2)_3O]_n$-H (T_d = 222 °C, T_{max} = 260 °C). Among the OH-protected polymers BnO-$[C(=O)(CH_2)_3O]_n$-R, the polymer with the silyl ether end group (R = $SiMe_2CMe_3$) exhibited the highest T_d of 334 °C and T_{max} of 402 °C, attributed to the more thermally stable and sterically more hindered silyl ether, which renders the transfer of the terminal R group during the decomposition process (*c.f.* Figure 4.1) more difficult. On the other hand, changing the chain end groups had little influence on the thermal transition temperatures T_g and T_m (Table 4.1, Figures S7-S11). Furthermore, the impact of the initiation end R'O on the thermal degradation profile was also negligible, as the T_d barely changed with replacing BnOH with Ph_2CHCH_2OH as the initiator (run 1 vs. 6, Table 4.1; Figures S5-S6). Overall, the large effect was seen on the thermal stability of the P*γ*BL polymer, and the T_d and T_{max} values of the end-capped polymer BnO-$[C(=O)(CH_2)_3O]_n$-R now become similar to those of the cyclic P*γ*BL without chain ends.[17] These results are consistent with the mechanistic scenario outlined in Figure 4.1, where the bulkiness and stability of the termination chain end R should

significantly enhance the resistance of BnO-[C(=O)$(CH_2)_3$O]$_n$-R towards thermal degradation, thus rendering them behaving much like the cyclic PγBL .

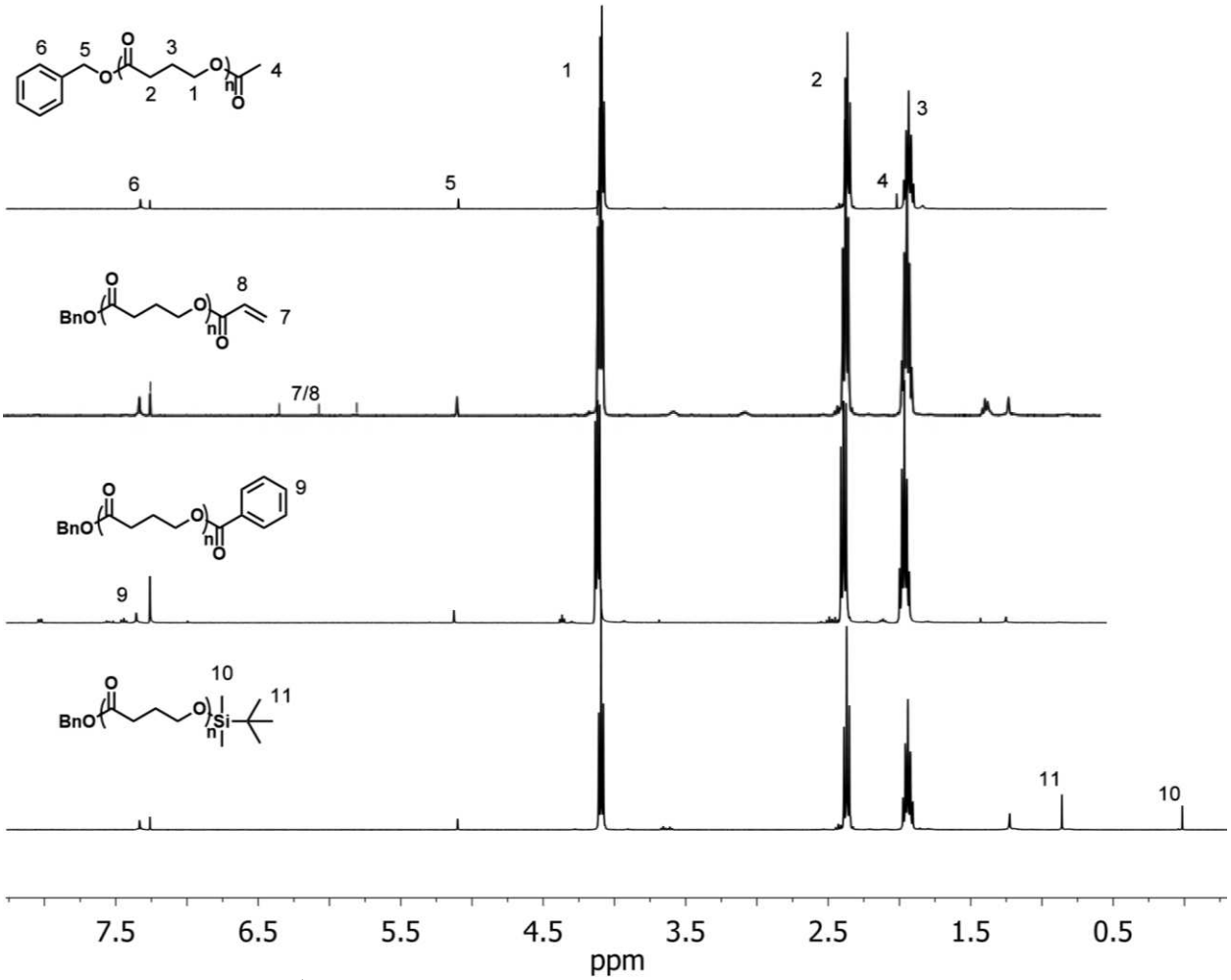

Figure 4.3 Overlay of ^{1}H NMR (400 MHz, $CDCl_3$, 25 ^{o}C) spectra of BnO-[C(=O)$(CH_2)_3$O]$_n$-R. For R = C(=O)CH=CH_2, minor signals due to residual solvent (hexanes, 0.88 and 1.26 ppm) and unknown impurities (~3.0 and 3.5 ppm) were also present.

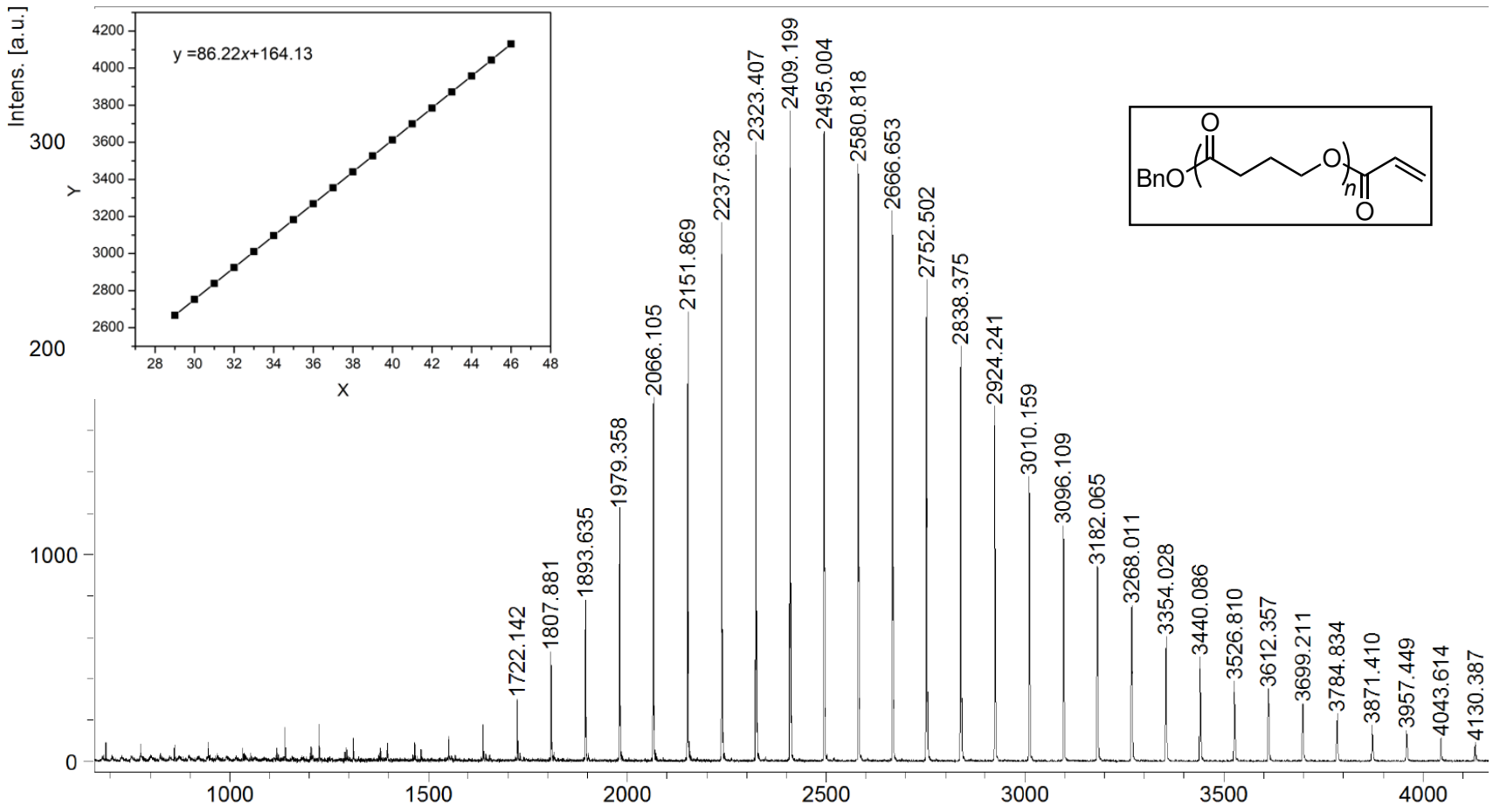

Figure 4.4 MALDI-TOF MS spectrum of BnO-[C(=O)$(CH_2)_3$O]$_n$-C(=O)CH=CH_2 and plot of *m*/*z* values vs γ-BL repeat units.

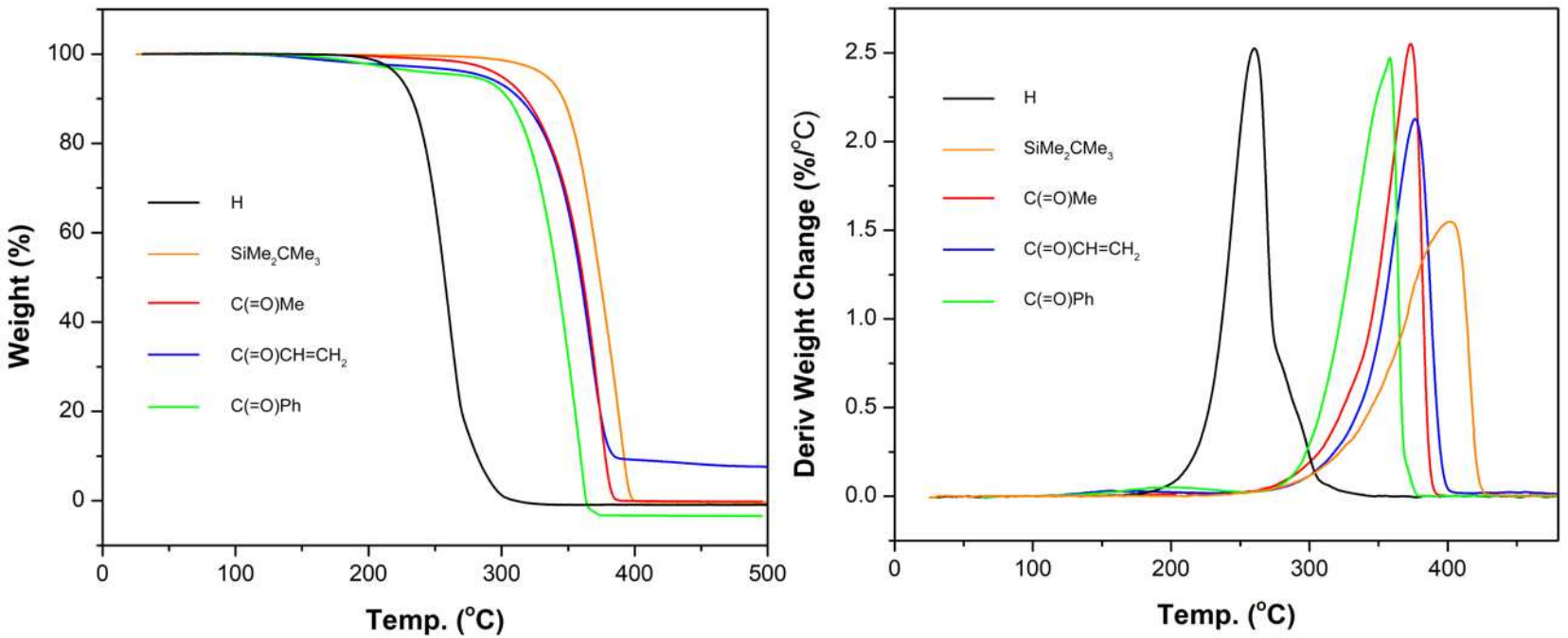

Figure 4.5 Overlay of TGA (top) and DTG (bottom) curves for BnO-[C(=O)$(CH_2)_3$O]$_n$-R. T_{max} = 260 °C (R = H), 373 °C [R = C(=O)Me], 367 °C [R = C(=O)CH=CH_2], 358 °C [R = C(=O)Ph], 402 °C (R = $SiMe_2CMe_3$).

4.4.3 Molecular Weight Effects on Degradation Temperature

The thermal properties of BnO-[C(=O)$(CH_2)_3$O]$_n$-H with different molecular weights were also investigated by TGA (Figure 4.6). In the low molecular weight regime (M_n from 5.0 to ~40 kg/mol), there showed a large effect of polymer molecular weight on the T_d value of the polymer; as the M_n increased from 4.95 kg/mol to 7.59 kg/mol to 42.2 kg/mol, the T_d value increased from 207 °C to 222 °C to 266 °C, respectively (runs 1–3, Table 2). However, In the higher molecular weight regime from 42.2 kg/mol to 83.2 kg/mol, there was essentially no further change in the T_d value (run 4 vs 3, Table 2). On the other hand, regardless of the molecular weight regime, T_g remained the same at –45 °C, while T_m varied to some extent.

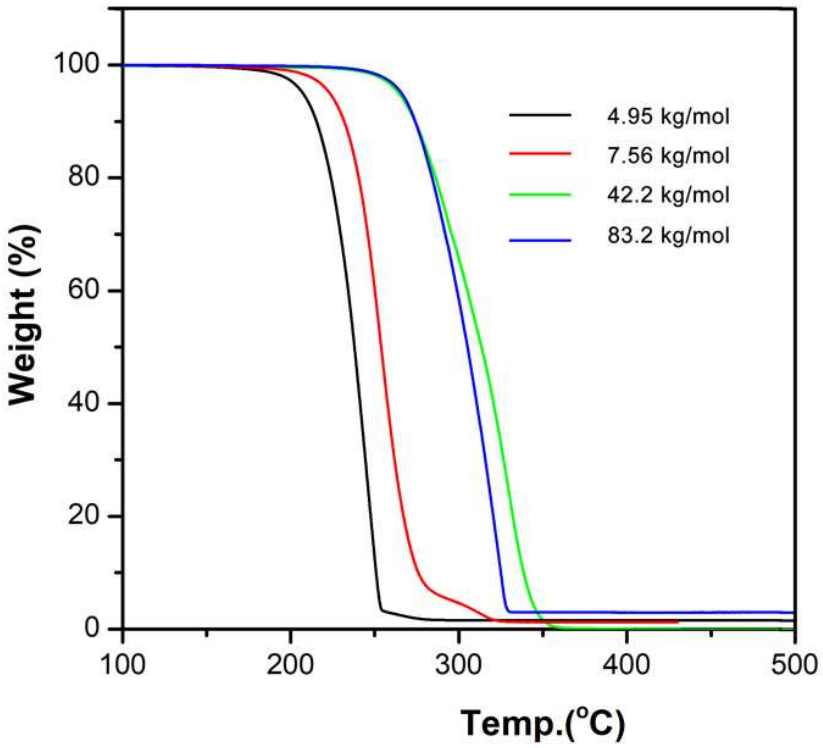

Figure 4.6 Overlay of TGA curves for BnO-[C(=O)$(CH_2)_3$O]$_n$-H with different molecular weights.

Table 2 T_d of BnO-[C(=O)$(CH_2)_3$O]$_n$-H with different molecular weights

Run #	M_n (kg/mol)	$Đ$	T_d (°C)	T_g (°C)	T_m (°C)		T_{max} (°C)
1	4.95	1.39	207	-44.8	54.9	58.6	239
2	7.56	1.59	222	-45.1	45.1	57.4	260
3	42.2	1,90	266	-44.8	50.9	63.3	343
4	83.2	2.29	264	-44.9	50.4	61.1	329

4.4.4 Thermal Recyclability of Chain-End Capped PγBL-OR

To address a question of whether chain-end capping would hinder the thermal recyclability of OH-protected P*γ*BL materials, the thermal recyclability of post-functionalized polymers was examined by heating the bulk material BnO-

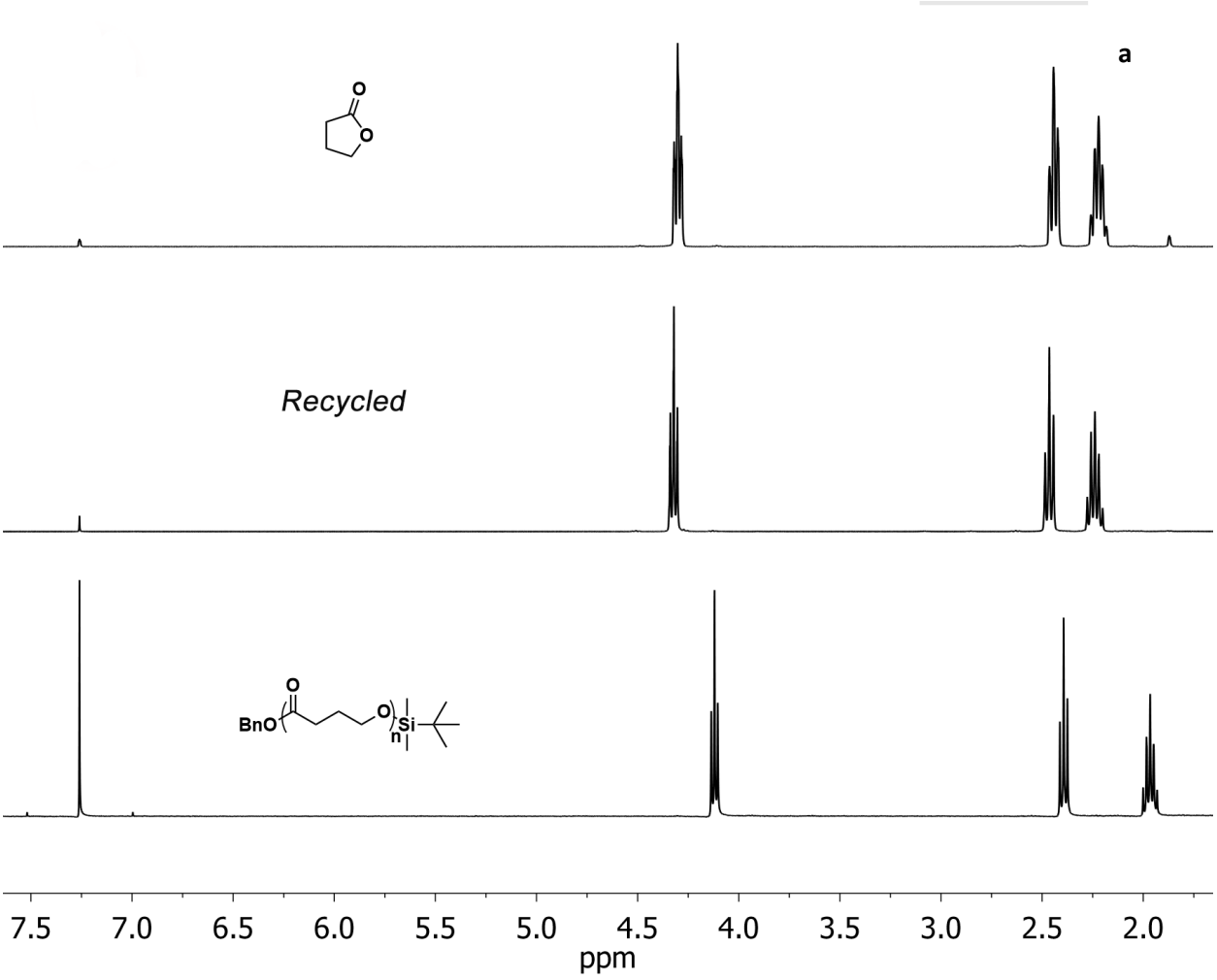

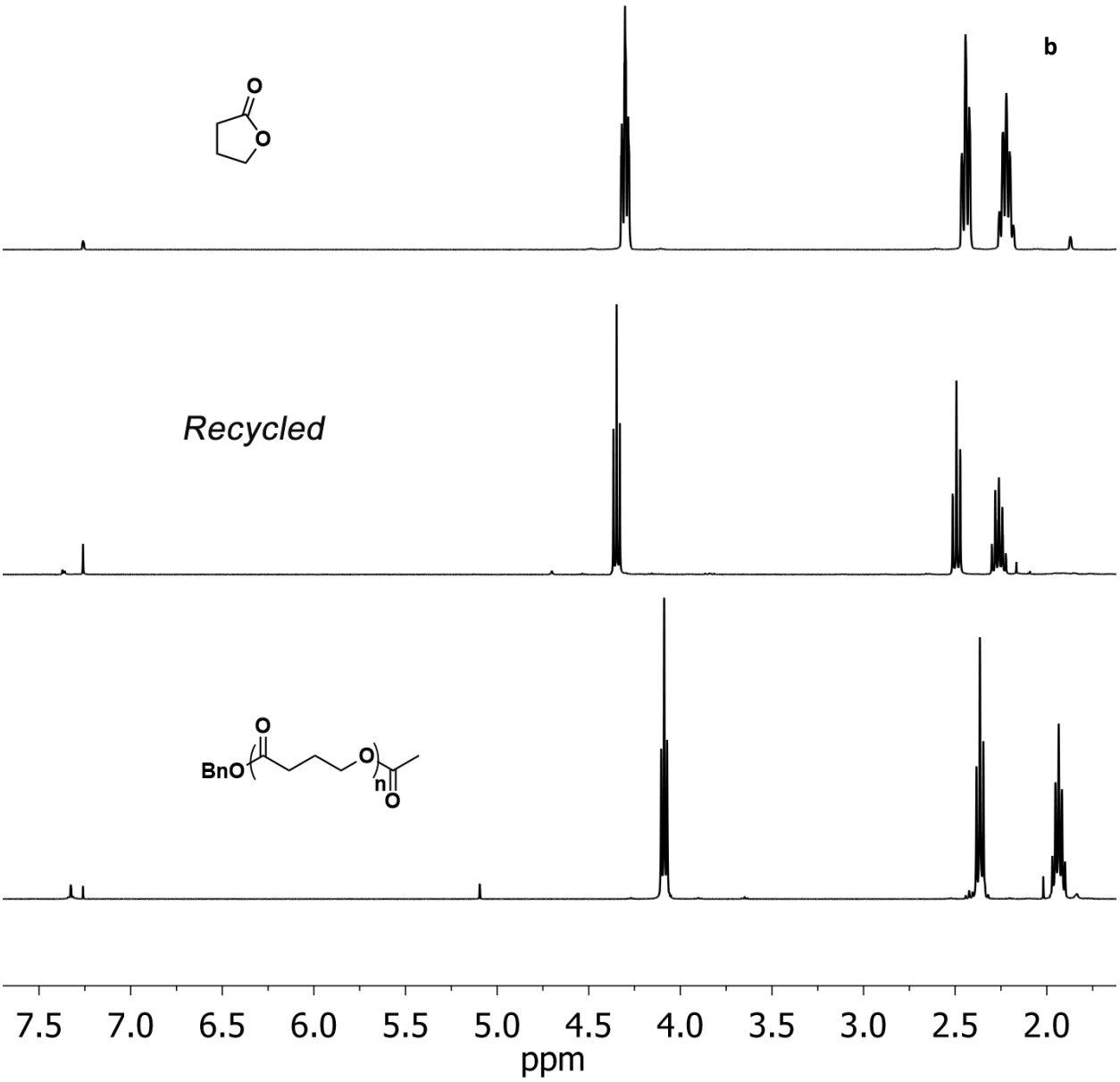

Figure 4.7 Overlays of ^{1}H NMR spectra (25 ^{o}C, $CDCl_3$, with residual solvent peaks at 7.26 and 1.56 ppm for $CHCl_3$ and H_2O, respectively): **a,** bottom, BnO-$[C(=O)(CH_2)_3O]_n$-$SiMe_2CMe_3$; middle, the liquid recovered after depolymerization; top, pure γ-BL monomer for comparison. **b,** bottom, BnO-$[C(=O)(CH_2)_3O]_n$-C(=O)Me; middle, the liquid recovered after depolymerization; top, pure γ-BL monomer for comparison.

$[C(=O)(CH_2)_3O]_n$-$SiMe_2CMe_3$ (M_n = 83.2 kg/mol) at 250 °C for 5 h and BnO-$[C(=O)(CH_2)_3O]_n$-C(=O)Me (M_n = 7.63 kg/mol) at the same temperature for 2 h under a nitrogen atmosphere in a sealed tube. After cooling to ambient temperature, the colorless liquid formed was directly (without any purification) analyzed by ^{1}H NMR spectroscopy (Figure. 6), which revealed the complete conversion of P*γ*BL back into *γ*-BL after thermal depolymerization. Noteworthy also is that the thermal decomposition of P*γ*BL back into its monomer *γ*-BL was quantitative for both silyl and acyl protected polymers, thereby demonstrating that the post-functionalized, chain-end capped P*γ*BL also exhibits full thermal recyclability, just like the unprotected P*γ*BL.

4.4.5 Hydrolytic Degradation Profiles of Chain-End Capped PγBL-OR

The hydrolytic degradation behavior of an end-capped P*γ*BL, BnO-$[C(=O)(CH_2)_3O]_n$-C(=O)Me, was examined in comparison with uncapped BnO-$[C(=O)(CH_2)_3O]_n$-H by monitoring the weight changes of the polymer film specimens immersed in neutral, acidic, and basic aqueous solutions. Figure 4.8 shows the weight remaining profiles of the polymer samples as a function of time (in days). As can be seen from the profiles depicted in Figure 4.8, the degradation rates of the polymer samples in different aqueous solutions are substantially different, which follow the degradation rate order of OH^-/H_2O >> H^+/H_2O > H_2O. Compared with uncapped BnO-$[C(=O)(CH_2)_3O]_n$-H, the hydrolytic degradation of end-capped BnO-$[C(=O)(CH_2)_3O]_n$-C(=O)Me is significantly slower, especially in the basic aqueous solution. For example, only 33.7 % of the weight remained for the uncapped polymer after 4 days, while the capped polymer still had 50.8% of the weight remained. The rate differences in neutral water and acidic aqueous solution were much smaller as both types of polymers degrade rather slowly under such conditions, but the overall trend was still the same. Overall, this study showed that chain-end capping by

removing the active, nucleophilic OH group enhances resistance towards hydrolytic degradation, especially the basic medium. These results are consistent with the hypothesis that the hydrolytic degradation prefers to proceed at the chain-end site due to the high surface area and higher reactivity of chain ends.

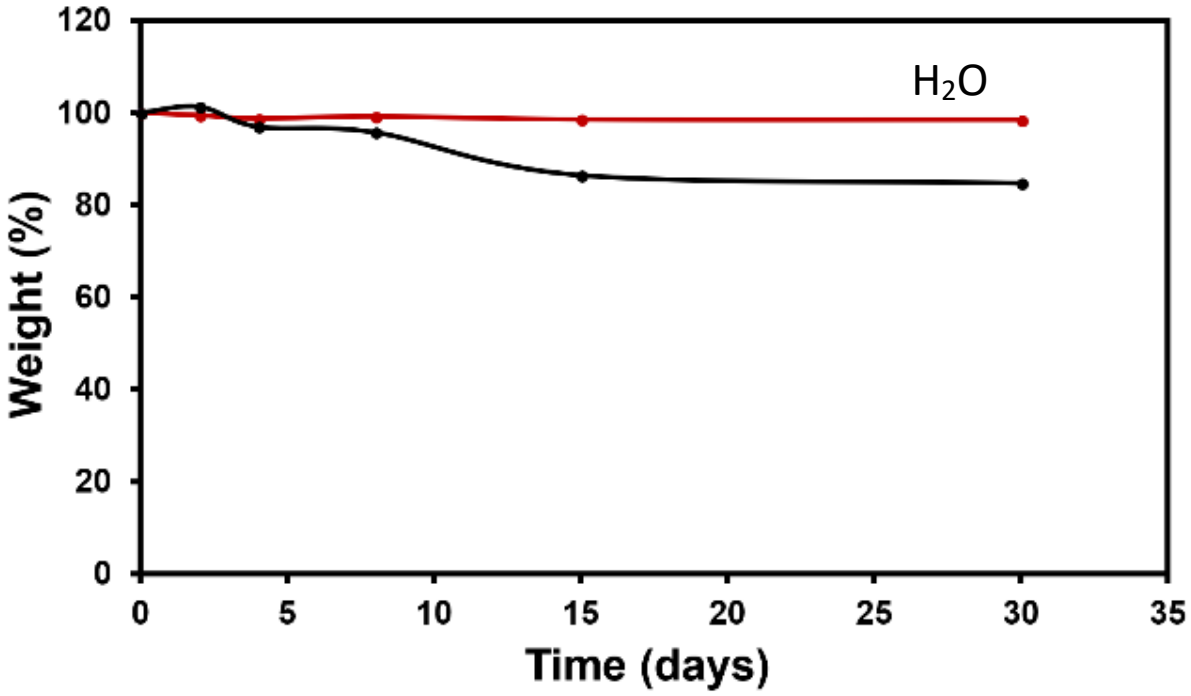

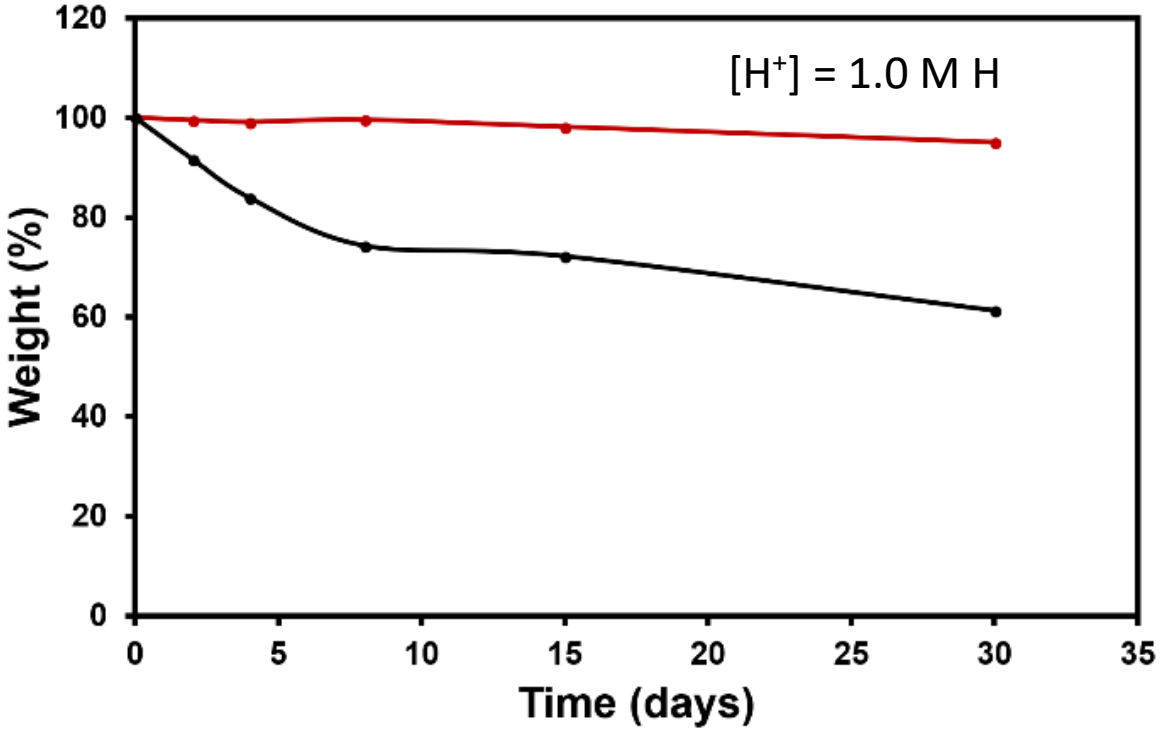
[H+] = 1.0 M H
Weight (%)
Time (days)
0
20
40
60
80
100
120
0
5
10
15
20
25
30
35

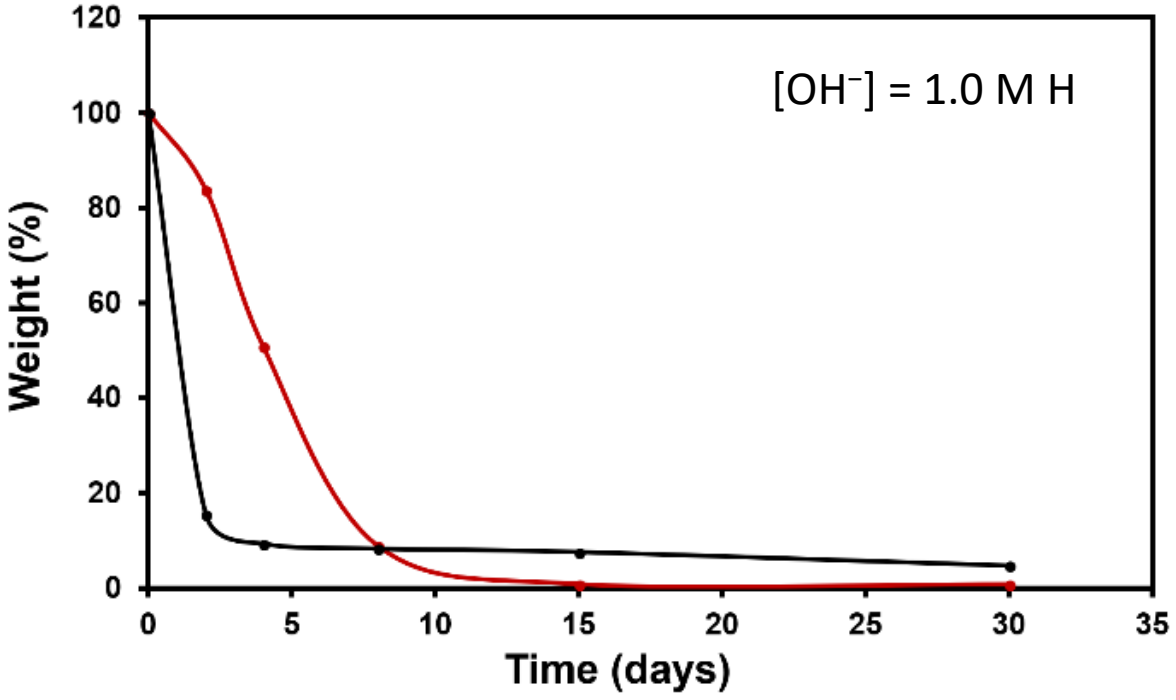
[OH−] = 1.0 M H
Weight (%)
Time (days)
0
20
40
60
80
100
120
0
5
10
15
20
25
30
35

Figure 4.8 Hydrolytic degradation profiles of BnO-[C(=O)$(CH_2)_3$O]$_n$-H (black) and BnO-[C(=O)$(CH_2)_3$O]$_n$-C(=O)Me (red) in deionized water (top), acidic aqueous solution (middle), and basic aqueous solution (bottom).

4.4.6 Dynamic Mechanical Behavior of Chain-End Capped PγBL-OR

Unprotected PγBL and end-capped BnO-[C(=O)$(CH_2)_3$O]$_n$-$SiMe_2CMe_3$ (M_n = 83.2 kg/mol) film specimens for dynamic mechanical analysis (DMA, Figure 4.9) were prepared by compression molding of the polymers. At ambient temperature of 25 °C (i.e., in the rubbery state), the unprotected PγBL-OH polymer had a storage modulus (E') of 260 MPa and a loss modulus (E'') of 7.8 MPa. In comparison, the PγBL end-capped by the $SiMe_2CMe_3$ group exhibited a somewhat lower E' of 220 MPa but a comparable E'' of 8.7 MPa, which indicates that the $SiMe_2CMe_3$ end-capped polymer is a somewhat more flexible material relative to the uncapped one. At a low temperature of –80 °C (i.e., in the glassy state), the difference in storage modulus was larger, with E' = 2.8 GPa and 2.4 GPa for the unprotected and end-capped polymer, respectively, showing again the more rigid chain for the uncapped polymer.

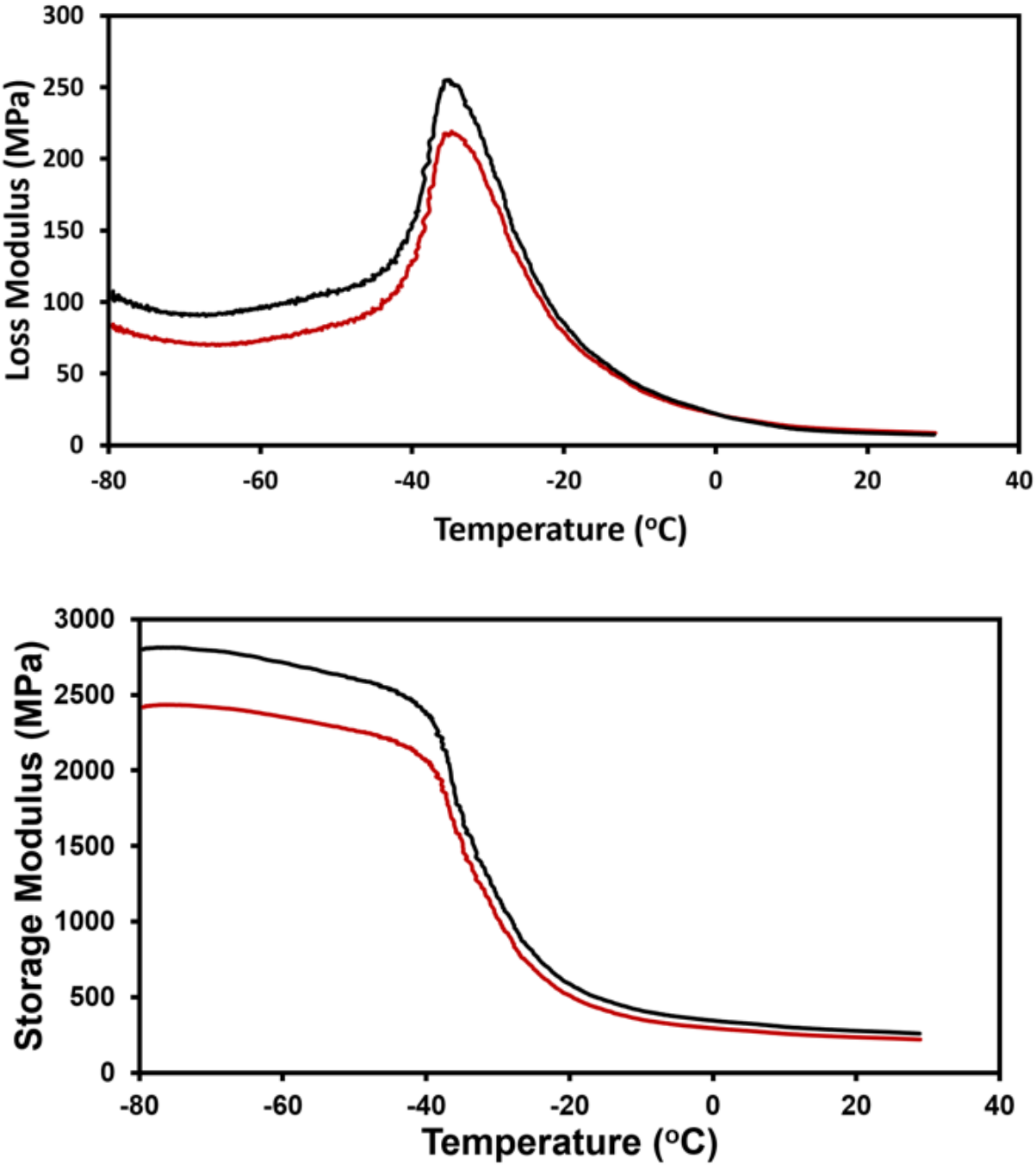

Figure 4.9 DMA (tension film mode) curves of unprotected BnO-[C(=O)$(CH_2)_3$O]$_n$-H (black) and end-capped BnO-[C(=O)$(CH_2)_3$O]$_n$-$SiMe_2CMe_3$ (red).

4.5 Conclusions

This work was centered on addressing a fundamental question of whether linear PγBL-OH can be modified to behave just like its cyclic analog in properties most sensitive to the OH group in the chain end by protecting the OH group with the more robust OR group in the form of PγBL-OR. To answer this question, we have examined the effects of PγBL polymers with different initiation and termination chain ends as well as molecular weight on five types of materials properties, including thermal stability, thermal transitions, thermal recyclability, hydrolytic degradation, and dynamic mechanical behavior. For this purpose, four different chain-end capped polymers with similar molecular weights, BnO-$[C(=O)(CH_2)_3O]_n$-R, where R = C(=O)Me, C(=O)CH=CH_2, C(=O)Ph, and $SiMe_2CMe_3$, along with a series of unprotected polymers, R'O-$[C(=O)(CH_2)_3O]_n$-H (R' = Bn, Ph_2CHCH_2) with M_n ranging from low (4.95 kg/mol) to high (83.2 kg/mol), have been synthesized. In the low molecular regime (M_n from 5.0 to ~40 kg/mol), there exhibited a large effect of molecular weight on the T_d value of the polymer, while in the higher molecular regime from 42.2 kg/mol to 83.2 kg/mol, there was essentially no further change in the T_d value.

While the initiation chain end was found to have a negligible effect on the polymer thermal stability, the termination chain end showed a large effect on polymer decomposition temperature. Thus, relative to the uncapped polymer with a similar molecular weight, chain-end capped PγBL-OR significantly enhanced the T_d value by 55, 65, 78, and 112 ^oC for R = C(=O)Ph, C(=O)CH=CH_2, C(=O)Me, and $SiMe_2CMe_3$, respectively. Chain-end capping also enhanced resistance towards hydrolytic degradation, especially in the basic medium. On the other hand, chain-end capping exerted minimal to negligible influence on polymer thermal transition temperatures, thermal recyclability, and dynamic mechanical behavior. Hence, for those

properties that are highly sensitive to the chain ends such as thermal stability and hydrolytic degradation, chain-end capping can indeed render the protected linear PγBL behaving much like the cyclic PγBL. Thus, OH end-group protection/ capping provides a simple and convenient approach to modulate the properties of PγBL-based materials. It is yet to be seen if the results reported herein could be extended to other polyesters.

References

(1) J.-F. Carpentier, *Organometllics* **2015**, *34*, 4175-4189.

(2) M. A. Hillmyer, W.B. Tolman, *Acc. Chem. Res.* **2014**, *47*, 2390-2396.

(3) A. Sauer, A. Kapelski, C. Fliedel, S. Dagorne, M. Kol, J. Okuda, *Dalton Trans.* **2013**, *42*, 9007–9023.

(4) C. Jérôme, P. Lecomte, *Adv. Polym. Sci.* **2012**, *245*, 173–217.

(5) N. E. Kamber, W. Jeong, R. M. Waymouth, R. C. Pratt, B. G. G. Lohmeijer, J. L. Hedrick, *Chem. Rev.* **2007**, *107*, 5813−5840.

(6) M. K. Kiesewetter, E. J. Shin, J. L. Hedrick, R. M. Waymouth, *Macromolecules* **2010**, *43*, 2093−2107.

(7) O. Coulembier, P. Degee, J. L. Hedrick, P. Dubois, *Prog. Polym. Sci.* **2006**, *31*, 723−747.

(8) C. Thomas, B. Bibal, *Green Chem.* **2014**, *16*, 1687−1699.

(9) A. P. Dove, *ACS Macro Lett.* **2012**, *1*, 1409−1412.

(10) C. M. Thomas, *Chem. Soc. Rev.* **2010**, *39*, 165−173.

(11) A.-C. Albertsson, I. K. Varma, *Biomacromolecules* **2003**, *4*, 1466 –1486.

(12) A.-C. Albertsson, I. K. Varma, *Adv. Polym. Sci.* **2002**, *157*, 1–40.

(13) B. J. OÏKeefe, M.A. Hillmyer, W. B. Tolman, *Dalton Trans.* **2001**, 2215 –2224.

(14) M. M. Bomgardner, *Chem. Eng. News* **2014**, *92*, 10–14.

(15) J. J. Bozell, G. R. *Petersen, Green Chem.* **2010**, *12*, 539-554.

(16) Top Value Added Chemicals from Biomass, T. Werpy, G. R. Petersen Eds.; U.S. Department of Energy report: DOE/GO-102004-101992, **2004**.

(17) M. Hong, E.Y.-X. Chen, *Nat. Chem.* **2016**, *8*, 42–49.

(18) H. R. Allcock, F. W. Lampe, J. E. Mark, *Contemporary Polymer Chemistry*, Pearson Education Inc., Upper Saddle River, 3rd ed., **2003**, p.155.

(19) G. Odian, *Principles of Polymerization*, Wiley-Interscience, New York, 3rd ed., **1991**, p.570.

(20) H. Sawada, *Thermodynamics of Polymerization*, Marcel Dekker, New York, **1976**, p.150.

(21) K. H. Houk, A. Jabbari, H. K. Hall, Jr. C. Alemán, *J. Org. Chem.* **2008**, 73, 2674–2678.

(22) M. Hong, E. Y.-X. Chen, *Angew. Chem. Int. Ed.* **2016**, *55*, 4188 –4193.

(23) N. Zhao, C. Ren, H. Li, Y. Li, S. Liu, Z. Li, *Angew. Chem. Int. Ed.* **2017**, *56*, 12987–12990.

(24) J.-B. Zhu, E. M. Watson, J. Tang, E. Y.-X. Chen, *Science* **2018**, *360*, 398-403.

(25) H. Sardon, A. P. Dove, *Science* **2018**, *360* 380-381.

(26) M. Hong, X. Tang, B. S. Newell, E. Y.-X. Chen, *Macromolecules* **2017**, *50*, 8469−8479.

(27) Y. Shen, J. Zhang, N. Zhao, F. Liu, Z. Li, *Polym. Chem.* **2018**, *9*, 2936-2941.

(28) J. A. Kaitz, C. E. Diesendruck, J. S. Moore, *J. Am. Chem. Soc.* **2013**, *135*, 12755−12761.

(29) W. Pyckhout-Hintzen, A. Wischnewski, D. Richter, *Polymer* **2016**, *105*, 378-392.

(30) Y. A. Chang, R. M. Waymouth, *J. Polym. Sci. Part A Polym. Chem.* **2017**, *55*, 2892–2902.

(31) G. Morgese, L. Trachsel, M. Romio, M. Divandari, S. N. Ramakrishna, E. M. Benetti, *Angew. Chem. Int. Ed.* **2016**, *55*, 15583 –15588.

(32) X.-Y. Tu, M.-Z. Liu, H. Wei, *J. Polym. Sci. Part A Polym. Chem.* **2016**, *54*, 1447–1458.

(33) D. R. Christopher, L. Hong, A. A. Khalil, B. W. Kenneth, S. V. Adam, *Nat. Chem.* **2016**, *8*, 791-796.

(34) P. Polanowski, J. K. Jeszka, A. Sikorski, *Macromolecules* **2014**, *47*, 4830-4839.

(35) Z. F. Jia, M. J. Monteiro, *J. Polym. Sci. Part A Polym. Chem.* **2012**, *50*, 2085-2097.

(36) T. Yamamoto, Y. Tezuka, *Polym. Chem.* **2011**, *2*, 1930-1941.

(37) H. R. Kricheldorf, *J. Polym. Sci. Part A Polym. Chem.* **2010**, *48*, 251-284.

(38) T. J. Farmer, J. W. Comerford, A. Pellis, T. Robert, *Polym. Int.* **2018**, DOI 10.1002/pi.5573.

(39) S. Agar, E. Baysak, G. Hizal, U, Tunca, H, Durmaz, *J. Polym. Sci. Part A Polym. Chem.* **2018**, *56*, 1181-1198.

(40) S. Li, L. T. Beringer, S. Y. Chen, S. Averick, *Polymer* **2015**, *78*, 37-41.

(41) I. Natori, H, Sato, S. Z. Natori, *Polym. Int.* **2008**, *57*, 219-225.

(42) M. Petenzi, T. Bavaro, C. Cornaggia, D. Ubiali, M. Pregnolato, D. Pasini, *Polym. Int.* **2012**, *61*, 1611-1618.

(43) C. E. Schweitzer, R. N. MacDonald, J. O. Punderson, *J. Appl. Polymer Sci.* **1959**, *1*, 158-163.

(44) W. H. Linton, H. H. Goodman, *J. Appl. Polymer Sci.* **1959**, *1*, 179-184.

(45) R. G. Alsup, J. O. Punderson, G. F. Leverett, *J. Appl. Polymer Sci.* **1959**, *1*, 185-191.

(46) A. D. Wong, M. A. DeWit, E. R. Gillies, *Adv. Drug Delivery Rev.* **2012**, *64*, 1031-1045.

(47) S. T. Phillips, A. M. DiLauro, *ACS Macro Lett.* **2014**, *3*, 298-304.

(48) G. I. Peterson, M. B. Larsen, A. J. Boydston, *Macromolecules* **2012**, *45*, 7317-7328.

(49) B. Fan, J. F. Trant, A. D. Wong, E. R. Gillies, *J. Am. Chem. Soc.* **2014**, *136*, 10116−10123.

(50) F. Burel, L. Rossignol, P. Pontvianne, J. Hartman, N. Couesnon, C. Bunel, *e-Polymers* **2003**, *3*, doi:10.1515/ epoly.2003.3.1.407

(51) H. Ito, C. G. Willson, *Polym. Eng. Sci.* **1983**, *23*, 1012– 1018.

(52) O. Vogl, *J. Polym. Sci. Part A Polym. Chem*. **2000***, 38*, 2293–2299.

(53) A. Fukuzawa, H. Sato, T. Masamune, *Tetrahedron Lett.* **1987**, *28*, 4303–4306.

(54) L. V. Hijfte; R. D. Little, *J. Org. Chem.* **1985**, *50*, 3940–3942.

(55) O. Sirkecioglu, B. Karliga, N. Talinli, *Tetrahedron Lett.* **2003**, *44*, 8483–8485.

(56) E. J. Corey, J.-L. Gras, P. Ulrich, *Tetrahedron Lett.* **1976**, *17*, 809–812.

(57) H. M. Lee, C. Nieto-Oberhuber, M. D. Shair, *J. Am. Chem. Soc.* **2008**, *130*, 16864–16866.

(58) D. Enders, G. Geibel, S. Osborne, *Chem. Eur. J.* **2000**, *6*, 1302–1309.

(59) J. L. Marco, J. A. Hueso-Rodríguez, *Tetrahedron Lett.* **1988**, *29*, 2459–2462.

(60) H., Takaku., K. Kamaike, T. Hiromichi, *J. Org. Chem.* **1984**, *49*, 51–56.

(61) B. M. Trost, J. Waser, A. Meyer, *J. Am. Chem. Soc.* **2007**, *129*, 14556–14557. T. Mukaiyama, I. Shiina, H. Iwadare, M. Saitoh, T. Nishimura, N. Ohkawa, H. Sakoh, K. Nishimura, Y.-I. Tani, *Chem. Eur. J.* **1999**, *5*, 121–161.

(62) E. J. Corey, A. Venkateswarlu, *J. Am. Chem. Soc.* **1972**, *94*, 6190–6191.

(63) E. J. Corey, H. Cho, C. Rücker; D. H. Hua, *Tetrahedron Lett.* **1981**, *22*, 3455–3458.

(64) P. G. McDougal, J. G. Rico, Y.-I. Oh, B. D. Condon, *J. Org. Chem.* **1986**, *51*, 3388–3390.

(65) W. R. Roush, H. R. Gillis, A. P. Essenfeld, *J. Org. Chem.* **1983**, *49*, 4674–4682.

(66) J. Macor, A. J. Sampognaro, P. R. Verhoest, R. A. Mack, *Organic Syntheses* **2000**, *77*, 45–49.

(67) M. J. Robins, S. D. Hawrelak, T. Kanai, J. M. Siefert, R. Mengel, *J. Org. Chem.* **1979**, *44*, 1317–1322.

(68) Cai, C. X; Amgoune, A.; Lehmannb, C. W.; Carpentier, J.-F. *Chem. Eur. J.* **2006**, *12*, 169–179.

Chapter 5

Summary

The work described within this dissertation is focused on the polymerization of the multifunctional and bioderived monomer Tulipalin B (βHMBL) catalyzed by organocatalysts such as *N*-heterocyclic carbenes and phosphazene superbases. The reactive exo-cyclic double bond and β-hydroxyl of the five-membered lactone lead to multiple reaction pathways and more complicated scenarios than analogues MBL and MMBL. Since MBL and MMBL always undergo vinyl addition, the study of such reactions provided no critical insights into the mechanisms of Tulipalin B polymerization. The observed isomerization of βHMBL into 3-HMFO in water led to the study of the polymerization behavior of 3-HMFO. To better understand the mechanisms of the polymerization of HMBL and 3-HMFO, we simplified the monomer structures and studied the polymerization behavior of FO and its derivatives. This study helped uncovering of the polymerization mechanism of 3-HMFO and βHMBL. First, with the reactive exo-cyclic double bond in βHMBL, vinyl addition polymerization proceeds smoothly resulting the expected vinyl addition product. An interesting ene-type mechanism involving two acrylates under basic conditions, one of which bearing OH groups, shed light on the reactions between two monomers in our system. A resulting molecule has two lactone rings connected together, one with an exo-cyclic double bond and another with endo-cyclic double bond and a reactive proton at the five position. This structure then undergoes both vinyl addition polymerization and a Michael addition after the proton transfer from the lactone ring. At the same time, a water molecule is generated during the ene-type reaction which is consistent with the MALDI-TOF spectra of P (βHMBL). With comparable reactivity, the OH proton and the lactone ring proton both undergo proton transfers, followed by oxa-Michael addition and Michael addition, respectively. Although only three types of reactions (ene-type reaction, oxa-Michael addition, and proton transfer) were involved

in the mechanism, the complexity herein is mainly caused by the competitive reactivity of multiple reaction sites.

There are two subunits that can be controlled in the reaction. One is the vinyl addition product, the amount of which will dramatically decrease if the reaction is carried out in water. Another subunit is U-II unit in described in Chapter 3. With the addition of BnOH as the initiator, a six-membered transition state facilitates the proton transfer of the five-position lactone ring proton, which limits the production of subunit U-II.

Chapters 2 and 3 have focused mainly on the discovery of the new P(βHMBL) structure and the effort to study the mechanism. In Chapter 4, we reported a strategy to post-functionalize PBL to tune the end-group related properties such as the thermal and hydrolytic stability. Six commonly used reagents were used for the end-capping of the polymer, and all of them were shown to improve the decomposition temperatures and hydrolytic stability of PBL, which suggest end capping is an effective and simple method for property modifications of polymers such as PBL.

Appendix A

Experiment Details and Supporting Information for Chapter 2

A.1. Materials, Reagents, and Methods

All manipulations with air- and moisture-sensitive chemicals and reagents were performed using standard Schlenk techniques on a dual-manifold line, on a high-vacuum line, or in an inert gas (Ar or N_2)-filled glovebox. NMR-scale reactions were conducted in Teflon-valve-sealed J. Young-type NMR tubes. NMR (^{1}H and ^{13}C) spectra were recorded on a Varian Inova 400 MHz or 500 MHz spectrometer. Chemical shifts for ^{1}H and ^{13}C spectra were referenced to internal solvent resonances and are reported as parts per million relative to $SiMe_4$. DMSO-d_6 was dried over CaH_2 overnight and vacuum-distilled. HPLC-grade organic solvents were first sparged extensively with nitrogen during filling 20 L solvent reservoirs and then dried by passage through activated alumina (for Et_2O, THF, and CH_2Cl_2) followed by passage through Q-5 supported copper catalyst (for toluene and hexanes) stainless steel columns. HPLC-grade DMF was degassed and dried over CaH_2 overnight, followed by vacuum distillation (CaH_2 was removed before distillation).

The superbase phosphazene, 1-tert-butyl-4,4,4-tris(dimethylamino)-2,2-bis[tris(di- methylamino) phosphoranylidenamino]-2λ^5,4λ^5-catenadi(phosphazene) (^{t}Bu-P_4), was purchased from Sigma-Aldrich as a 1.0 M solution in hexanes; the solvent was removed under vacuum prior to use. BHT-H (2,6-di-tert-butyl-4-methylphenol) was purchased from Alfa Aesar and recrystallized from hexanes prior to use. Azobisisobutyronitrile (AIBN) was purchased from Sigma-Aldrich and recrystallized from methanol before use. NHC catalyst 1,3-di-tert-butylimidazol-2-ylidene (I^{t}Bu) and α-methylene-γ-butyrolactone (MBL) were purchased from TCI America, and selenium dioxide was purchased from Alfa Aesar Chemical Co. All other commercial reagents were used as received. NHC catalyst 1,3,4-

triphenyl-4,5-dihydro-1H-1,2,4-triazol-5-ylidene (TPT)[1] was prepared according to literature procedures.

Preparation of *β*-Hydroxy-*α*-Methylene-*γ*-Butyrolactone (βHMBL). Literature procedures[2] were modified for the preparation of βHMBL from MBL. To a solution of MBL (5.0 mL, 45.6 mmol) in dioxane (50 mL) was added SeO_2 (7.0 g, 63.1 mmol) and the reaction mixture was stirred at 80 ºC for 10 h. The resulting mixture was concentrated and the crude product was purified by flash chromatography on silica gel (CH_2Cl_2) to give βHMBL (1.5 g, 30% yield) as a pale yellow liquid at room temperature. Seven batches of the resulted βHMBL were collected for further purification by distillation at 50 ºC/10^{-5} Torr to give βHMBL (10.2 g) as colorless crystals at –40 ºC, which melts at room temperature.

^{1}H NMR (400 MHz, $CDCl_3$) for βHMBL: δ 6.37 (d, J = 2.1 Hz, 1H), 6.02 (d, J = 1.8 Hz, 1H), 4.95–4.90 (m, 1H), 4.48 (dd, J = 10.0, 3.6 Hz, 1H), 4.15 (dd, J = 10.0, 3.6 Hz, 1H), 3.86 (d, J = 5.7 Hz, 1H).

General Polymerization Procedures.

Polymerizations were performed either in 25 mL flame-dried Schlenk flasks interfaced to a dual-manifold Schlenk line for runs using external temperature bath, or in 20 mL glass reactors inside the glovebox for room temperature (~25 °C) runs. The reactor was charged with a predetermined amount of solvent and initiator. After equilibration at the desired polymerization temperature for 10 min, the polymerization was initiated by rapid addition of 200 mg monomer via a gastight syringe. After a measured time interval, a 0.1 mL aliquot was taken from the reaction mixture via syringe and quickly quenched into a 1.5 mL septum cap sealed vial containing 0.6 mL of "wet" $CDCl_3$ stabilized by 250

ppm of BHT-H; the quenched aliquots were later analyzed by ^{1}H NMR to obtain monomer conversion data. The remaining bulk polymerization reaction was immediately quenched after the removal of the last aliquot by addition of 5.0 mL of 5% HCl-acidified methanol. The quenched mixture was precipitated into 50 mL of cold methanol, filtered, washed with methanol to remove any unreacted monomer, and dried in a vacuum oven at 50 °C to a constant weight.

Polymer Characterization. Polymer number-average molecular weights (M_n) and molecular weight distributions ($Đ = M_w/M_n$) were measured by gel permeation chromatography (GPC) analyses carried out at 40 °C and a flow rate of 1.0 mL min-1, with DMF (0.02 mol/L LiBr) as the eluent, on a Waters University 1500 GPC instrument equipped with four PLgel 5 μm mixed-C columns (Polymer Laboratories; linear range of molecular weight = 200–2,000,000) and calibrated using 10 PMMA standards. Chromatograms were processed with Waters Empower software (version 2002).

Glass transition temperatures (T_g) of the polymers were measured by differential scanning calorimetry (DSC) on a Q20 DSC, TA Instruments. Polymer samples were first heated to 180 °C at 20°C/min, equilibrated at this temperature for 4 min, cooled to −80 °C at 10 °C/min, and reheated to 250 °C at 10 °C/min. All T_g values were obtained from the second scan after the thermal history was removed from the first scan. Maximum rate decomposition temperatures (T_{max}) and decomposition onset temperatures (T_{onset}) of the polymers were measured by thermal gravimetric analysis (TGA) on a Q50 TGA Thermogravimetric Analyzer, TA Instrument. Polymer samples were heated from 20 °C to 700 °C at a rate of 20 °C/min. FT-IR spectra were recorded on a Nicolet iS-50 FT-IR spectrometer for powder samples

The low molecular weight sample was analyzed by matrix-assisted laser desorption/ionization time-of-flight mass spectroscopy (MALDI-TOF MS). The experiment was performed on an Ultraflex MALDI-TOF mass spectrometer (Bruker Daltonics) operated in positive ion, reflector mode using a Nd:YAG laser at 355 nm and 25 kV accelerating voltage. The sample (1 µl) was mixed with 1µl of 2,5-dihydroxy benzoic acid (DHB, 10 mg/ml in 50% ACN, 0.1% TFA). The mixture was spotted on the MALDI target and allowed to air dry. External calibration was done using a peptide calibration mixture (4−6 peptides) on a spot adjacent to the sample. The raw data were processed in the FlexAnalysis software (version 2.4, Bruker Daltonics).

A.2. Additional Figures and Tables

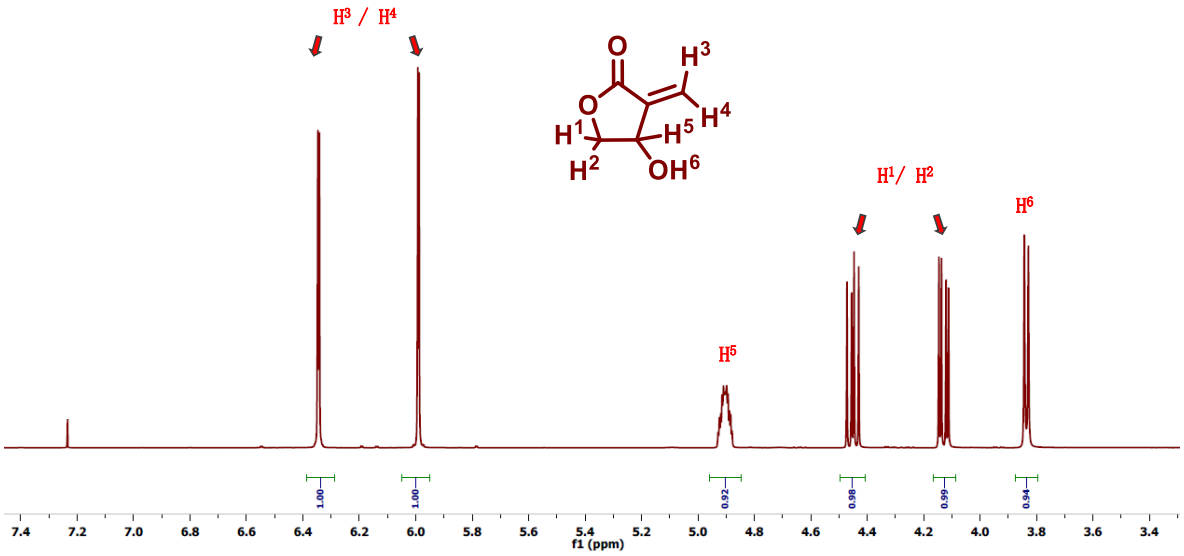

Figure S2.1. ^{1}H NMR (400 MHz, $CDCl_3$, 25 ºC) spectrum of βHMBL.

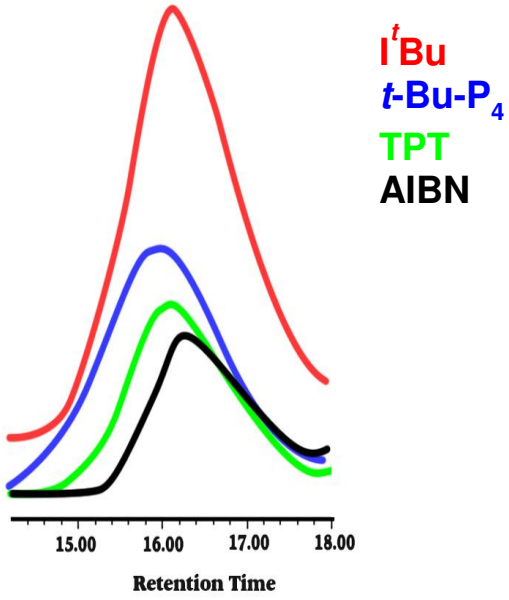

Figure S2.2 Representative GPC traces of the polymers produced by I^{t}Bu (red), ^{t}Bu-P$_4$ (blue), TPT (green), and AIBN (black).

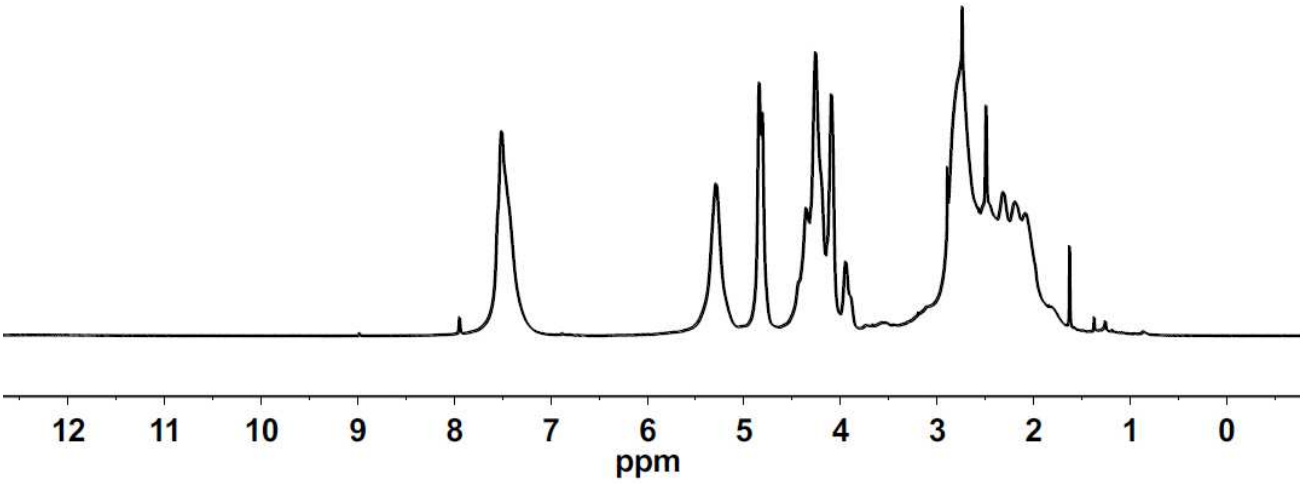

Figure S2.3. ^{1}H NMR (DMSO-d_6, 500 MHz, 80 °C) spectrum of the polymer produced by I^{t}Bu.

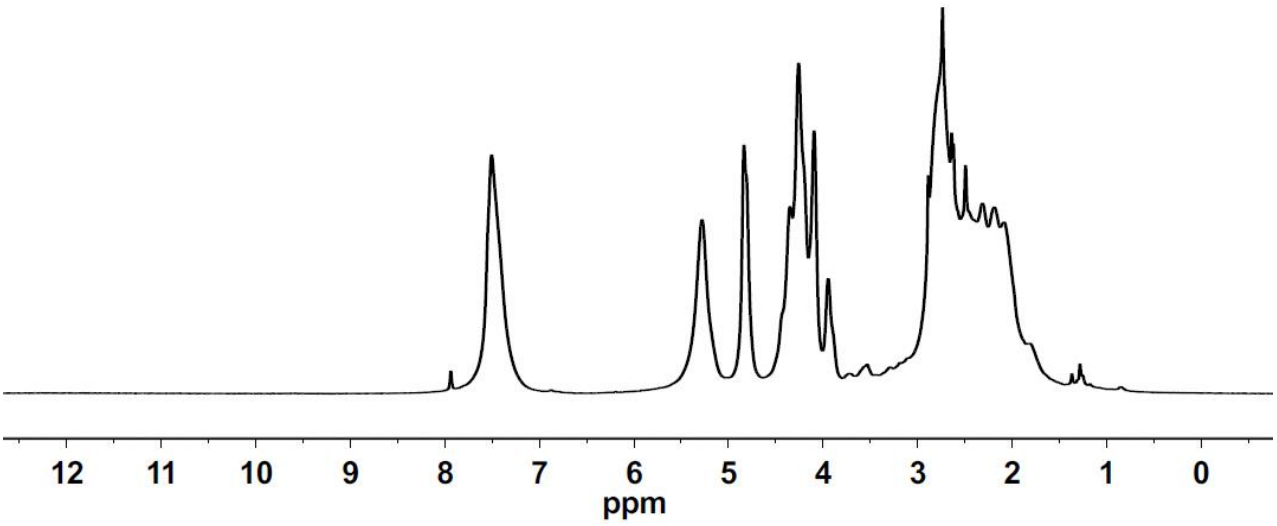

Figure S2.4. ^{1}H NMR (DMSO-d_6, 500 MHz, 80 °C) spectrum of the polymer produced by ^{t}Bu-P$_4$.

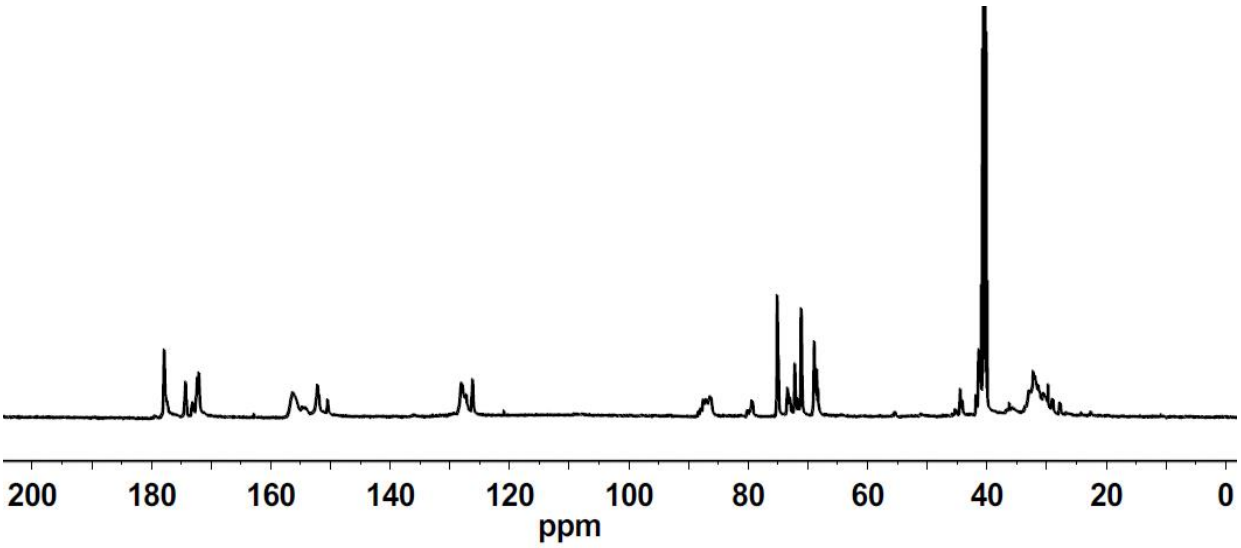

Figure S2.5. ^{13}C NMR (DMSO-d_6, 125 MHz, 80 °C) spectrum of the polymer produced by I^{t}Bu.

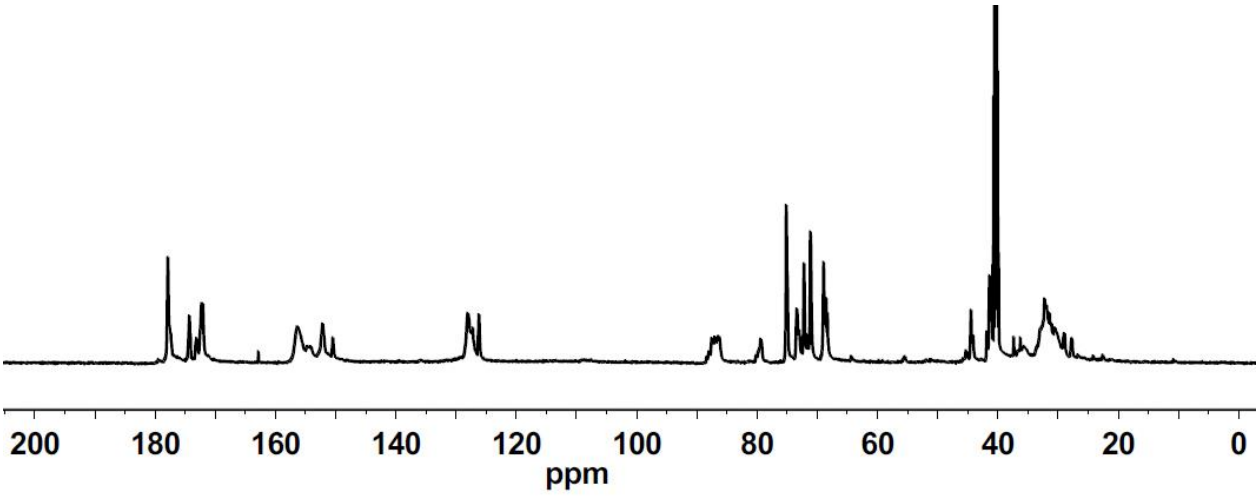

Figure S2.6. ^{13}C NMR (DMSO-d_6, 125 MHz, 80 °C) spectrum of the polymer produced by ^{t}Bu-P$_4$.

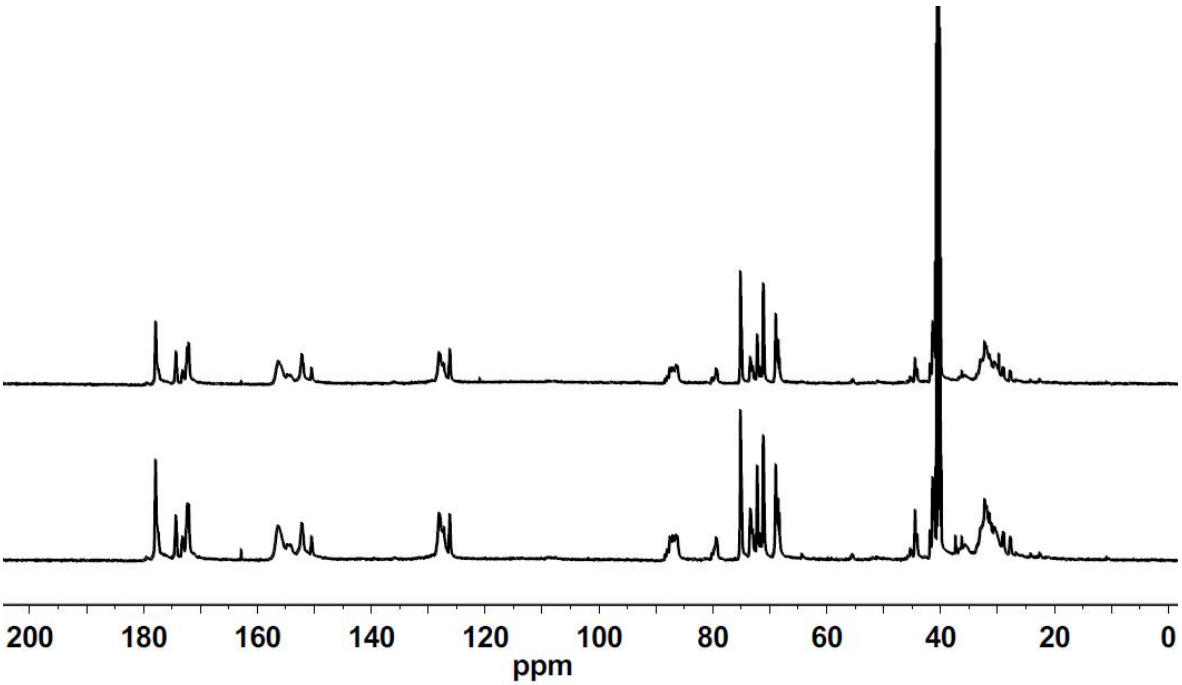

Figure S2.7. Overlay of ^{13}C NMR (DMSO-d_6, 125 MHz, 80 °C) spectra of the polymers produced by I^{t}Bu (top) and ^{t}Bu-P$_4$ (bottom).

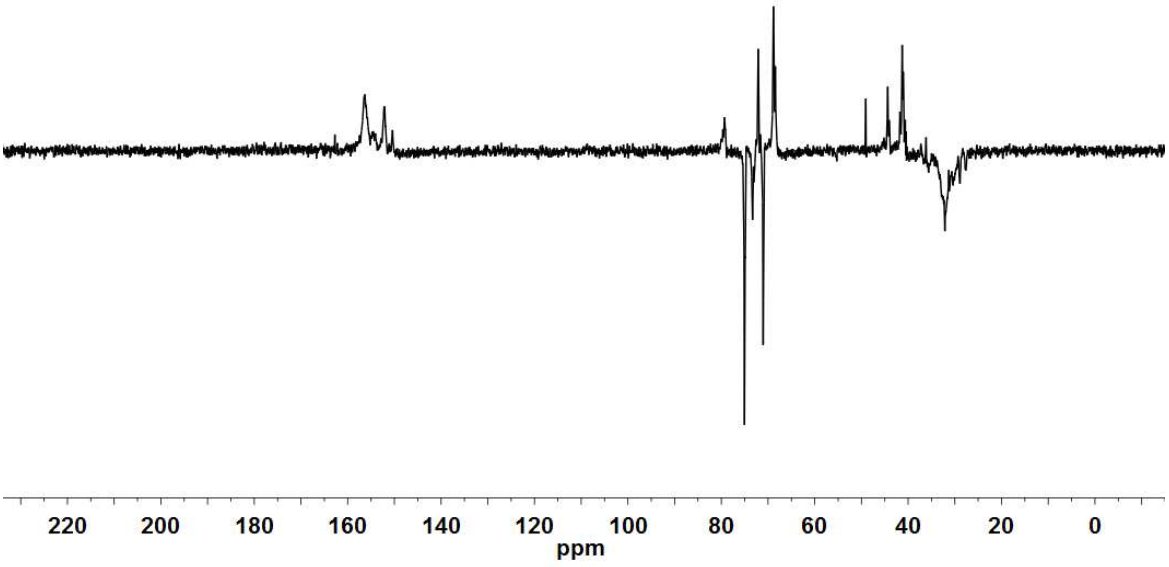

Figure S2.8. 135-DEPT (DMSO-d_6, 125 MHz, 80 °C) spectrum of the polymer produced by I^{t}Bu.

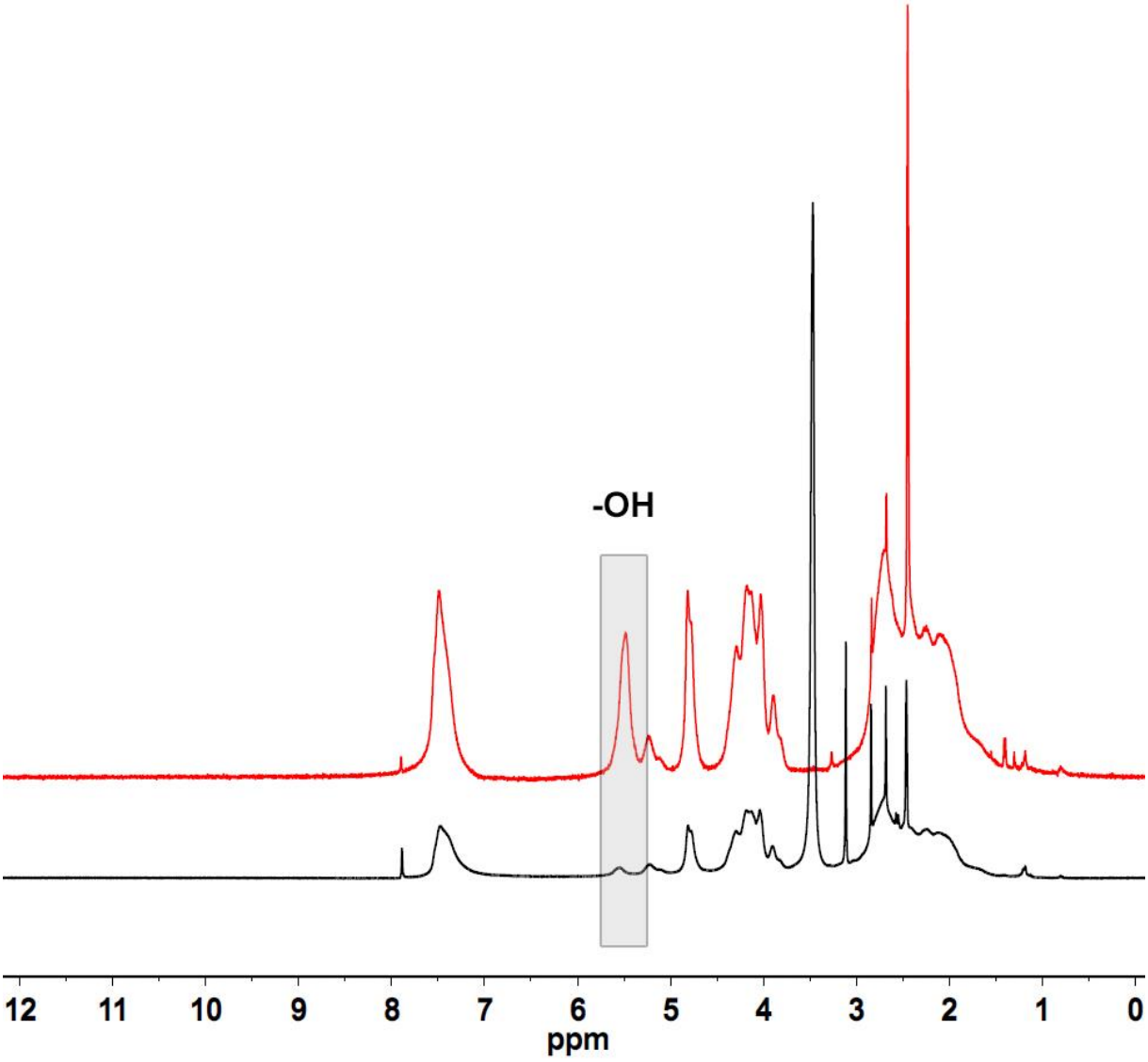

Figure S2.9. ^{1}H NMR (DMSO-d_6, 400 MHz, 25 °C) spectrum of the polymer produced by I^{t}Bu before (top, red) and after (bottom, black) addition of D_2O.

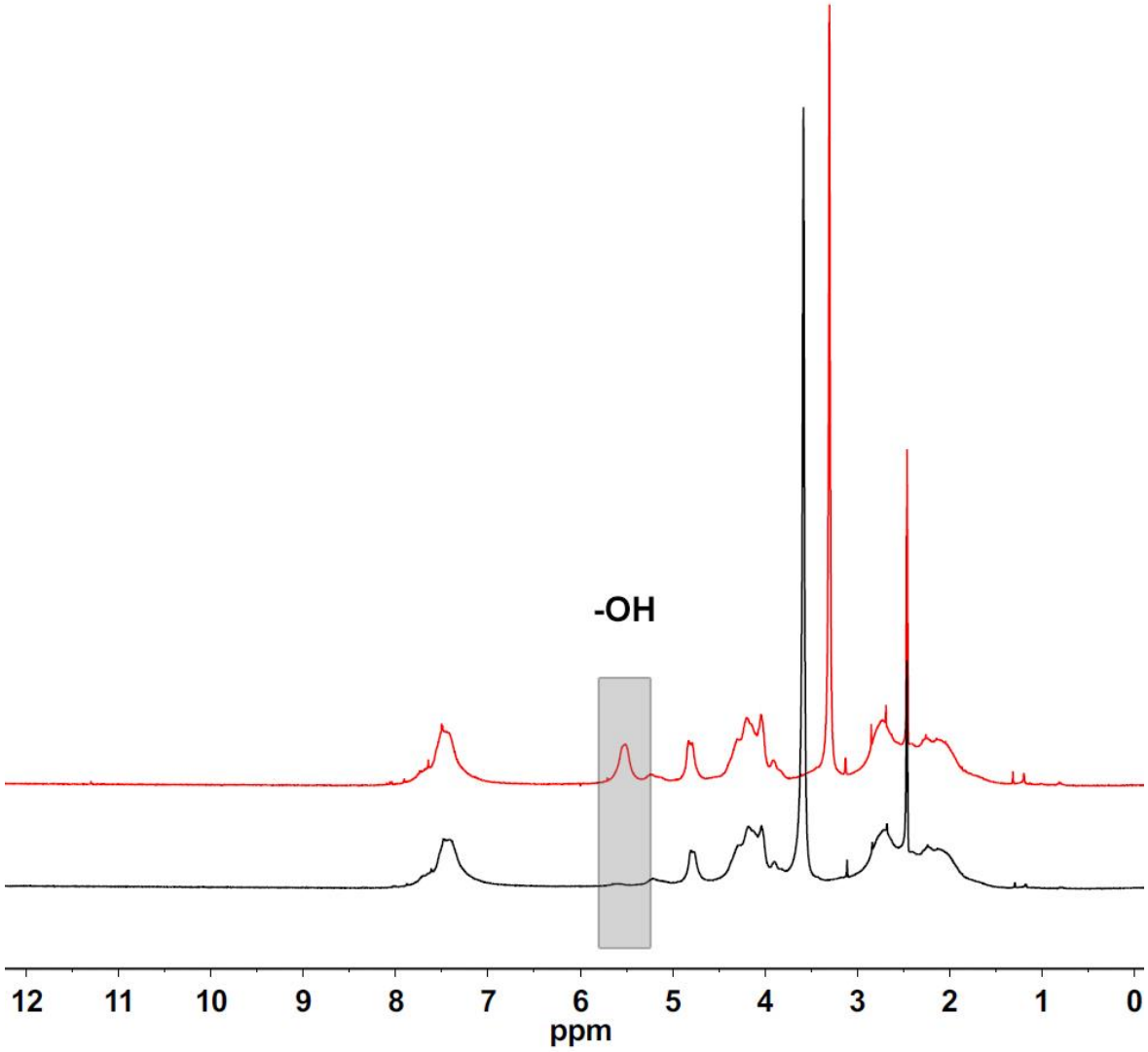

Figure S2.10. ^{1}H NMR (DMSO-d_6, 400 MHz, 25 °C) spectrum of the polymer produced by TPT before (top, red) and after (bottom, black) addition of D_2O.

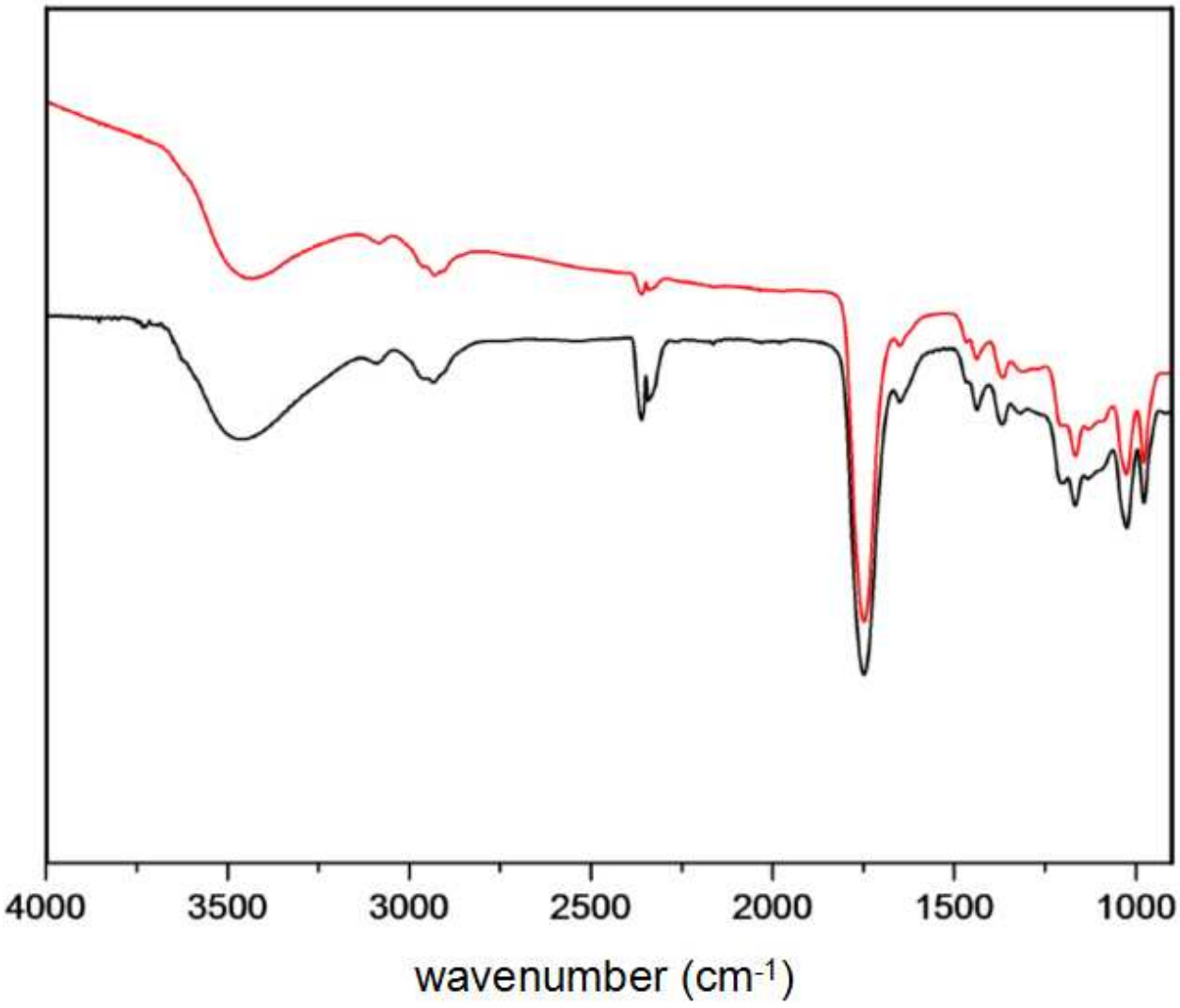

Figure S2.11. FT-IR spectra of the polymers produced by I^{t}Bu (red) and ^{t}Bu-P$_4$ (black)

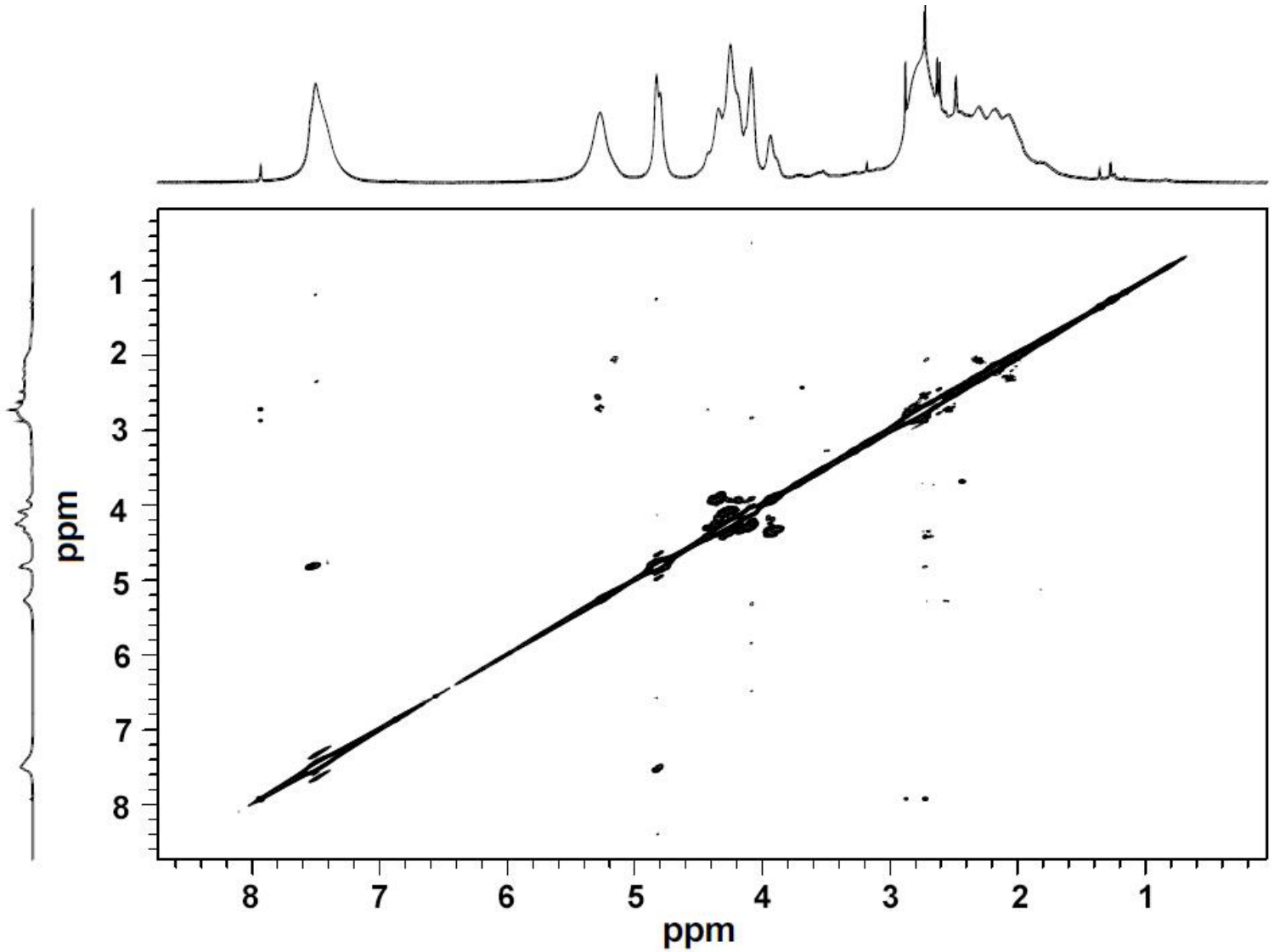

Figure S2.12. ^{1}H-^{1}H gCOSY (DMSO-d_6, 500 MHz, 80 °C) spectra of the polymer produced by I^{t}Bu.

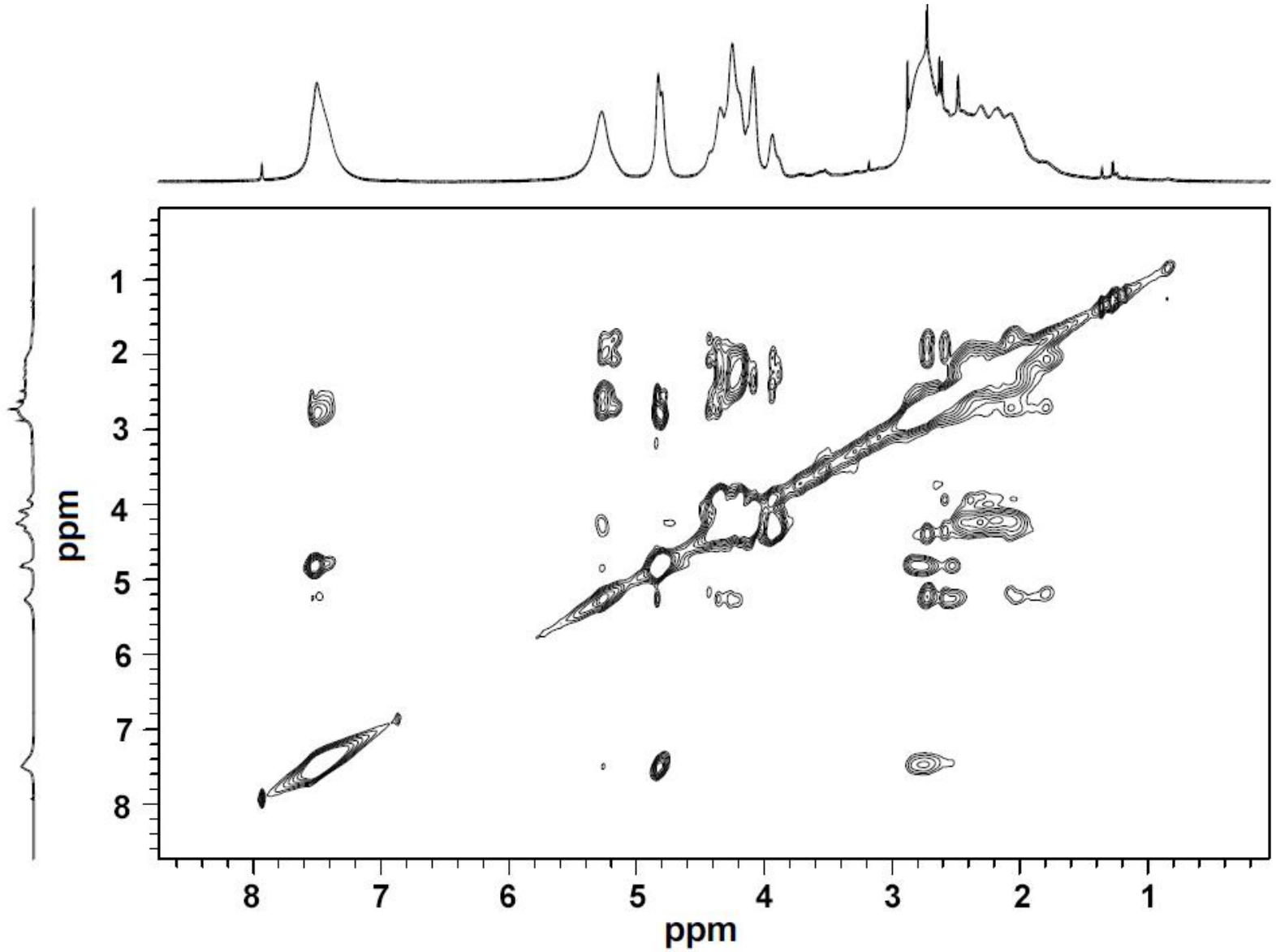

Figure S2.13. ^{1}H-^{1}H zTOCSY (DMSO-d6, 500 MHz, 80 °C) spectra of the polymer produced by I^{t}Bu.

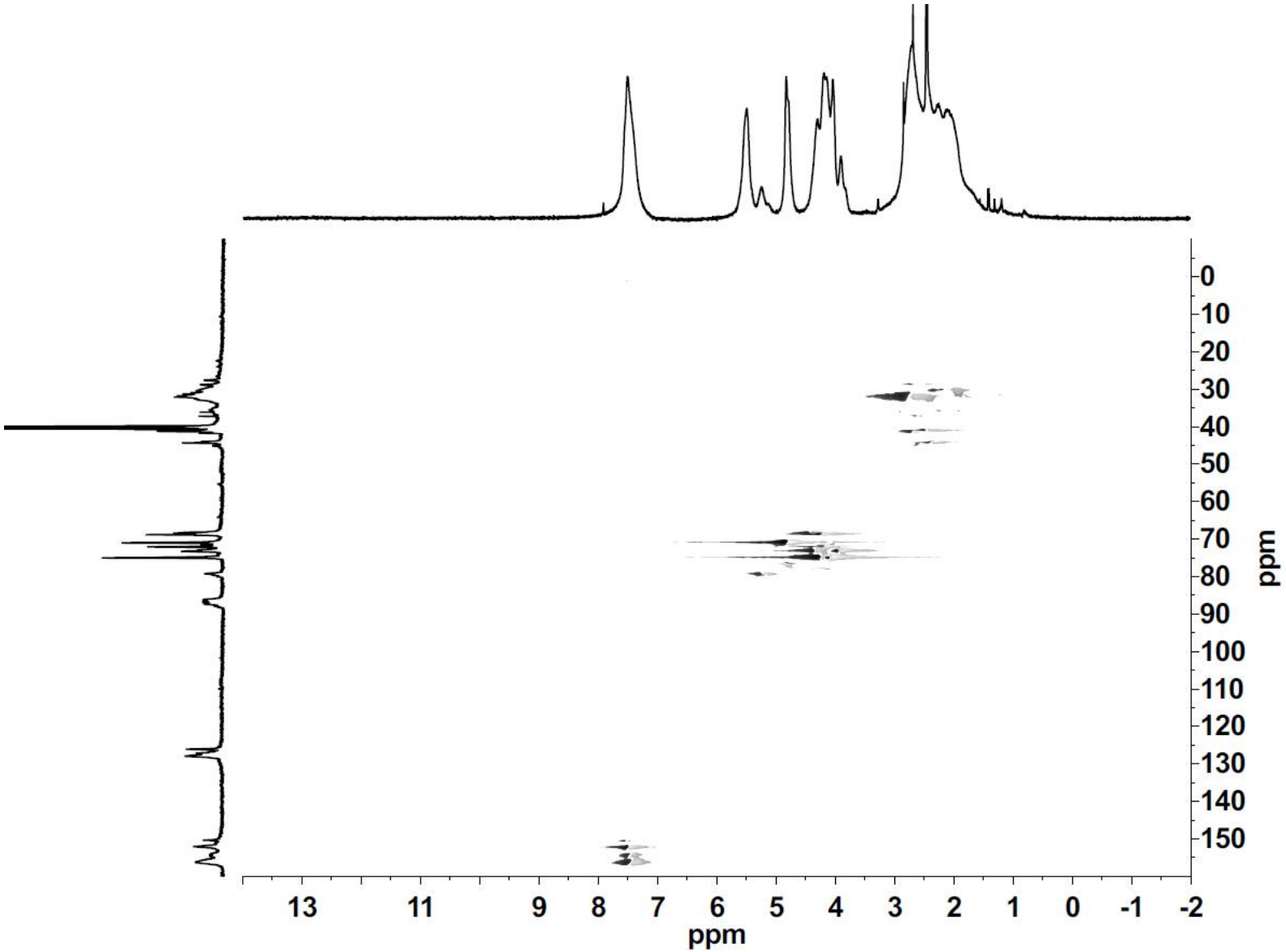

Figure S2.14. ^{1}H-^{13}C gHMQC (DMSO-d_6, 500 MHz, 80 °C) spectra of the polymer produced by I^{t}Bu.

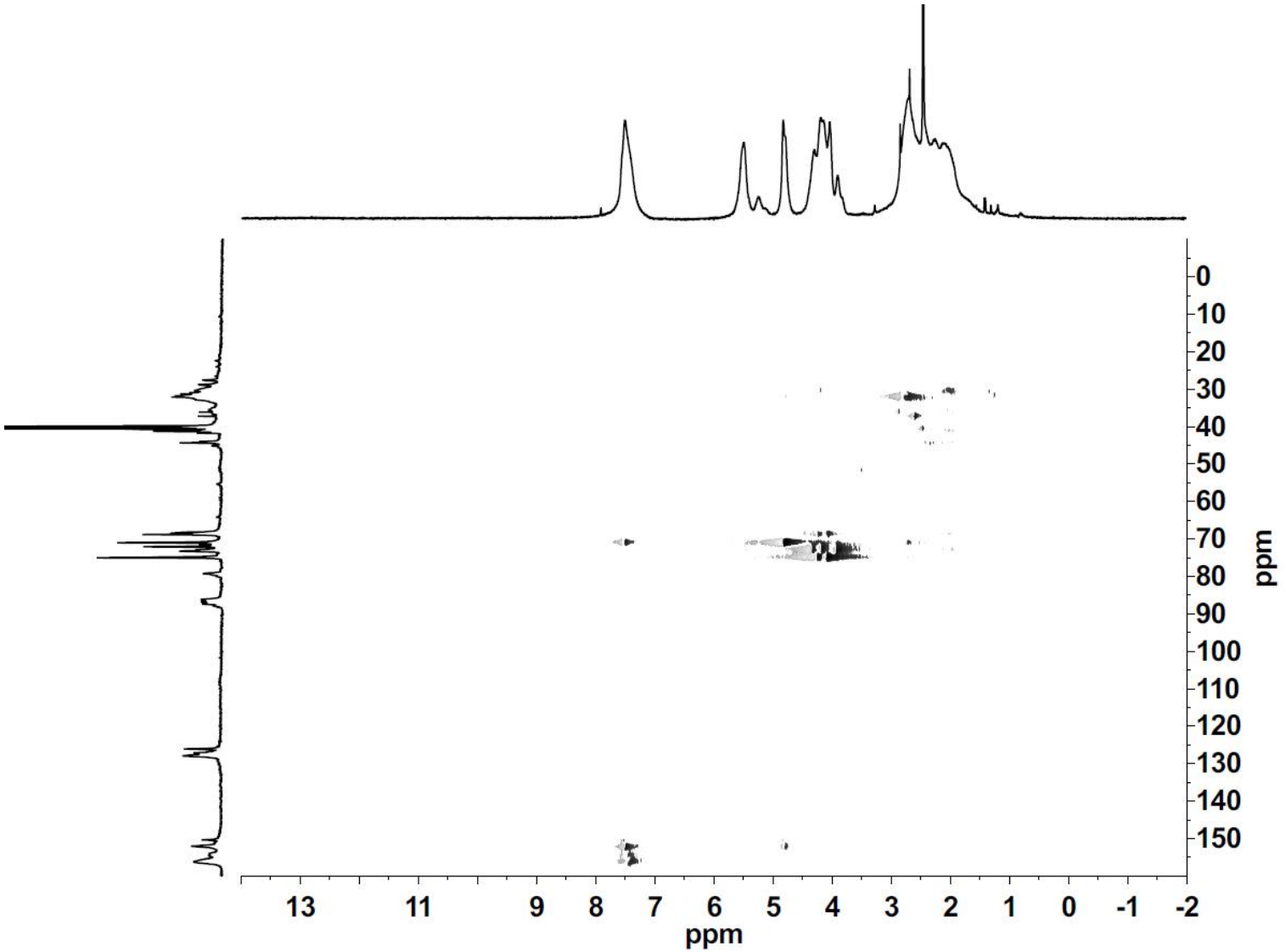

Figure S2.15. ^{1}H-^{13}C gHMQC-TOCSY (DMSO-d_6, 500 MHz, 80 °C) spectra of the polymer produced by I^{t}Bu.

References

(1) (a) Enders, D.; Breuer, K.; Raabe, G.; Runsink, J.; Teles, J. H.; Melder, J. P.; Ebel, K.; Brode, S. *Angew. Chem. Int. Ed. Engl.* **1995**, *34*, 1021−1023. (b) Enders, D.; Breuer, K.; Kallfass, U.; Balensiefer, T. *Synthesis* **2003**, 1292–1295.

(2) Mendgen, T.; Scholz, T.; Klein, C. D. Bioorg. *Med. Chem. Lett.* **2010**, *20*, 5757–5762.

Appendix B

Experiment Details and Supporting Information for Chapter 3

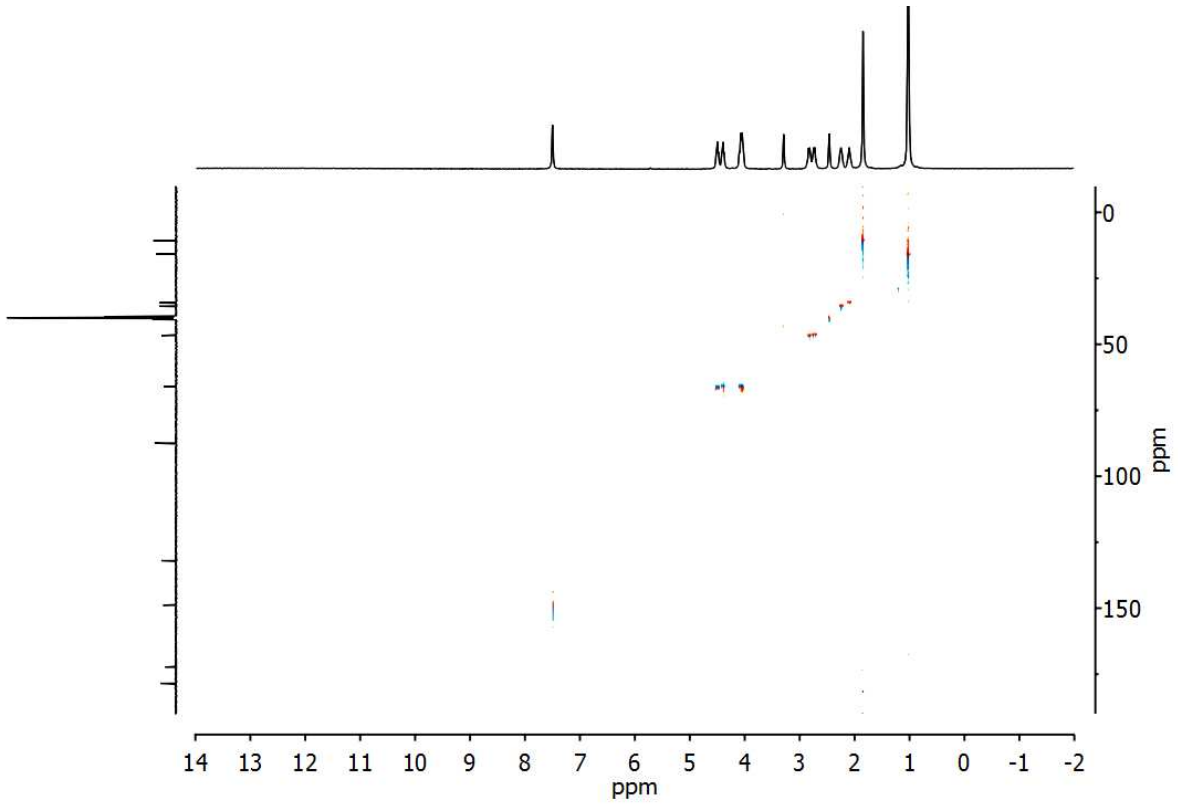

Figure S3.1. ^{1}H-^{13}C HSQCAD (DMSO-d_6, 400 MHz, 25 °C) spectrum of T(3-MFO) produced by I^{t}Bu.

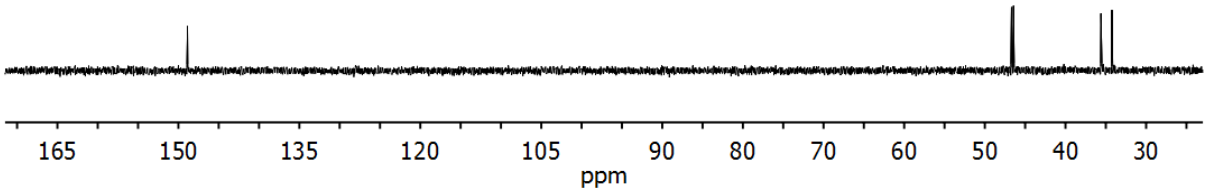

Figure S3.2. 90-DEPT (DMSO-d_6, 100 MHz, 25 °C) spectrum of T(3-MFO) produced by I^{t}Bu.

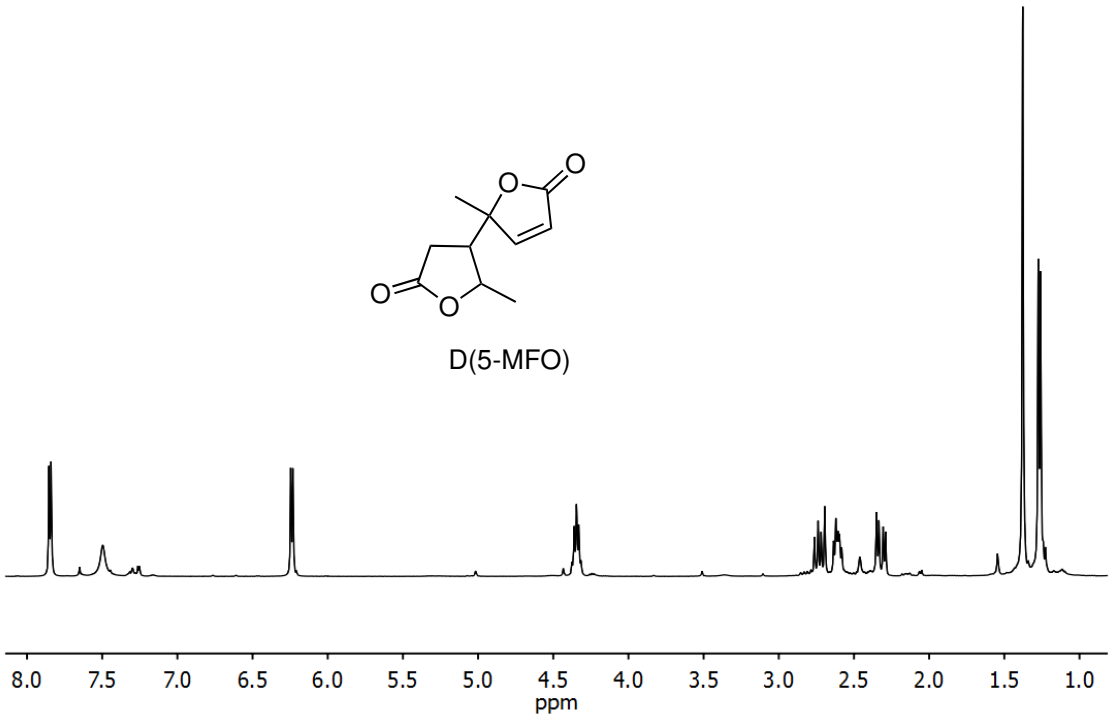

Figure S3.3. ^{1}H NMR (DMSO-d_6, 400 MHz, 25 °C) spectrum of the crude product D(5-MFO) produced by La.

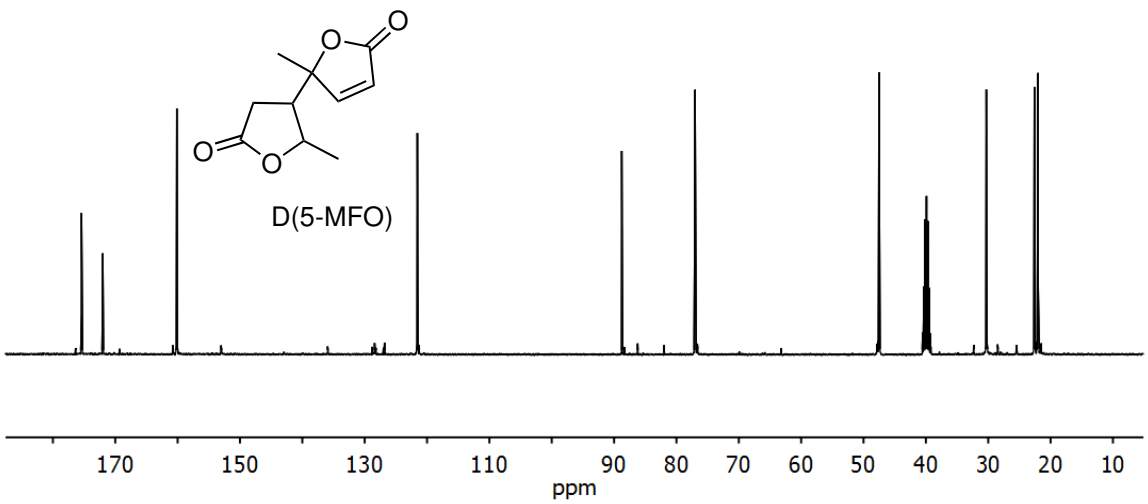

Figure S3.4. ^{13}C NMR (DMSO-d_6, 100 MHz, 25 °C) spectrum of the crude product D(5-MFO) produced by La.

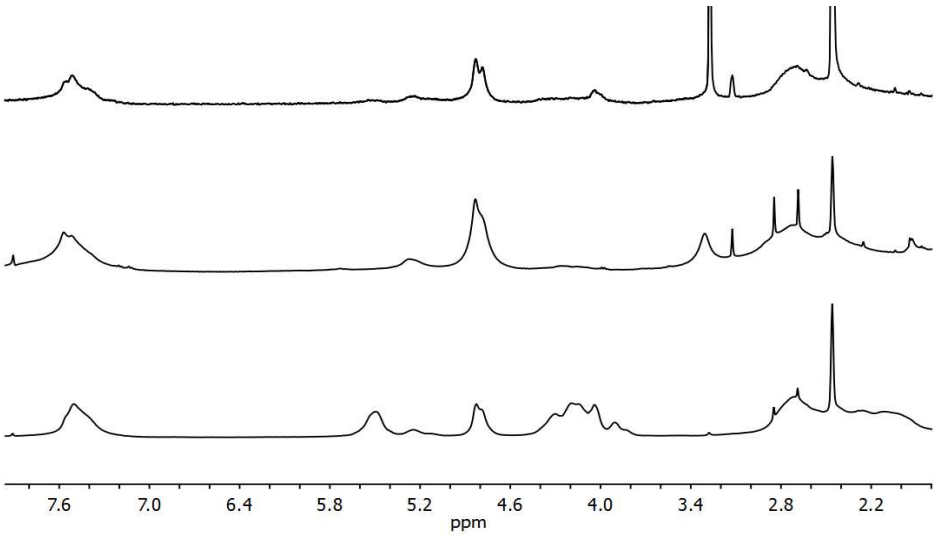

Figure S3.5. Overlay of ^{1}H NMR (DMSO-d_6, 400 MHz, 25 °C) spectra. Top: P(βHMBL) produced by KOH in water; middle: P(3-HMFO); bottom: P(βHMBL) produced by ^{t}Bu-P$_4$ in DMF.

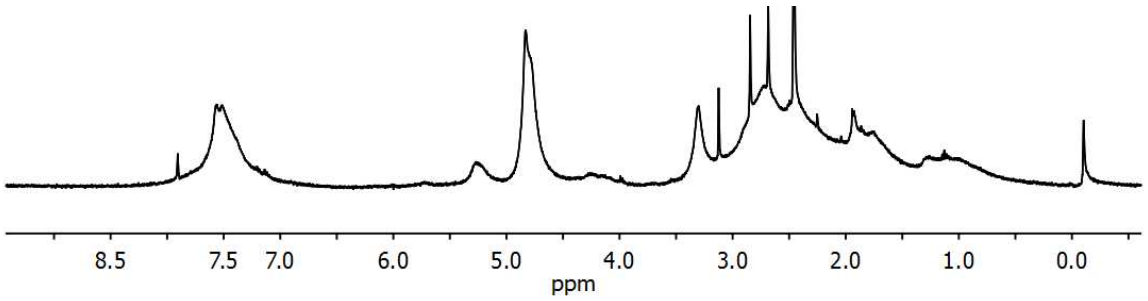

Figure S3.6. ^{1}H NMR (DMSO-d_6, 400 MHz, 25 °C) spectrum of Poly(3-HMFO).

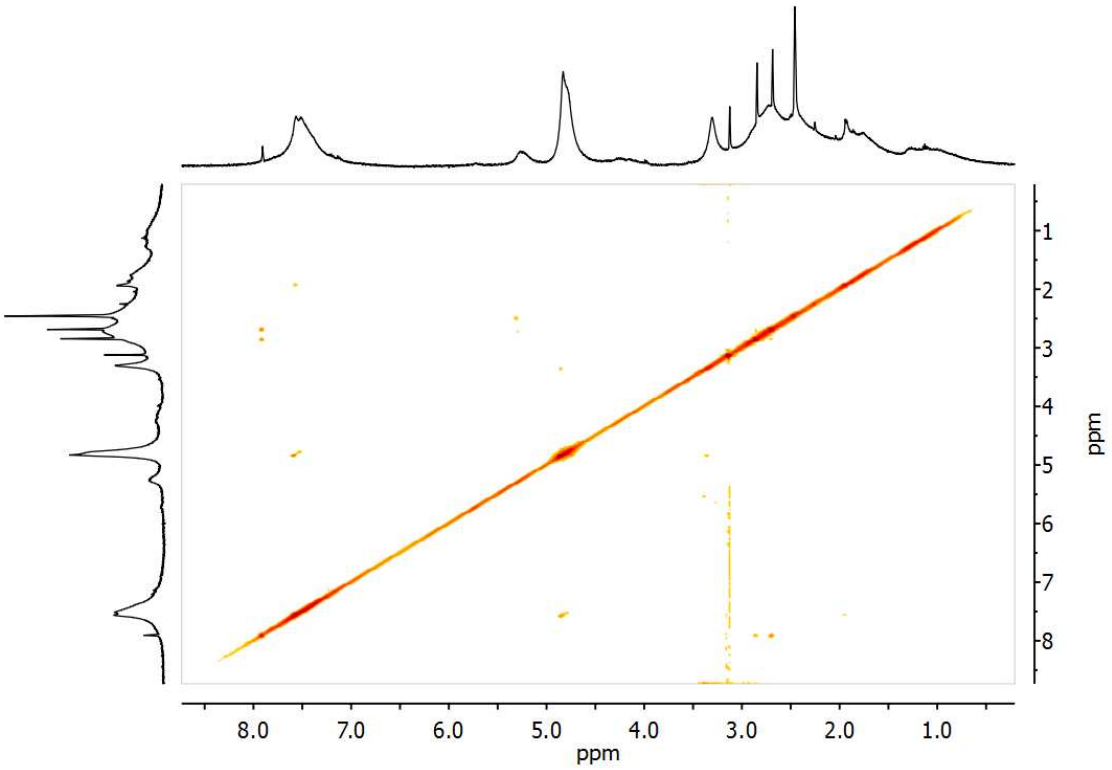

Figure S3.7. ^{1}H-^{1}H g COSY (DMSO-d_6, 400 MHz, 25 °C) spectrum of Poly(3-HMFO).

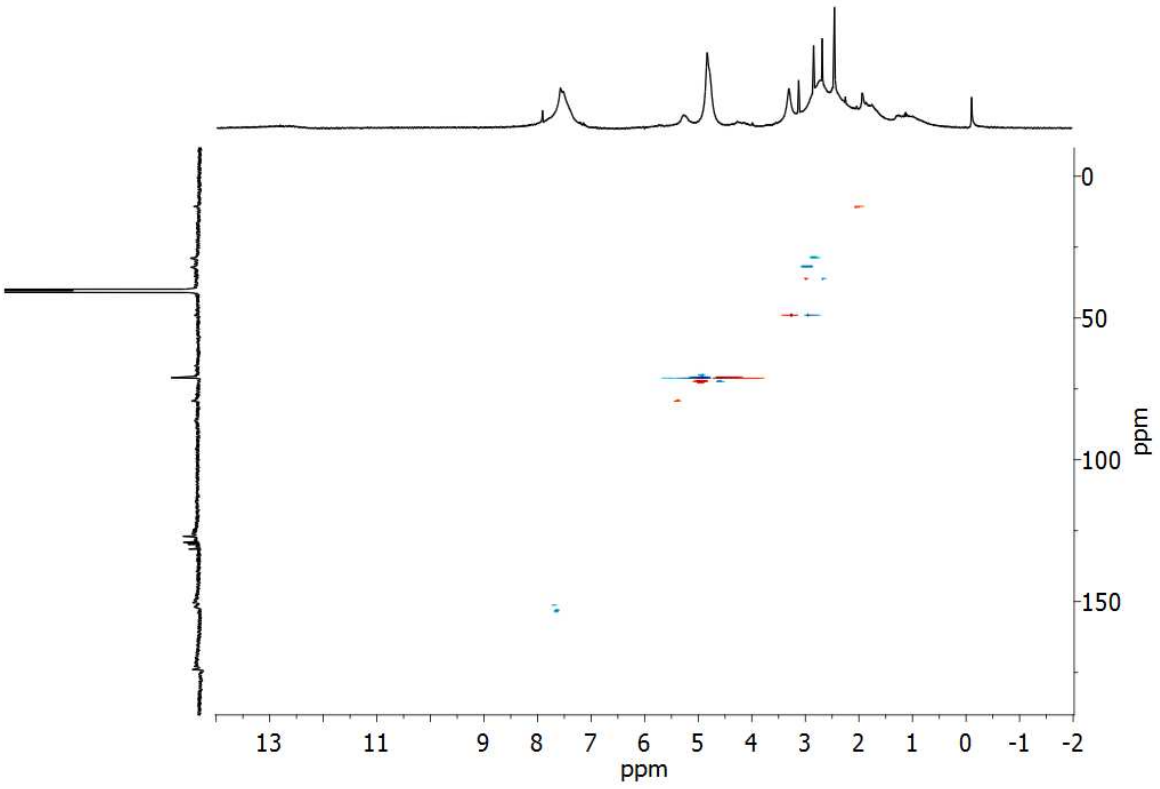

Figure S3.8. ^{1}H-^{13}C HSQCAD (DMSO-d_6, 400 MHz, 25 °C) spectrum of Poly(3-HMFO).

Appendix C

Experiment Details and Supporting Information for Chapter 4

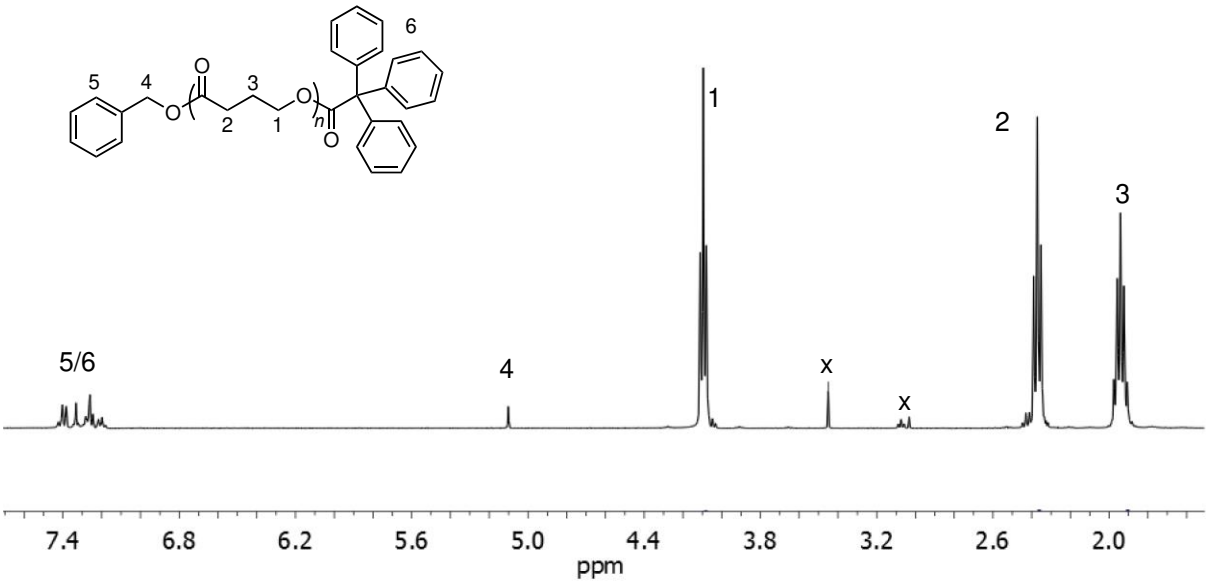

Figure S4.1 ^{1}H NMR (400 MHz, $CDCl_3$, 25 ºC) spectrum of $BnO\text{-}[C(=O)(CH_2)_3O]_n\text{-}C(=O)CPh_3$. Minor signals marked with "x" were due to the presence of unknown impurities.

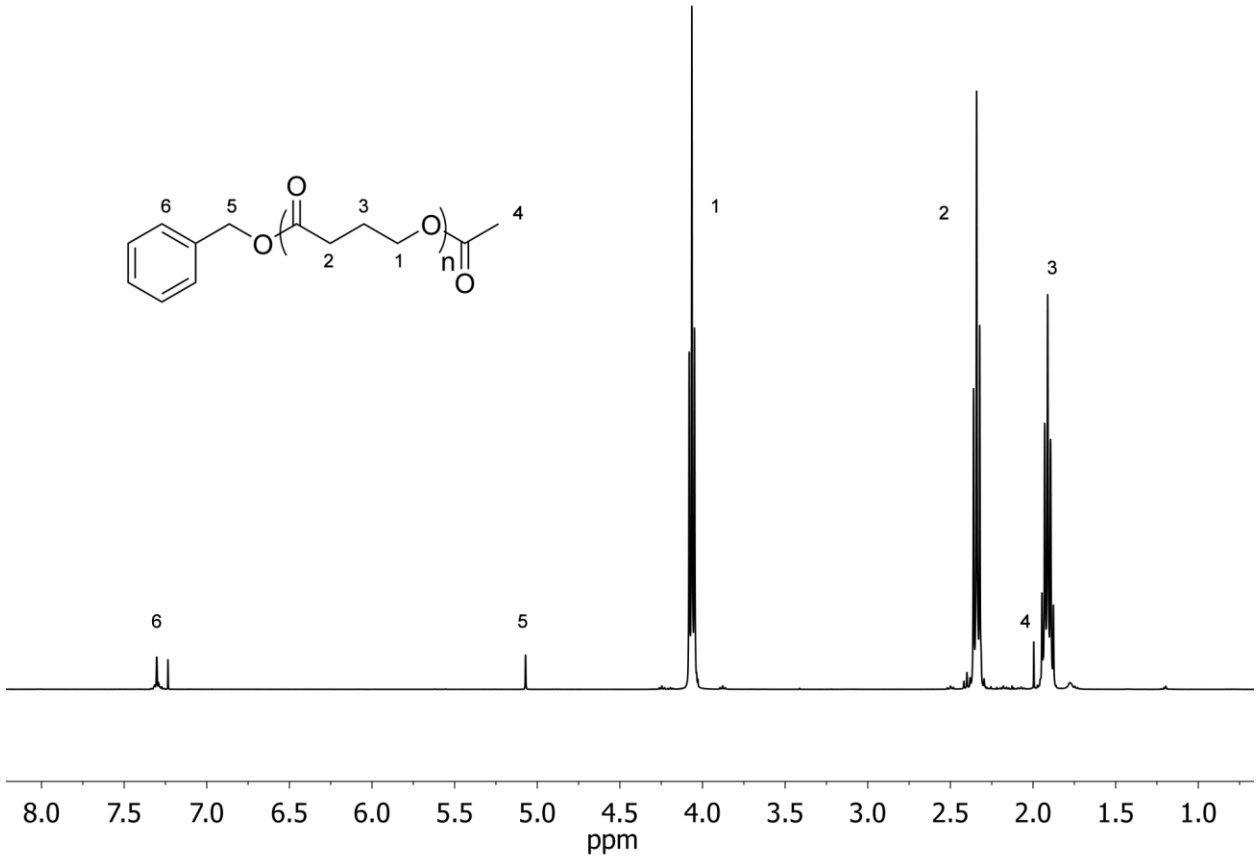

Figure S4.2 ^{1}H NMR (400 MHz, $CDCl_3$, 25 ºC) spectrum of BnO-[C(=O)$(CH_2)_3$O]$_n$-C(=O)Me prepared by acetic anhydride.

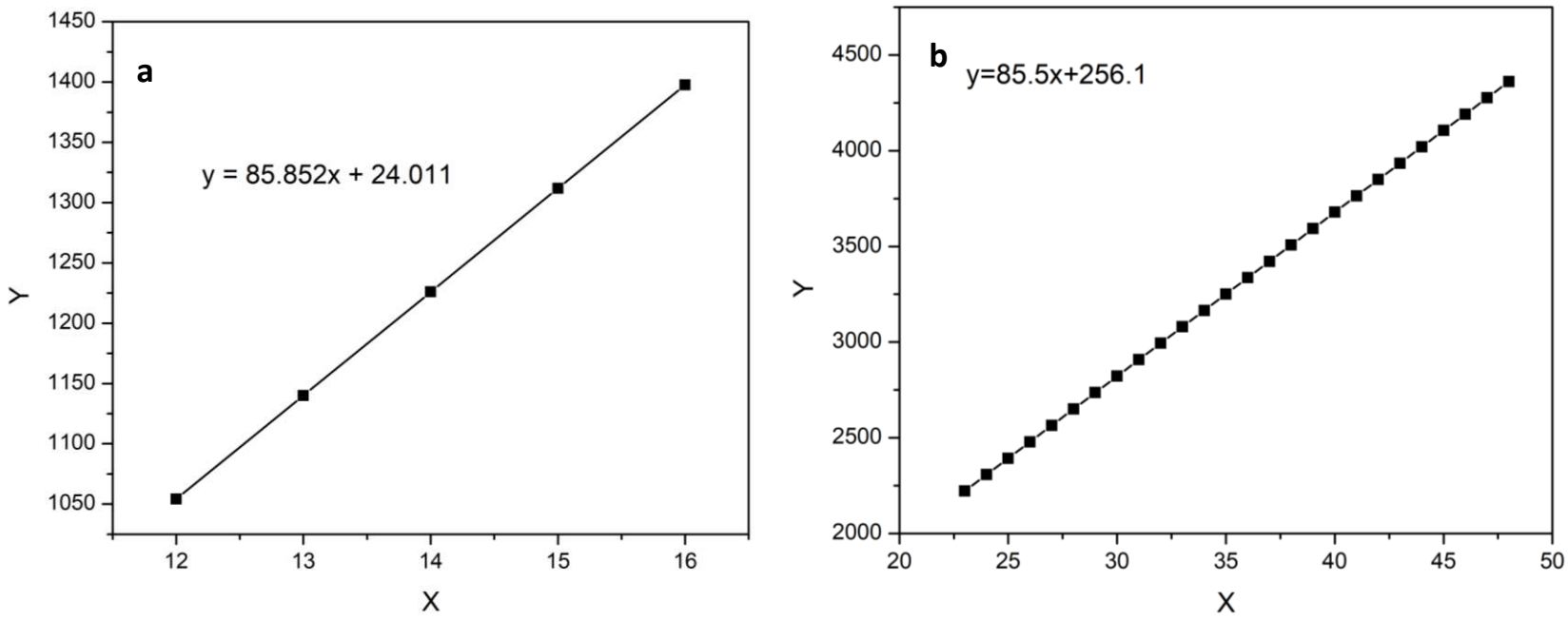
a
y = 85.852x + 24.011
Y
X
1450
1400
1350
1300
1250
1200
1150
1100
1050
12
13
14
15
16
b
y=85.5x+256.1
Y
X
4500
4000
3500
3000
2500
2000
20
25
30
35
40
45
50

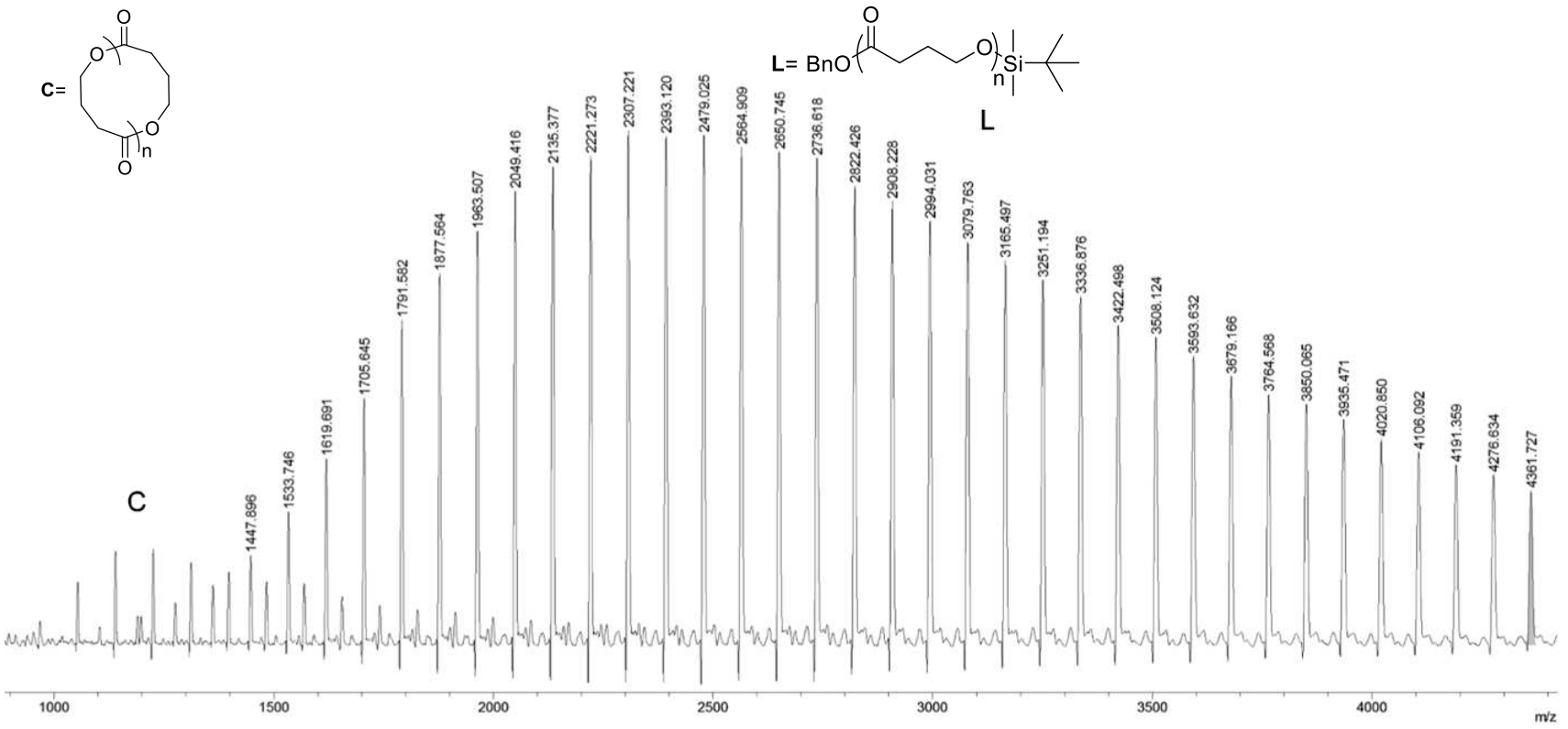

Figure S4.3 MALDI-TOF MS spectra of BnO-[C(=O)$(CH_2)_3$O]$_n$-$SiMe_2CMe_3$ and plots of *m*/*z* values vs γ-BL repeat units for the cyclic structure (**a**) and linear structure (**b**).

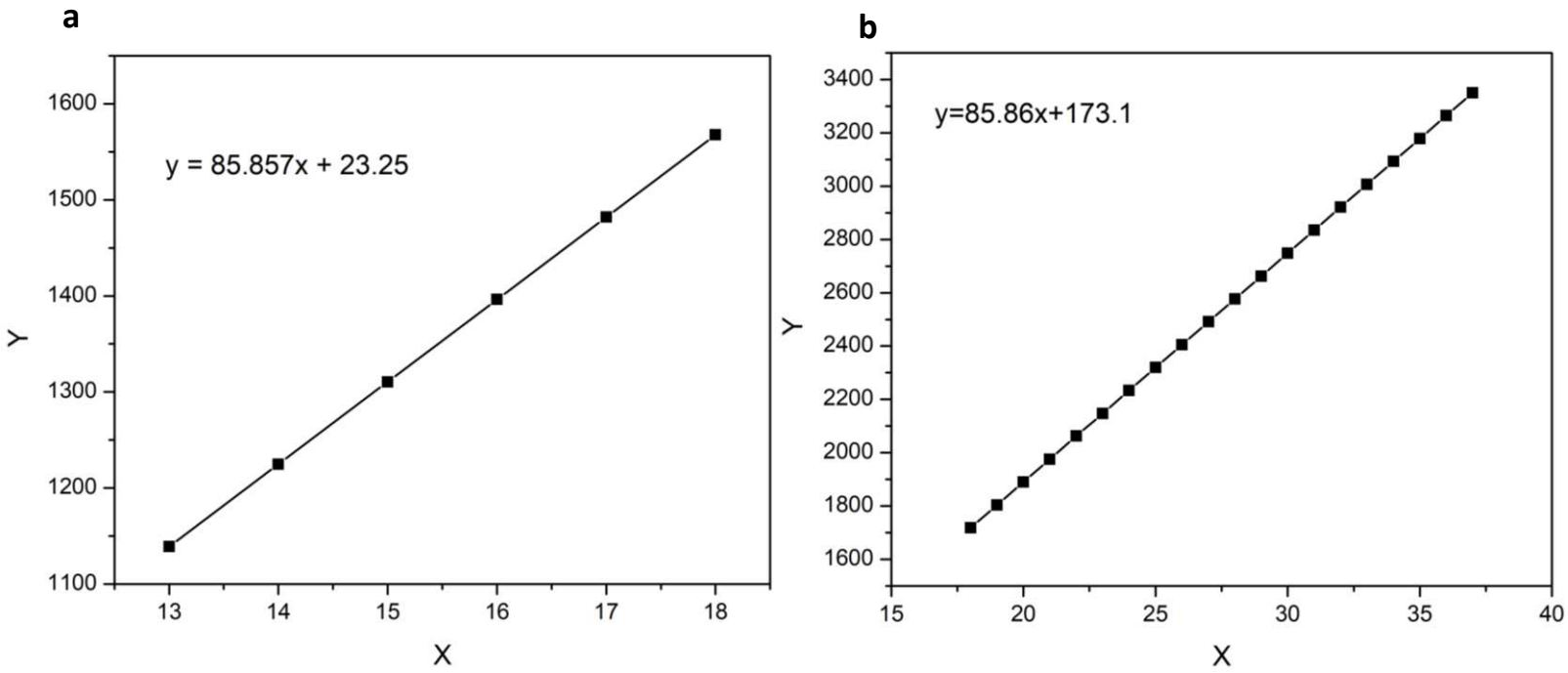
a
y = 85.857x + 23.25
Y
X
1600
1500
1400
1300
1200
1100
13
14
15
16
17
18
b
y=85.86x+173.1
Y
X
3400
3200
3000
2800
2600
2400
2200
2000
1800
1600
15
20
25
30
35
40

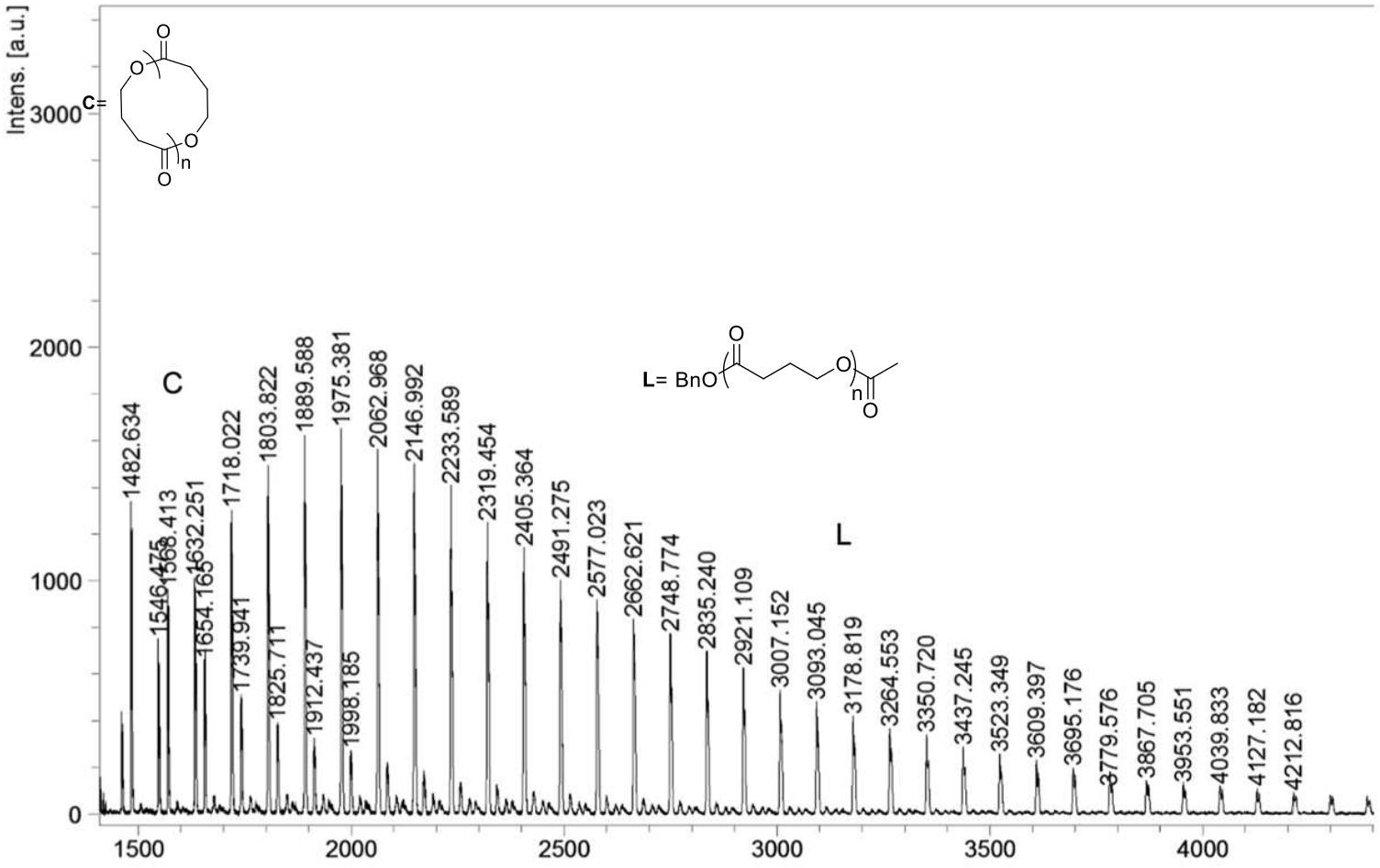

Figure S4.4 MALDI-TOF MS spectra of BnO-[C(=O)(CH_2)$_3$O]$_n$-C(=O)Me and plots of *m*/*z* values vs *γ*-BL repeat units for the cyclic structure (**a**) and linear structure (**b**).

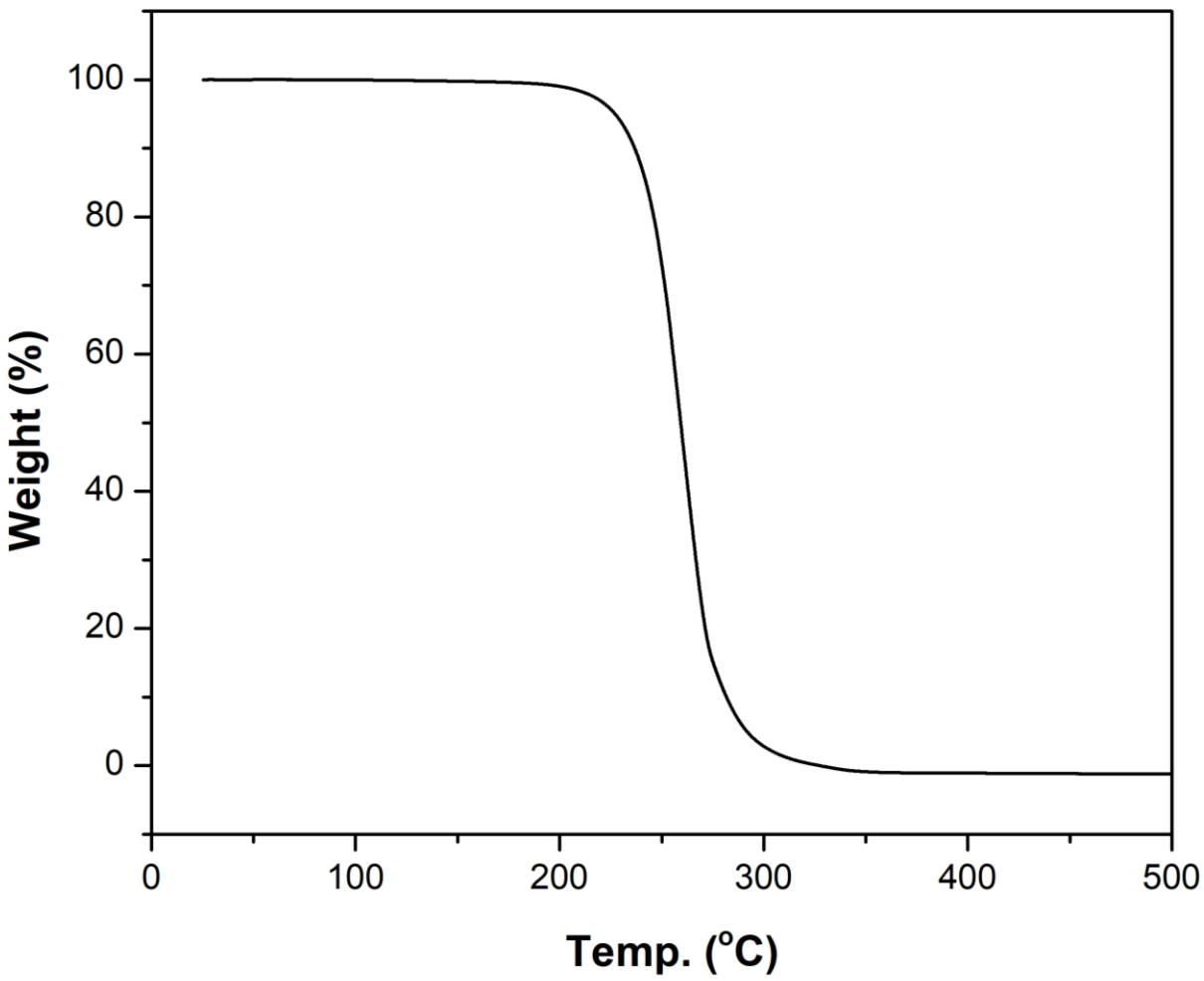

Figure S4.5 TGA curve for Ph_2CHCH_2O-$[C(=O)(CH_2)_3O]_n$-H.

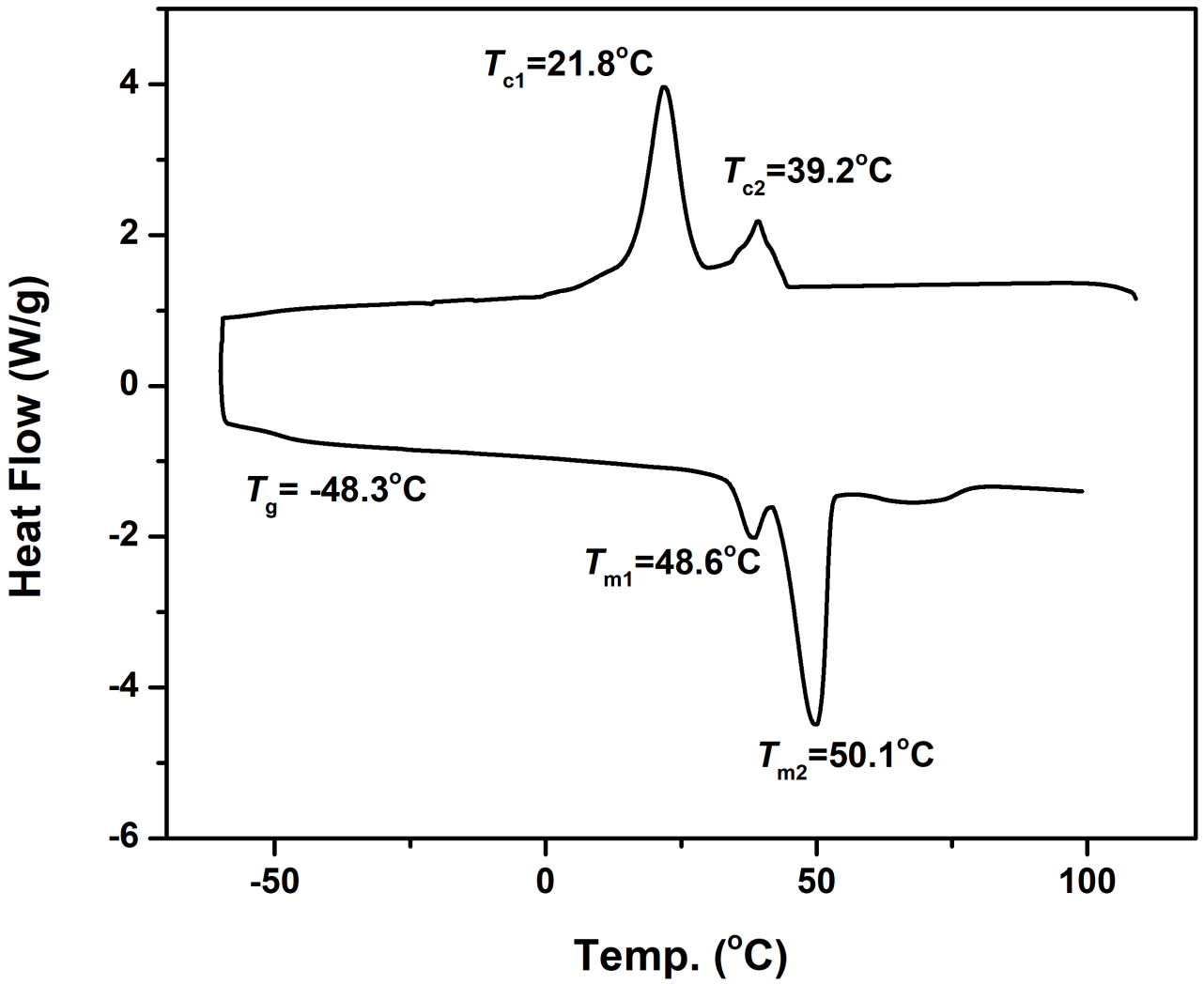

Figure S4.6 DSC curve for Ph_2CHCH_2O-$[C(=O)(CH_2)_3O]_n$-H.

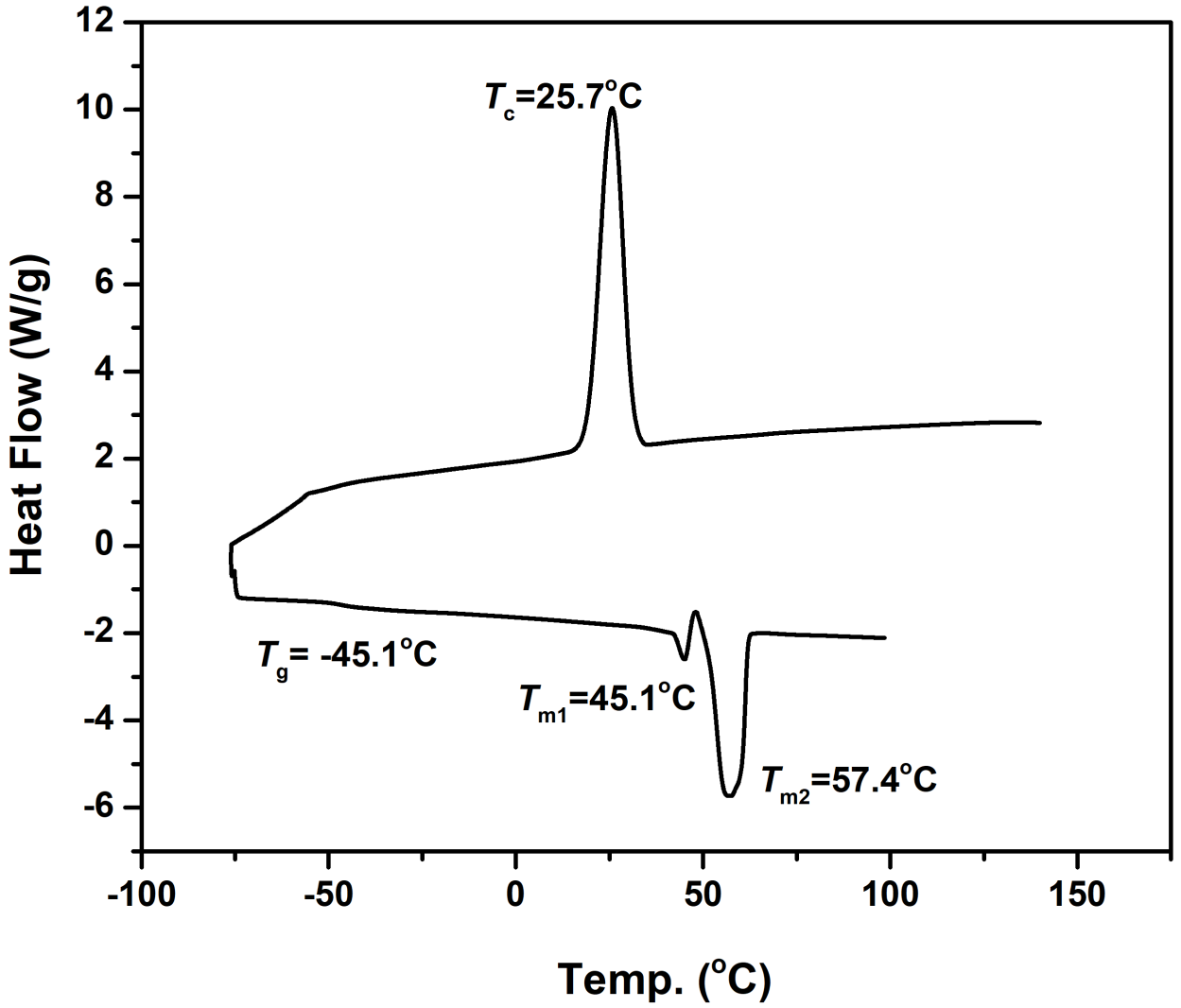

Figure S4.7 DSC curve for BnO-[C(=O)$(CH_2)_3$O]$_n$-H.

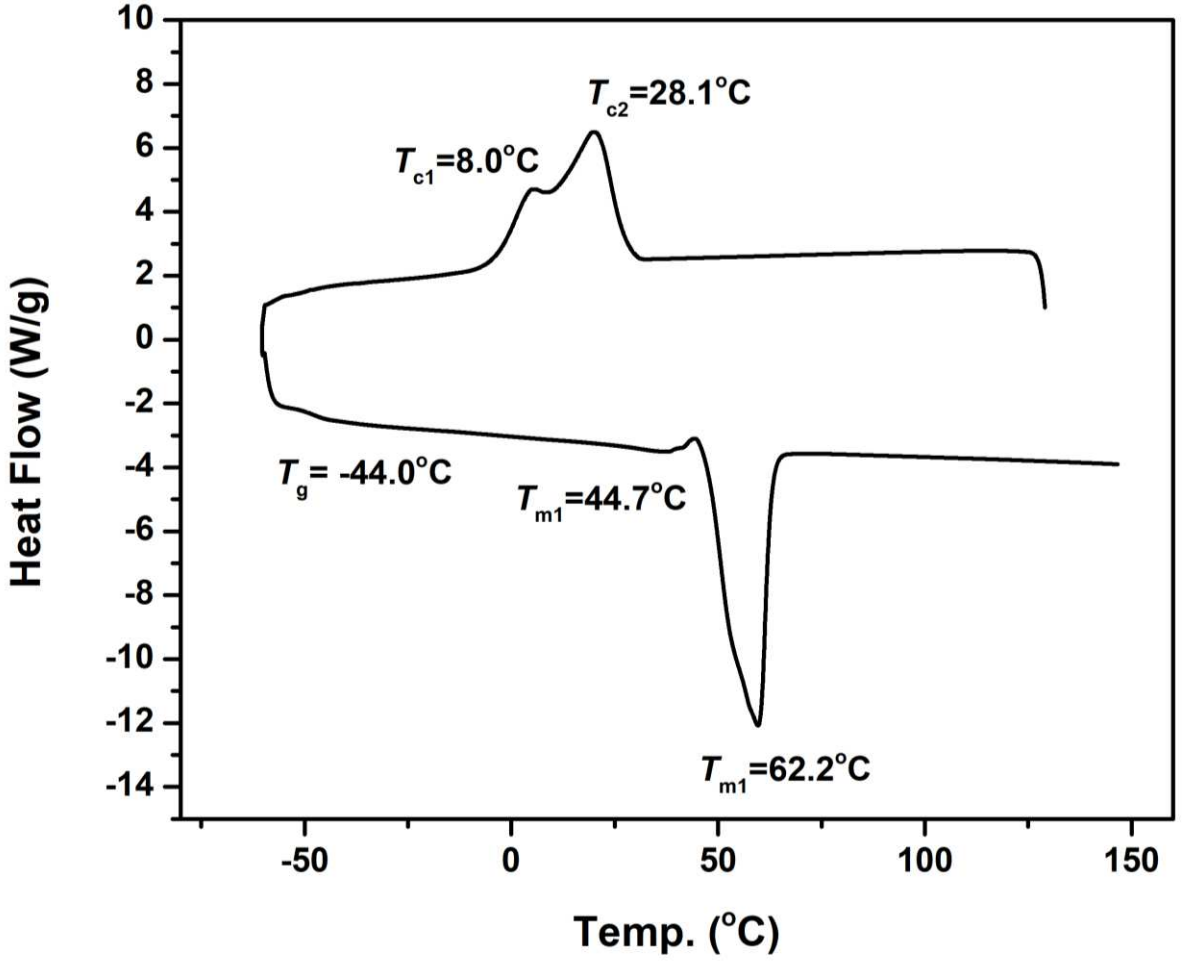

Figure S4.8 DSC curve for BnO-[C(=O)$(CH_2)_3$O]$_n$-C(=O)Me.

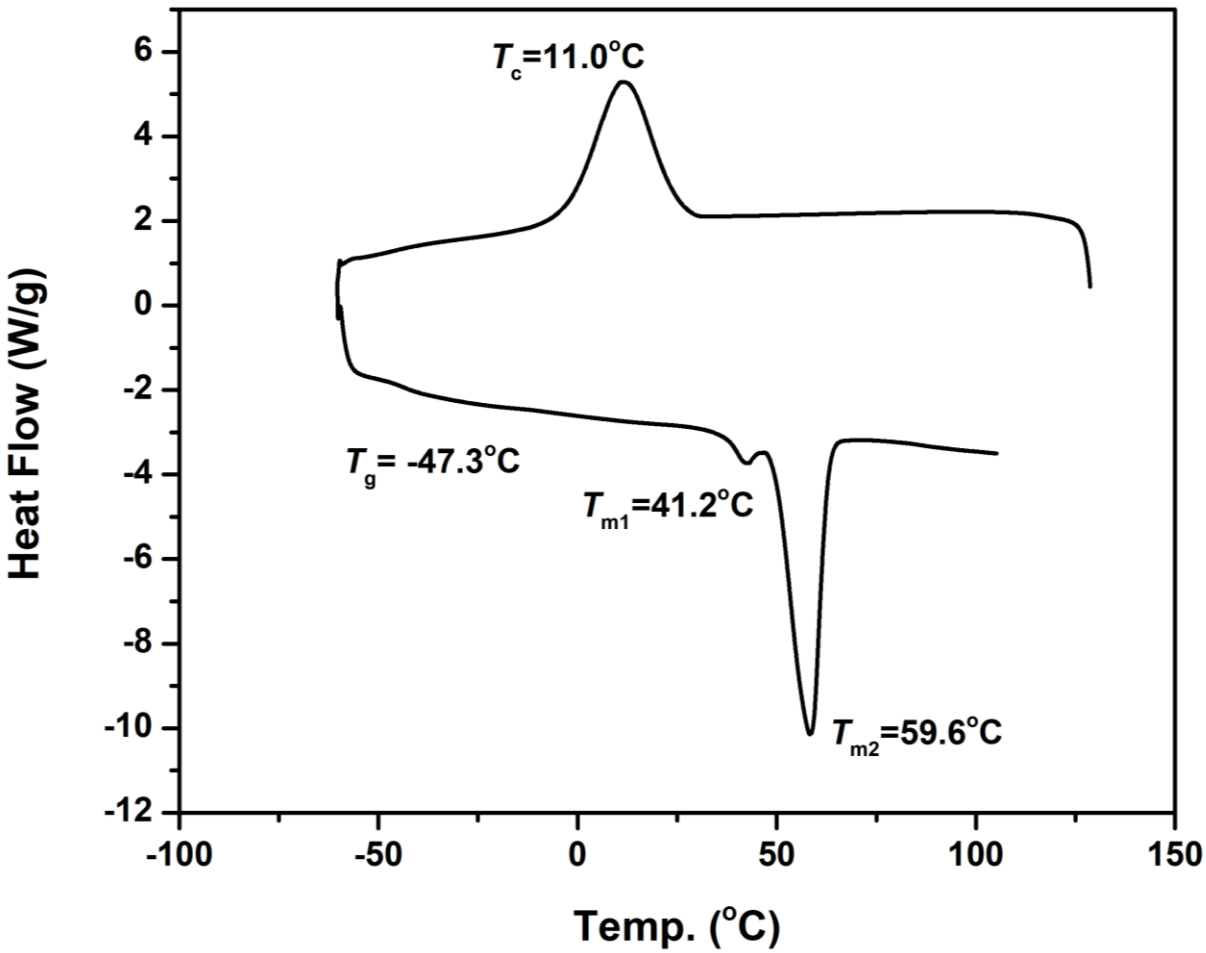

Figure S4.9 DSC curve for BnO-[C(=O)$(CH_2)_3$O]$_n$-C(=O)CH=CH_2.

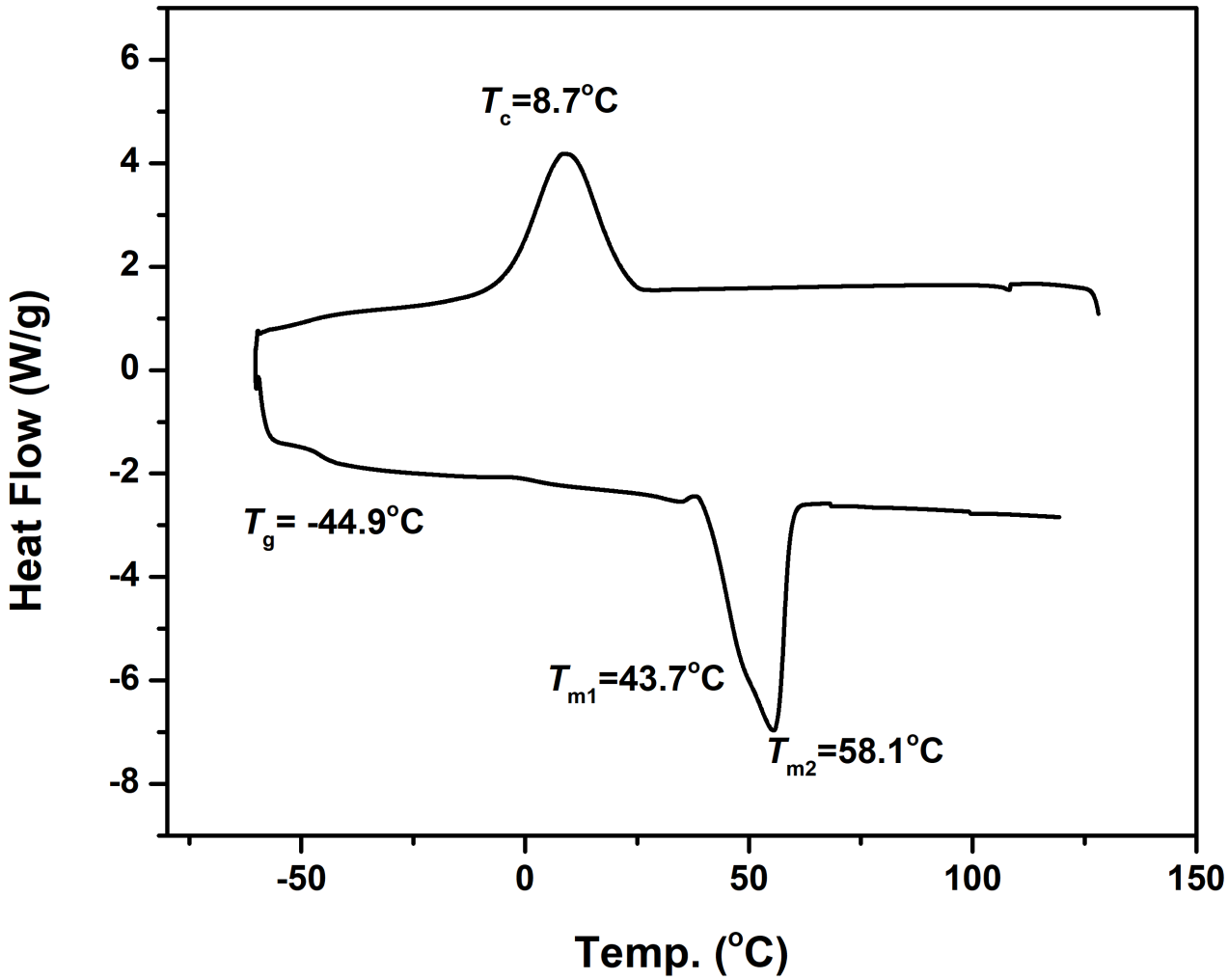

Figure S4.10 DSC curve for BnO-[C(=O)(CH_2)$_3$O]$_n$-C(=O)Ph.

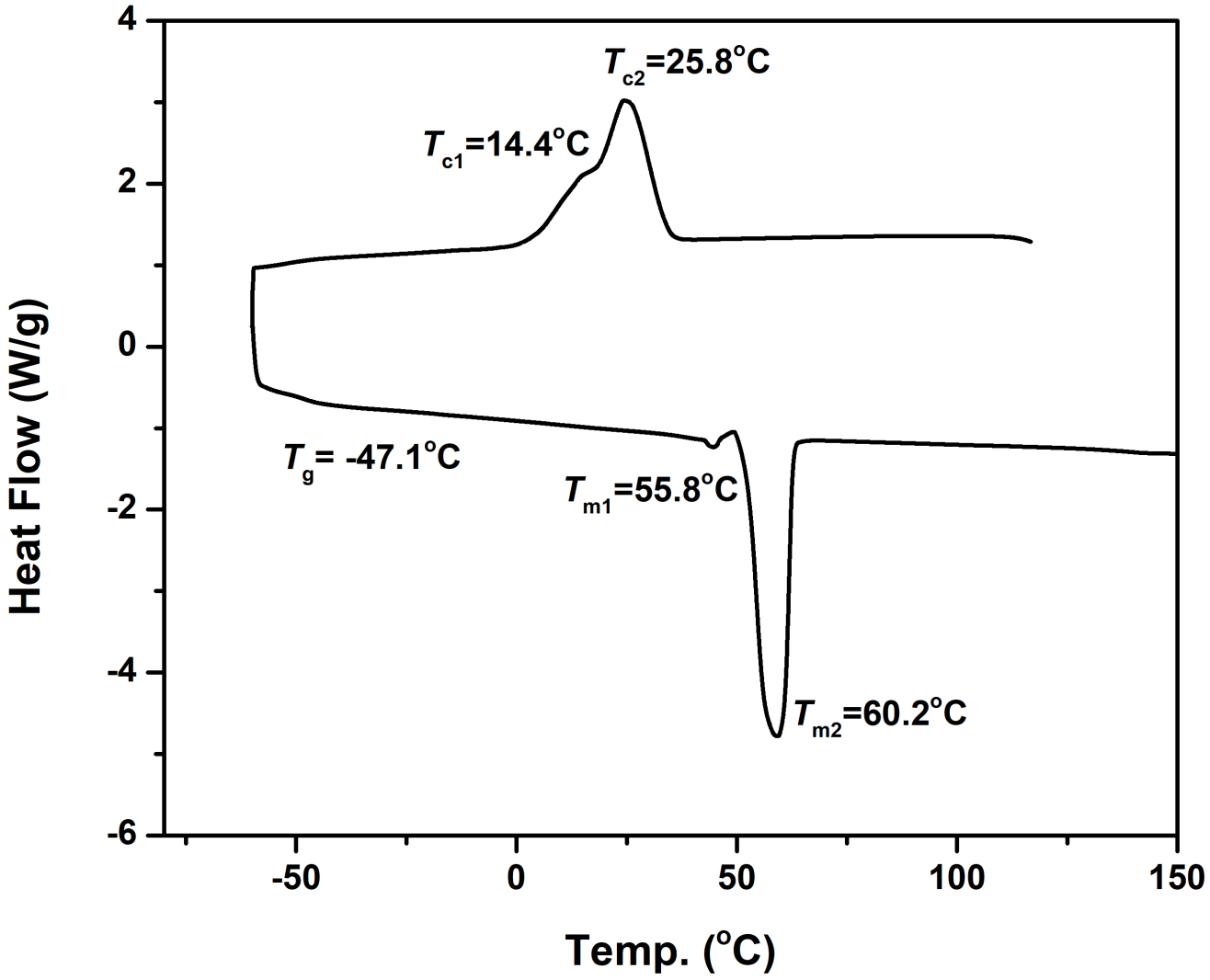

Figure S4.11 DSC curve for BnO-[C(=O)$(CH_2)_3$O]$_n$